DISSERTATION

GENERAL MODEL-BASED DECOMPOSITION FRAMEWORK FOR

POLARIMETRIC SAR IMAGES

Submitted by

Stephen Dauphin

Department of Mathematics

In partial fulfillment of the requirements

For the Degree of Doctor of Philosophy

Colorado State University

Fort Collins, Colorado

Spring 2017

Doctoral Committee:

Advisor: Margaret Cheney

Michael Kirby
Jade Morton
Olivier Pinaud

ABSTRACT

GENERAL MODEL-BASED DECOMPOSITION FRAMEWORK FOR
POLARIMETRIC SAR IMAGES

Polarimetric synthetic aperture radars emit a signal and measure the magnitude, phase, and polarization of the return. Polarimetric decompositions are used to extract physically meaningful attributes of the scatterers. Of these, model-based decompositions intend to model the measured data with canonical scatter-types. Many advances have been made to this field of model-based decomposition and this work is surveyed by the first portion of this dissertation.

A general model-based decomposition framework (GMBDF) is established that can decompose polarimetric data with different scatter-types and evaluate how well those scatter-types model the data by comparing a residual term. The GMBDF solves for all the scatter-type parameters simultaneously that are within a given decomposition by minimizing the residual term. A decomposition with a lower residual term contains better scatter-type models for the given data. An example is worked through that compares two decompositions with different surface scatter-type models.

As an application of the polarimetric decomposition analysis, a novel terrain classification algorithm of polSAR images is proposed. In the algorithm, the results of state-of-the-art polarimetric decompositions are processed for an image. Pixels are then selected to represent different terrain classes. Distributions of the parameters of these selected pixels are determined for each class. Each pixel in the image is given a score according to how well its parameters fit the parameter distributions of each class. Based on this score, the pixel is either assigned to a predefined terrain class or labeled unclassified.

ACKNOWLEDGEMENTS

Many people helped make this dissertation possible. I would like to thank my advisor from Colorado State University, Margaret Cheney, through whom the possibility of pursuing my degree was made possible.

I would like to thank L.J. Nickisch, Chad Spooner, and the other guys at Northwest Research Associates for giving me an opportunity and igniting my passion for applied mathematical research.

Robert Riley and Derek West have been my mentors during my internship at Sandia National Laboratories. They continue to encourage me in my research efforts. I am very lucky to have such supportive coworkers. Many others at Sandia have helped me throughout my internship including Steve Castillo, David Yocky, Andrew Pound, Kristina Czuchlewski, Katherine Simonson, amongst many others.

I would like to thank the National Nuclear Security Administration, Defense Nuclear Nonproliferation Research and Development, for sponsoring this work. I would also like to thank the UNESE team, a multi-institutional and interdisciplinary group of scientists and engineers, for its technical contributions.

I absolutely must thank my amazing wife, Nikki. She takes great care of our six children, she runs her own business, and still has the strength to encourage and support me in achieving my educational and professional goals. Nikki, this would not be possible without you. I love you. I would also like to thank my children, Isaac, Caleb, Joshua, Elliana, Nathan, and Timothy, who were gracious to me on many nights and weekends when I had to go and fight off mathematical dragons.

This dissertation is typeset in LaTeX using a document class designed by Leif Anderson.

TABLE OF CONTENTS

LIST OF FIGURES

INTRODUCTION: POLSAR PRIMER

The primary function of a radar (**RA**dio **D**etection **A**nd **R**anging) is to calculate the distance to an object. The radar accomplishes this by the following: 1) The radar emits an electromagnetic signal; 2) the signal interacts with the scene; 3) the scene reradiates the signal; and 4) the radar measures the magnitude and phase of the reradiated return. The larger the antenna aperture, the higher the resolution. Synthetic Aperture Radar (SAR) synthesizes a large aperture by placing a radar in motion relative to a scene and utilizes advanced signal processing to create a high-resolution image of the scene's measured electromagnetic reradiation. During the relative motion, the radar emits a series of polarized electromagnetic pulses. These pulses interact with the scatterers in the scene and are reradiated. A radar then receives and measures the reradiated signals. For a monostatic SAR system (which is to say the same radar sends and receives the electromagnetic signals), the emitter and receiver are the same radar. As the radar and the scene continue in their relative motion, multiple sets of these signals are emitted, interact with the ground, and the backscatter is measured. Through mathematical algorithms, a complex image is constructed from the returned signals (magnitude and phase). A great resource that explains the signal processing details is Jakowatz's book [1]. An informative mathematical approach is Cheney's monograph [2]. For a brief, yet informative, tutorial of SAR and some of its applications, see the article by Moreira, et al., [3].

Polarimetric Synthetic Aperture Radar (polSAR) measures the magnitude and phase of the returned signal as well as the return's polarization state [4, 5, 6]. Signals in two orthogonal polarization states are emitted and both polarization states of the return are measured.
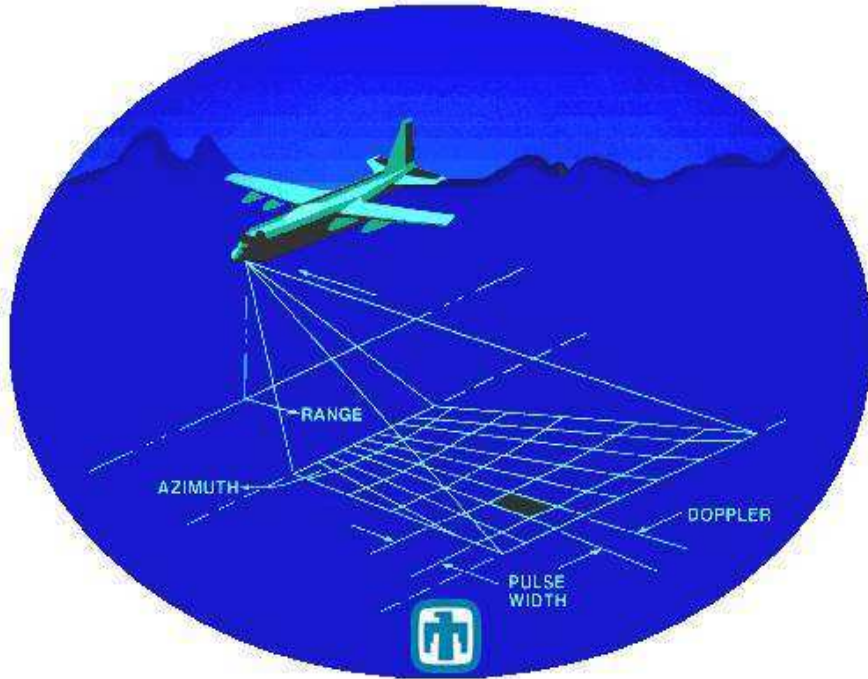
FIGURE 1.1. Diagram of the Geometry of SAR

The four images are referred to as S_{XX}, S_{XY}, S_{YX}, and S_{YY}, where S_{XY} represents the image created with the Y-polarized backscatter return of a X-polarized emitted signal. It is common to use polarization emitters and receivers that are linearly polarized and horizontally and vertically oriented. For the case where horizontally and vertically polarized signals are sent and received, the four images are referred to as S_{HH}, S_{HV}, S_{VH}, and S_{VV}, where S_{HV} represents the image created with the vertical backscatter return of a horizontally emitted signal. Based on the orientation of the returned signal, information about the scatterers (such as the geometry of the scatterers) is retrievable.

1.1. BUILDING BLOCKS FOR POLSAR DECOMPOSITIONS

The four measured returns are commonly placed in a 2×2 matrix referred to as the Sinclair scattering matrix representing the polarized backscatter,

$$
(1) \qquad \boldsymbol{S} = \begin{bmatrix} S_{\mathrm{HH}} & S_{\mathrm{HV}} \\ S_{\mathrm{VH}} & S_{\mathrm{VV}} \end{bmatrix}.
$$

These four polarization configurations form a basis for the polarization information of the returned signal [4] and therefore the complete polarization information of the backscatter is contained in the Sinclair scatter matrix. For polarimetric SAR systems that are monostatic, reciprocity is assumed, that is $S_{\mathrm{HV}} = S_{\mathrm{VH}}$ [4]. Monostatic systems and therefore reciprocity are assumed throughout the rest of this dissertation.

Two of the main tools to analyze polSAR images are the Pauli feature vector, $\underline{\boldsymbol{k}}$, and the corresponding coherency matrix, $\boldsymbol{T}$ [4]. For the monostatic case, $\underline{\boldsymbol{k}}$ is a three element vector

$$
(2) \qquad \underline{\boldsymbol{k}} = \frac{1}{\sqrt{2}} \begin{bmatrix} S_{\mathrm{HH}} + S_{\mathrm{VV}} \\ S_{\mathrm{HH}} - S_{\mathrm{VV}} \\ 2S_{\mathrm{HV}} \end{bmatrix},
$$

and $\boldsymbol{T}$ is a 3×3 matrix

$$
(3) \quad \langle \boldsymbol{T} \rangle = \left\langle \underline{\boldsymbol{k}} \cdot \underline{\boldsymbol{k}}^{*\mathrm{T}} \right\rangle = \frac{1}{2} \left\langle \begin{bmatrix} |S_{\mathrm{HH}}+S_{\mathrm{VV}}|^2 & (S_{\mathrm{HH}}+S_{\mathrm{VV}})(S_{\mathrm{HH}}-S_{\mathrm{VV}})^* & 2(S_{\mathrm{HH}}+S_{\mathrm{VV}})S_{\mathrm{HV}}^* \\ (S_{\mathrm{HH}}-S_{\mathrm{VV}})(S_{\mathrm{HH}}+S_{\mathrm{VV}})^* & |S_{\mathrm{HH}}-S_{\mathrm{VV}}|^2 & 2(S_{\mathrm{HH}}-S_{\mathrm{VV}})S_{\mathrm{HV}}^* \\ 2S_{\mathrm{HV}}(S_{\mathrm{HH}}+S_{\mathrm{VV}})^* & 2S_{\mathrm{HV}}(S_{\mathrm{HH}}-S_{\mathrm{VV}})^* & 4|S_{\mathrm{HV}}|^2 \end{bmatrix} \right\rangle.
$$

Both quantities are built from the complex images where $\langle \cdot \rangle$ is a spatial ensemble average, S_{HV}^* is the conjugate of S_{HV}, and $\underline{\boldsymbol{k}}^{*\mathrm{T}}$ the conjugate transpose of $\underline{\boldsymbol{k}}$. The ensemble-averaged

coherency matrix contains valuable second-order statics of the data as well as reduces the effects of speckle. Speckle is the result of the coherent interference of waves reflected from the scene. This interference causes variation in pixel intensities across the image and produces a granular effect which is typically undesirable. Averaging the coherency matrix with nearby coherency matrices reduces the speckle effect by averaging the constructive and destructive interference. This dissertation makes use of a 3×3 box-filter at the pixel. A larger box-filter will reduce the speckle further at the cost of losing resolution. The ensemble-averaged coherency matrix can be created other ways [**4, 7, 8**]. Polarimetric decompositions utilize these building blocks to extract physical information from the data.

MODEL-BASED POLARIMETRIC

DECOMPOSITIONS

In order to better understand and analyze polarimetric images, various methods exist to decompose the data to extract physical meaning. The vast majority of polarimetric decompositions fall into two categories. Eigen-decompositions begin with the eigenvalues and eigenvectors of the coherency matrix and attempt to construct physically relevant parameters, with the seminal paper being Cloude and Pottier's decomposition [9]. Model-based decompositions, the strain of decompositions that this dissertation is concerned with, separate the power of the measured return into contributions of canonical scatter-types:

$$\langle \boldsymbol{T} \rangle = \sum_{i=1}^{n} f_i \left[\boldsymbol{T} \right]_i,$$

(4)

where f_i is a scalar, and the theoretical coherency matrix $\left[\boldsymbol{T} \right]_i$ represents the ith canonical scatter-type.

The trace of the measured coherency matrix is referred to as the total power, TP, of the response.

$$TP = \text{tr} \left\{ \langle \boldsymbol{T} \rangle \right\} = \left\langle |S_{\text{HH}} + S_{\text{VV}}|^2 \right\rangle + \left\langle |S_{\text{HH}} - S_{\text{VV}}|^2 \right\rangle + \left\langle 4|S_{\text{HV}}|^2 \right\rangle$$

(5)
$$= T_{11} + T_{22} + T_{33}$$

The convention is to describe the power of a scatter-type with

$$P_i = f_i \left(\text{tr} \left\{ T_i \right\} \right).$$

(6)

As a small side note, the above calculation of the total power of the matrix is almost universally referred to as the *span* of the coherency matrix in polarimetric SAR literature. The span of a set of vectors refers to the space that contains all linear combinations of the vectors. From [**10**] the span and the trace are defined as

$$\text{(7)} \qquad \text{span}\left\{\vec{v}_1, \cdots, \vec{v}_n\right\} = \left\{\sum_{j=1}^{n} \beta_j \vec{v}_j : \beta_j \in \mathbb{R}\right\},$$

$$\text{(8)} \qquad \text{tr}\,(A) = \sum_{i=1}^{m} a_{ii}.$$

According to these definitions, the correct term for the sum of the diagonal elements of a matrix is the trace and will be used throughout the rest of this dissertation.

2.1. FREEMAN-DURDEN

The Freeman-Durden decomposition [**11**] popularized model-based decompositions using canonical scatter models for surface scattering (s), double-bounce scattering (d), and volume scattering (v). The averaged coherency matrix is decomposed as follows:

$$\text{(9)} \qquad \langle \boldsymbol{T} \rangle = f_{\text{s}} \langle \boldsymbol{T} \rangle_{\text{s}} + f_{\text{d}} \langle \boldsymbol{T} \rangle_{\text{d}} + f_{\text{v}} \langle \boldsymbol{T} \rangle_{\text{v}}.$$

2.1.1. **Surface scattering**. A surface that can be modeled by the small perturbation model (SPM) [**12**], also referred to as a Bragg surface [**4**], satisfies the following:

- $2\pi|h(x,y)|/\lambda \ll 1$
- $|\nabla h(x,y)| \ll 1,$

where $h(x, y)$ is the surface height in the xy-plane and λ is the wavelength of the emitted signal [12]. The Sinclair scattering matrix that models the response from such a surface is

$$
(10) \qquad S_\text{s} = \begin{bmatrix} R_\text{H} & 0 \\ 0 & R_\text{V} \end{bmatrix}.
$$

The reflection coefficients for horizontally and vertically polarized waves are given by [12]

$$
(11) \qquad R_\text{H} = \frac{\mu_r \cos \phi - \sqrt{\varepsilon_r \mu_r - \sin^2 \phi}}{\mu_r \cos \phi + \sqrt{\varepsilon_r \mu_r - \sin^2 \phi}}
$$

$$
(12) \qquad R_\text{V} = \frac{\varepsilon_r \cos \phi - \sqrt{\varepsilon_r \mu_r - \sin^2 \phi}}{\varepsilon_r \cos \phi + \sqrt{\varepsilon_r \mu_r - \sin^2 \phi}}.
$$

By assuming $\mu_r \approx 1$, which is true for most surfaces, we can simplify the equations to

$$
(13) \qquad R_\text{H} = \frac{\cos \phi - \sqrt{\varepsilon_r - \sin^2 \phi}}{\cos \phi + \sqrt{\varepsilon_r - \sin^2 \phi}}
$$

$$
(14) \qquad R_\text{V} = \frac{(\varepsilon_r - 1) \left\{ \sin^2 \phi - \varepsilon_r (1 + \sin^2 \phi) \right\}}{\left(\varepsilon_r \cos \phi + \sqrt{\varepsilon_r - \sin^2 \phi} \right)^2},
$$

where ϕ is the local incidence angle and ε_r is the relative dielectric constant [4].

The corresponding Pauli feature vector to the Sinclair scattering matrix that represents a small perturbation surface is

$$
(15) \qquad \underline{\boldsymbol{k}} = \frac{1}{\sqrt{2}} \begin{bmatrix} R_\text{H} + R_\text{V} \\ R_\text{H} - R_\text{V} \\ 0 \end{bmatrix}.
$$

The corresponding coherency matrix is

$$
(16) \qquad \boldsymbol{T}_\mathrm{s} = \frac{1}{2} \begin{bmatrix} |R_\mathrm{H} + R_\mathrm{V}|^2 & (R_\mathrm{H} + R_\mathrm{V})(R_\mathrm{H} - R_\mathrm{V})^* & 0 \\ (R_\mathrm{H} - R_\mathrm{V})(R_\mathrm{H} + R_\mathrm{V}) & |R_\mathrm{H} - R_\mathrm{V}|^2 & 0 \\ 0 & 0 & 0 \end{bmatrix}.
$$

After dividing through by $|R_\mathrm{H} + R_\mathrm{V}|^2$ we get the common expression for the surface coherency matrix:

$$
(17) \qquad \boldsymbol{T}_\mathrm{s} = \begin{bmatrix} 1 & \beta^* & 0 \\ \beta & |\beta|^2 & 0 \\ 0 & 0 & 0 \end{bmatrix} \qquad \text{where} \quad \beta = \frac{R_\mathrm{H} - R_\mathrm{V}}{R_\mathrm{H} + R_\mathrm{V}}, \quad |\beta| < 1.
$$

This construction of the β parameter differs slightly from the Freeman-Durden paper [11]. There, elements of the covariance matrix (a unitary transformation of the coherency matrix) are used and $\beta_\mathrm{FD} = \frac{R_\mathrm{H}}{R_\mathrm{V}}$. The β from the coherency matrix can be expressed in terms of the Freeman-Durden surface parameter β_FD:

$$
(18) \qquad \beta = \frac{R_\mathrm{H} - R_\mathrm{V}}{R_\mathrm{H} + R_\mathrm{V}} = \frac{\frac{R_\mathrm{H}}{R_\mathrm{V}} - 1}{\frac{R_\mathrm{H}}{R_\mathrm{V}} + 1} = \frac{\beta_\mathrm{FD} - 1}{\beta_\mathrm{FD} + 1}.
$$

From Van Zyl [13], the phase difference between R_H and R_V for natural surfaces is nearly zero. From this, Freeman and Durden [11] claim that β_FD is real. This claim implies that the β calculated from the coherency matrix also is real.

2.1.2. **Double-bounce scattering**. Double-bounce scattering is modeled by the scattering from a dihedral corner reflector, such as ground-wall backscatter:

$$(19) \qquad \boldsymbol{S}_{\mathrm{d}} = \begin{bmatrix} e^{j2\gamma_{\mathrm{H}}} R_{\mathrm{WH}} R_{\mathrm{GH}} & 0 \\ 0 & e^{j2\gamma_{\mathrm{V}}} R_{\mathrm{WV}} R_{\mathrm{GV}} \end{bmatrix}.$$

The horizontal and vertical reflection coefficients are

$$(20) \qquad R_{i\mathrm{H}} = \frac{\cos\phi_i - \sqrt{\varepsilon_i - \sin^2\phi_i}}{\cos\phi_i + \sqrt{\varepsilon_i - \sin^2\phi_i}}$$

$$(21) \qquad R_{i\mathrm{V}} = \frac{\varepsilon_i \cos\phi_i - \sqrt{\varepsilon_i - \sin^2\phi_i}}{\varepsilon_i \cos\phi_i + \sqrt{\varepsilon_i - \sin^2\phi_i}},$$

where $i \in \{\mathrm{G}, \mathrm{W}\}$, the ground surface and vertical surface dielectric constants are ε_{G} and ε_{W}, and the corresponding incidence angles $\phi_{\mathrm{G}} = \theta$ and $\phi_{\mathrm{W}} = \frac{\pi}{2} - \theta$.

The scaled corresponding coherency matrix is

$$(22) \qquad \boldsymbol{T}_{\mathrm{d}} = \begin{bmatrix} |\alpha|^2 & \alpha & 0 \\ \alpha^* & 1 & 0 \\ 0 & 0 & 0 \end{bmatrix},$$

where

$$(23) \qquad \alpha = \frac{R_{\mathrm{WH}} R_{\mathrm{GH}} + e^{j\phi} R_{\mathrm{WV}} R_{\mathrm{GV}}}{R_{\mathrm{WH}} R_{\mathrm{GH}} - e^{j\phi} R_{\mathrm{WV}} R_{\mathrm{GV}}}, \quad \phi = 2\gamma_{\mathrm{V}} - 2\gamma_{\mathrm{H}}, \quad |\alpha| < 1.$$

2.1.3. **Volume scattering**. The volume scattering model in the Freeman-Durden decomposition is modeled as the contribution of a cloud of randomly oriented dipoles. The

Sinclair scattering matrix of a dipole that is horizontally oriented is given by

$$(24) \qquad \boldsymbol{S}_{\text{dipole}} = \begin{bmatrix} a & 0 \\ 0 & b \end{bmatrix}_{|a| \gg |b|},$$

where a and b are the complex scattering coefficients. This scattering matrix can be rotated about the radar line of sight:

$$\boldsymbol{S}(\theta)_{\text{dipole}} = \boldsymbol{R}(\theta)\,\boldsymbol{S}_{\text{dipole}}\,\boldsymbol{R}(\theta)^T$$

$$(25) \qquad = \begin{bmatrix} \cos\theta & \sin\theta \\ -\sin\theta & \cos\theta \end{bmatrix} \begin{bmatrix} a & 0 \\ 0 & b \end{bmatrix} \begin{bmatrix} \cos\theta & -\sin\theta \\ \sin\theta & \cos\theta \end{bmatrix}$$

$$= \begin{bmatrix} a\cos^2\theta + b\sin^2\theta & (b-a)\sin\theta\cos\theta \\ (b-a)\sin\theta\cos\theta & a\sin^2\theta + b\cos^2\theta \end{bmatrix}.$$

If it is assumed that the thin cylinder scatterers are randomly oriented about the radar line of sight, the second-order statistics of the resulting coherency matrix $\boldsymbol{T}$ are given by

$$\langle (S_{\text{HH}} + S_{\text{VV}})(S_{\text{HH}} + S_{\text{VV}})^* \rangle = |a+b|^2$$

$$\langle (S_{\text{HH}} + S_{\text{VV}})(S_{\text{HH}} - S_{\text{VV}})^* \rangle = \left(|a|^2 + 2\mathbf{Im}\,\{a^*b\} - |b|^2 \right) I_1$$

$$\langle (S_{\text{HH}} + S_{\text{VV}})(2S_{\text{HV}})^* \rangle = \left(|b|^2 + 2\mathbf{Im}\,\{ab^*\} - |a|^2 \right) I_2$$

$$\langle (S_{\text{HH}} - S_{\text{VV}})(S_{\text{HH}} - S_{\text{VV}})^* \rangle = |a-b|^2\, I_3$$

$$\langle (S_{\text{HH}} - S_{\text{VV}})(2S_{\text{HV}})^* \rangle = -\frac{1}{2}\left(|a|^2 - 2\mathbf{Re}\,\{ab^*\} + |b|^2 \right) I_4$$

$$(26) \qquad \langle (2S_{\text{HV}})(2S_{\text{HV}})^* \rangle = |b-a|^2\, I_5,$$

where

$$I_1 = \int_{-\pi}^{\pi} \cos 2\theta \, p\left(\theta\right) \mathrm{d}\theta$$

$$I_2 = \int_{-\pi}^{\pi} \sin 2\theta \, p\left(\theta\right) \mathrm{d}\theta$$

(27)
$$I_3 = \int_{-\pi}^{\pi} \cos^2 2\theta \, p\left(\theta\right) \mathrm{d}\theta$$

$$I_4 = \int_{-\pi}^{\pi} \sin 4\theta \, p\left(\theta\right) \mathrm{d}\theta$$

$$I_5 = \int_{-\pi}^{\pi} \sin^2 2\theta \, p\left(\theta\right) \mathrm{d}\theta.$$

In matrix form

(28) $$\boldsymbol{T}_{\mathrm{v}} = \begin{bmatrix} |a+b|^2 & \left(|a|^2 + 2\mathbf{Im}\{a^*b\} - |b|^2\right)I_1 & \left(|b|^2 + 2\mathbf{Im}\{ab^*\} - |a|^2\right)I_2 \\ \left(|a|^2 + 2\mathbf{Im}\{a^*b\} - |b|^2\right)I_1 & |a-b|^2 I_3 & -\frac{1}{2}\left(|a|^2 - 2\mathbf{Re}\{ab^*\} + |b|^2\right)I_4 \\ \left(|b|^2 + 2\mathbf{Im}\{ab^*\} - |a|^2\right)I_2 & -\frac{1}{2}\left(|a|^2 - 2\mathbf{Re}\{ab^*\} + |b|^2\right)I_4 & |b-a|^2 I_5 \end{bmatrix}.$$

If the probability density function of the orientation angle is assumed to be uniform,

(29) $$p\left(\theta\right) = \frac{1}{2\pi}, \qquad \text{then} \qquad I_1, I_2, I_4 = 0 \quad I_3, I_5 = \frac{1}{2}.$$

With these values for I_i and considering the width of the dipoles going to zero we have

(30) $$\boldsymbol{T}_{\mathrm{v}} = \lim_{b \to 0} \begin{bmatrix} |a+b|^2 & 0 & 0 \\ 0 & \frac{|a-b|^2}{2} & 0 \\ 0 & 0 & \frac{|b-a|^2}{2} \end{bmatrix} = \frac{|a|^2}{2} \begin{bmatrix} 2 & 0 & 0 \\ 0 & 1 & 0 \\ 0 & 0 & 1 \end{bmatrix}.$$

11

Normalizing this volume scattering matrix so that its trace equals one, gives

$$
(31) \qquad \boldsymbol{T}_{\mathrm{v}} = \frac{1}{4} \begin{bmatrix} 2 & 0 & 0 \\ 0 & 1 & 0 \\ 0 & 0 & 1 \end{bmatrix}.
$$

2.1.4. **Assigning Powers**. We can now represent a measured coherency matrix with contributions of these three models. This decomposition assumes reflection symmetry, which is to say $T_{13} = T_{31} = T_{23} = T_{32} = 0$.

$$
(32) \qquad \langle \boldsymbol{T} \rangle = \begin{bmatrix} T_{11} & T_{12} & 0 \\ T_{21} & T_{22} & 0 \\ 0 & 0 & T_{33} \end{bmatrix} = f_{\mathrm{s}} \begin{bmatrix} 1 & \beta^* & 0 \\ \beta & |\beta|^2 & 0 \\ 0 & 0 & 0 \end{bmatrix} + f_{\mathrm{d}} \begin{bmatrix} |\alpha|^2 & \alpha & 0 \\ \alpha^* & 1 & 0 \\ 0 & 0 & 0 \end{bmatrix} + \frac{f_{\mathrm{v}}}{4} \begin{bmatrix} 2 & 0 & 0 \\ 0 & 1 & 0 \\ 0 & 0 & 1 \end{bmatrix}
$$

This yields the following equations:

$$
(33) \qquad T_{11} = f_{\mathrm{s}} + f_{\mathrm{d}}|\alpha|^2 + \frac{f_{\mathrm{v}}}{2}
$$

$$
(34) \qquad T_{22} = f_{\mathrm{s}}|\beta|^2 + f_{\mathrm{d}} + \frac{f_{\mathrm{v}}}{4}
$$

$$
(35) \qquad T_{33} = \frac{f_{\mathrm{v}}}{4}
$$

$$
(36) \qquad T_{12} = f_{\mathrm{s}}\beta^* + f_{\mathrm{d}}\alpha.
$$

This model gives four equations with five unknown parameters. Freeman and Durden [11] choose to set either α or β equal to zero. To make this decision, the contributions of the surface model and double-bounce model are compared. If $\langle |S_{\mathrm{HH}} + S_{\mathrm{VV}}|^2 \rangle > \langle |S_{\mathrm{HH}} - S_{\mathrm{VV}}|^2 \rangle$, the coherency matrix is dominated by surface model and α is set to zero. Likewise, if

$\langle |S_{\mathrm{HH}} + S_{\mathrm{VV}}|^2 \rangle < \langle |S_{\mathrm{HH}} - S_{\mathrm{VV}}|^2 \rangle$, the coherency matrix is dominated by double-bounce scattering and β is set to zero.

For surface-dominant scattering and setting $\alpha = 0$,

$$\text{(37)} \qquad f_{\mathrm{s}} = T_{11} - \frac{f_{\mathrm{v}}}{2}$$

$$\text{(38)} \qquad \beta = \left(\frac{T_{12}}{f_{\mathrm{s}}} \right)^{*}$$

$$\text{(39)} \qquad f_{\mathrm{d}} = T_{22} - f_{\mathrm{s}}|\beta|^2 - \frac{f_{\mathrm{v}}}{4}.$$

For dihedral-dominant scattering and setting $\beta = 0$,

$$\text{(40)} \qquad f_{\mathrm{d}} = T_{22} - \frac{f_{\mathrm{v}}}{4}$$

$$\text{(41)} \qquad \alpha = \frac{T_{12}}{f_{\mathrm{d}}}$$

$$\text{(42)} \qquad f_{\mathrm{s}} = T_{11} - f_{\mathrm{d}}|\alpha|^2 - \frac{f_{\mathrm{v}}}{2}.$$

Therefore, the TP (5) is separated into surface power, P_{s}, double-bounce power, P_{d}, and volume power, P_{v}. From equation (32), we can set the trace of the coherency matrix equal to an expression containing our five parameters:

$$\text{(43)} \qquad \mathrm{tr}\left\{ \langle \boldsymbol{T} \rangle \right\} = \underbrace{f_{\mathrm{s}} \left(1 + |\beta|^2 \right)}_{P_{\mathrm{s}}} + \underbrace{f_{\mathrm{d}} \left(1 + |\alpha|^2 \right)}_{P_{\mathrm{d}}} + \underbrace{f_{\mathrm{v}}}_{P_{\mathrm{v}}}$$

As the first mainstream model-based decomposition, the Freeman-Durden decomposition is an excellent first step. In practice, there is an issue of overestimating the volume power that leads to negative surface or dihedral power, which is a physical impossibility.

The Freeman-Durden model assumes reflection symmetry which is to say that the coherency matrix has the following form [4]:

$$
(44) \qquad \langle \boldsymbol{T} \rangle = \begin{bmatrix} T_{11} & T_{12} & 0 \\ T_{12}^* & T_{22} & 0 \\ 0 & 0 & T_{33} \end{bmatrix}.
$$

These five values of the measured coherency matrix, the real values T_{11}, T_{22}, T_{33} and the real and imaginary parts of the complex value T_{12} are accounted for in the Freeman-Durden decomposition. The real and imaginary parts of the complex values T_{13}, and T_{23} are not accounted for. (Note that the complex values T_{21}, T_{31}, and T_{32} are the conjugates of T_{12}, T_{13} and T_{23} and therefore do not contain any extra information.) To address situations where the reflection symmetry assumption does not hold, another canonical scattering model is needed.

2.2. YAMAGUCHI'S FOUR-COMPONENT DECOMPOSITION

Yamaguchi, et al., introduce a fourth scattering model (helical) to address nonreflection symmetric conditions [14] by accounting for $\mathbf{Im}\{T_{23}\}$, and considers alternative volume scattering models created with different probability density functions from (29).

2.2.1. **Helical scattering**. The Pauli feature vector and coherency matrix that represent left-helical scattering is derived from the Jones vector that represents left circularly polarized waves, $\hat{u}_{\mathrm{L}}$, and its associated Sinclair scattering matrix. For more on representing a wave's polarization with its Jones vector; see Appendix A.

$$
(45) \qquad \hat{\boldsymbol{u}}_{\mathrm{L}} = \frac{1}{\sqrt{2}} \begin{bmatrix} 1 \\ j \end{bmatrix} \qquad \boldsymbol{S}_{\mathrm{L}} = \frac{1}{2} \begin{bmatrix} 1 & j \\ j & -1 \end{bmatrix}
$$

14

$$(46) \qquad \underline{\boldsymbol{k}}_{\mathrm{P(L)}} = \frac{1}{\sqrt{2}} \begin{bmatrix} 0 \\ 1 \\ j \end{bmatrix} \qquad \boldsymbol{T}_{\mathrm{L}} = \underline{\boldsymbol{k}}_{\mathrm{P(L)}} \cdot \underline{\boldsymbol{k}}_{\mathrm{P(L)}}^{*\mathrm{T}} = \frac{1}{2} \begin{bmatrix} 0 & 0 & 0 \\ 0 & 1 & j \\ 0 & -j & 1 \end{bmatrix}$$

Similarly, for right-circular polarization

$$(47) \qquad \hat{\underline{\boldsymbol{u}}}_{\mathrm{R}} = \frac{1}{\sqrt{2}} \begin{bmatrix} 1 \\ -j \end{bmatrix} \qquad \boldsymbol{S}_{\mathrm{R}} = \hat{\underline{\boldsymbol{u}}}_{\mathrm{L}} \cdot \hat{\underline{\boldsymbol{u}}}_{\mathrm{R}}^{*\mathrm{T}} = \frac{1}{2} \begin{bmatrix} 1 & -j \\ -j & -1 \end{bmatrix}$$

$$(48) \qquad \underline{\boldsymbol{k}}_{\mathrm{P(R)}} = \frac{1}{\sqrt{2}} \begin{bmatrix} 0 \\ 1 \\ -j \end{bmatrix} \qquad \boldsymbol{T}_{\mathrm{R}} = \underline{\boldsymbol{k}}_{\mathrm{P(R)}} \cdot \underline{\boldsymbol{k}}_{\mathrm{P(R)}}^{*\mathrm{T}} = \frac{1}{2} \begin{bmatrix} 0 & 0 & 0 \\ 0 & 1 & -j \\ 0 & j & 1 \end{bmatrix}.$$

Therefore, the generalized coherency matrix that represents the helical scattering component is

$$(49) \qquad \boldsymbol{T}_{\mathrm{c}} = \frac{1}{2} f_{\mathrm{c}} \begin{bmatrix} 0 & 0 & 0 \\ 0 & 1 & \pm j \\ 0 & \mp j & 1 \end{bmatrix}.$$

Note that $\boldsymbol{R}(\theta_{\mathrm{c}}) \boldsymbol{T}_{\mathrm{c}} \boldsymbol{R}(\theta_{\mathrm{c}})^{*\mathrm{T}} = \boldsymbol{T}_{\mathrm{c}}$. Therefore, $\boldsymbol{T}_{\mathrm{c}}$ is invariant to rotation about the radar line of sight.

2.2.2. **Alternative Volume Scattering Models**. Yamaguchi et al. assert that a vertical structure of trunks and branches is dominant and therefore should not be modeled with randomly oriented dipoles with a uniform distribution around the line of sight [**14**]. They propose the following probability distribution function to more accurately represent

15

the mostly vertical nature of trees:

$$(50) \qquad p(\theta) = \begin{cases} \frac{1}{2}\sin\theta, & \text{for } 0 < \theta < \pi \\ 0, & \text{for } \pi < \theta < 2\pi \end{cases} \qquad \text{with } \int_0^{2\pi} p(\theta)\mathrm{d}\theta = 1 .$$

Using the integrals from (27) and the newly defined pdf, the volumetric model becomes

$$(51) \qquad \boldsymbol{T}_{\mathrm{v}} = \frac{1}{30} \begin{bmatrix} 15 & 5 & 0 \\ 5 & 7 & 0 \\ 0 & 0 & 8 \end{bmatrix} .$$

Another pdf is proposed that represents dipoles that are mostly horizontal:

$$(52) \qquad p(\theta) = \begin{cases} \frac{1}{2}\cos\theta, & \text{for } 0 < \theta < \frac{\pi}{2} \text{ or } \frac{3}{2}\pi < \theta < 2\pi \\ 0, & \text{otherwise} \end{cases} .$$

The associated volumetric model is

$$(53) \qquad \boldsymbol{T}_{\mathrm{v}} = \frac{1}{30} \begin{bmatrix} 15 & -5 & 0 \\ -5 & 7 & 0 \\ 0 & 0 & 8 \end{bmatrix} .$$

The data-driven decision to choose the appropriate volumetric model utilizes the expression

$$(54) \qquad 10\log\left(\frac{\langle |S_{\mathrm{VV}}|^2 \rangle}{\langle |S_{\mathrm{HH}}|^2 \rangle} \right) = 10\log\left(\frac{t_{11} + t_{22} - 2\mathbf{Re}\left\{t_{12}\right\}}{t_{11} + t_{22} + 2\mathbf{Re}\left\{t_{12}\right\}} \right) .$$

For vertically dominated volumetric scattering, $\langle |S_{\mathrm{VV}}|^2 \rangle \gg \langle |S_{\mathrm{HH}}|^2 \rangle$. For horizontally dominated volumetric scattering, $\langle |S_{\mathrm{VV}}|^2 \rangle \ll \langle |S_{\mathrm{HH}}|^2 \rangle$. From the volumetric model representing vertically dominant volumetric scattering,

$$(55) \quad 10 \log \left(\frac{t_{11} + t_{22} - 2\mathbf{Re}\left\{t_{12}\right\}}{t_{11} + t_{22} + 2\mathbf{Re}\left\{t_{12}\right\}} \right) = 10 \log \left(\frac{15 + 7 - 2(5)}{15 + 7 + 2(5)} \right) = 10 \log \left(\frac{3}{8} \right) \approx -4.26 \mathrm{dB},$$

and the volumetric model representing horizontally dominant volumetric scattering

$$(56) \quad 10 \log \left(\frac{t_{11} + t_{22} - 2\mathbf{Re}\left\{t_{12}\right\}}{t_{11} + t_{22} + 2\mathbf{Re}\left\{t_{12}\right\}} \right) = 10 \log \left(\frac{15 + 7 - 2(-5)}{15 + 7 + 2(-5)} \right) = 10 \log \left(\frac{8}{3} \right) \approx 4.26 \mathrm{dB}.$$

Yamaguchi, et al., set the threshold of $\pm 2\mathrm{dB}$ for the logarithmic expression. This way, the appropriate volumetric scattering model is chosen based on the measured data.

$$(57) \quad \text{If} \quad 10 \log \left(\frac{t_{11} + t_{22} - 2\mathbf{Re}\left\{t_{12}\right\}}{t_{11} + t_{22} + 2\mathbf{Re}\left\{t_{12}\right\}} \right) > 2 \text{then set} \quad \boldsymbol{T}_{\mathrm{v}} = \frac{1}{30} \begin{bmatrix} 15 & -5 & 0 \\ -5 & 7 & 0 \\ 0 & 0 & 8 \end{bmatrix}.$$

$$(58) \quad \text{If} \quad \left| 10 \log \left(\frac{t_{11} + t_{22} - 2\mathbf{Re}\left\{t_{12}\right\}}{t_{11} + t_{22} + 2\mathbf{Re}\left\{t_{12}\right\}} \right) \right| \leq 2 \text{then set} \quad \boldsymbol{T}_{\mathrm{v}} = \frac{1}{4} \begin{bmatrix} 2 & 0 & 0 \\ 0 & 1 & 0 \\ 0 & 0 & 1 \end{bmatrix}.$$

$$(59) \quad \text{If} \quad 10 \log \left(\frac{t_{11} + t_{22} - 2\mathbf{Re}\left\{t_{12}\right\}}{t_{11} + t_{22} + 2\mathbf{Re}\left\{t_{12}\right\}} \right) < -2 \text{then set} \quad \boldsymbol{T}_{\mathrm{v}} = \frac{1}{30} \begin{bmatrix} 15 & 5 & 0 \\ 5 & 7 & 0 \\ 0 & 0 & 8 \end{bmatrix}.$$

2.2.3. **Assigning Powers**. The coherency matrix is divided into contributions of canonical scattering models. Similar to Freeman-Durden, the power of each scatter-type is computed by multiplying the coefficient with the trace of the associated canonical scatter-type

matrix.

$$(60) \qquad \langle \boldsymbol{T} \rangle = f_{\mathrm{s}} \langle \boldsymbol{T} \rangle_{\mathrm{s}} + f_{\mathrm{d}} \langle \boldsymbol{T} \rangle_{\mathrm{d}} + f_{\mathrm{v}} \langle \boldsymbol{T} \rangle_{\mathrm{v}} + f_{\mathrm{c}} \langle \boldsymbol{T} \rangle_{\mathrm{c}}$$

$$(61) \qquad P_{\mathrm{s}} = f_{\mathrm{s}} \left(1 + |\beta|^2 \right) \qquad P_{\mathrm{v}} = f_{\mathrm{v}}$$

$$P_{\mathrm{d}} = f_{\mathrm{d}} \left(1 + |\alpha|^2 \right) \qquad P_{\mathrm{c}} = f_{\mathrm{c}}$$

The imaginary part of element T_{23} appears only in the helical scattering model. Therefore, f_{c} can be solved for first by

$$(62) \qquad \mathbf{Im}\,\{T_{23}\} = \pm \frac{f_{\mathrm{c}}}{2} \Rightarrow f_{\mathrm{c}} = 2\,|\mathbf{Im}\,\{T_{23}\}|\,.$$

The helical power is set $P_{\mathrm{c}} = f_{\mathrm{c}} \mathrm{tr}\,\{T_c\} = f_{\mathrm{c}}$. The T_{33} element is determined by the volume and helical scattering models. The next step is to select the appropriate volumetric scattering model for the measured data from equations (57), (58), and (59).

If (57) or (59) is satisfied, then

$$(63) \qquad T_{33} = \frac{4}{15} f_{\mathrm{v}} + \frac{1}{2} f_{\mathrm{c}} \qquad \Rightarrow \qquad f_{\mathrm{v}} = \frac{15}{4} \left(T_{33} - \frac{1}{2} f_{\mathrm{c}} \right).$$

If (58) is satisfied, then

$$(64) \qquad T_{33} = \frac{1}{4} f_{\mathrm{v}} + \frac{1}{2} f_{\mathrm{c}} \qquad \Rightarrow \qquad f_{\mathrm{v}} = 4 \left(T_{33} - \frac{1}{2} f_{\mathrm{c}} \right).$$

Now that both P_{c} and P_{v} have been calculated, we are left with three equations and four unknowns. P_{s} and P_{d} are calculated in a similar way to Freeman-Durden's decomposition by setting α or β equal to zero if the coherency matrix is dominated by double-bounce or surface

scattering respectively. If $\langle|S_{\text{HH}} + S_{\text{VV}}|^2\rangle > \langle|S_{\text{HH}} - S_{\text{VV}}|^2\rangle$, the coherency matrix is dominated by surface model and α is set to zero. Likewise, if $\langle|S_{\text{HH}} + S_{\text{VV}}|^2\rangle < \langle|S_{\text{HH}} - S_{\text{VV}}|^2\rangle$, the coherency matrix is dominated by double-bounce scattering and β is set to zero. Using the volumetric scattering model from (57), we get the equations

$$(65) \qquad T_{11} = f_{\text{s}} + f_{\text{d}}|\alpha|^2 + \frac{f_{\text{v}}}{2}$$

$$(66) \qquad T_{22} = f_{\text{s}}|\beta|^2 + f_{\text{d}} + \frac{7}{30}f_{\text{v}} + \frac{f_{\text{c}}}{2}$$

$$(67) \qquad T_{12} = f_{\text{s}}\beta^* + f_{\text{d}}\alpha - \frac{f_{\text{v}}}{6}.$$

For surface-dominant scattering and setting $\alpha = 0$,

$$(68) \qquad f_{\text{s}} = T_{11} - \frac{f_{\text{v}}}{2}$$

$$(69) \qquad \beta = \left(\frac{T_{12} + \frac{f_{\text{v}}}{6}}{f_{\text{s}}}\right)^*$$

$$(70) \qquad f_{\text{d}} = T_{22} - f_{\text{s}}|\beta|^2 - \frac{7}{30}f_{\text{v}} - \frac{f_{\text{c}}}{2}.$$

For dihedral-dominant scattering and setting $\beta = 0$,

$$(71) \qquad f_{\text{d}} = T_{22} - \frac{7}{30}f_{\text{v}} - \frac{f_{\text{c}}}{2}$$

$$(72) \qquad \alpha = \frac{T_{12} + \frac{f_{\text{v}}}{6}}{f_{\text{d}}}$$

$$(73) \qquad f_{\text{s}} = T_{11} - f_{\text{d}}|\alpha|^2 - \frac{f_{\text{v}}}{2}.$$

Using the volumetric scattering model from (58), we get the equations

$$(74) \qquad T_{11} = f_{\text{s}} + f_{\text{d}}|\alpha|^2 + \frac{f_{\text{v}}}{2}$$

$$(75) \qquad T_{22} = f_\text{s}|\beta|^2 + f_\text{d} + \frac{f_\text{v}}{4} + \frac{f_\text{c}}{2}$$

$$(76) \qquad T_{12} = f_\text{s}\beta^* + f_\text{d}\alpha.$$

For surface-dominant scattering and setting $\alpha = 0$,

$$(77) \qquad f_\text{s} = T_{11} - \frac{f_\text{v}}{2}$$

$$(78) \qquad \beta = \left(\frac{T_{12}}{f_\text{s}}\right)^*$$

$$(79) \qquad f_\text{d} = T_{22} - f_\text{s}|\beta|^2 - \frac{f_\text{v}}{4} - \frac{f_\text{c}}{2}.$$

For dihedral-dominant scattering and setting $\beta = 0$,

$$(80) \qquad f_\text{d} = T_{22} - \frac{f_\text{v}}{4} - \frac{f_\text{c}}{2}$$

$$(81) \qquad \alpha = \frac{T_{12}}{f_\text{d}}$$

$$(82) \qquad f_\text{s} = T_{11} - f_\text{d}|\alpha|^2 - \frac{f_\text{v}}{2}.$$

Using the volumetric scattering model from (59), we get the equations

$$(83) \qquad T_{11} = f_\text{s} + f_\text{d}|\alpha|^2 + \frac{f_\text{v}}{2}$$

$$(84) \qquad T_{22} = f_\text{s}|\beta|^2 + f_\text{d} + \frac{7}{30}f_\text{v} + \frac{f_\text{c}}{2}$$

$$(85) \qquad T_{12} = f_\text{s}\beta^* + f_\text{d}\alpha + \frac{f_\text{v}}{6}.$$

For surface-dominant scattering and setting $\alpha = 0$,

$$(86) \qquad f_\text{s} = T_{11} - \frac{f_\text{v}}{2}$$

$$(87) \qquad \beta = \left(\frac{T_{12} - \frac{f_v}{6}}{f_s} \right)^*$$

$$(88) \qquad f_d = T_{22} - f_s |\beta|^2 - \frac{7}{30} f_v - \frac{f_c}{2}.$$

For dihedral-dominant scattering and setting $\beta = 0$,

$$(89) \qquad f_d = T_{22} - \frac{7}{30} f_v - \frac{f_c}{2}$$

$$(90) \qquad \alpha = \frac{T_{12} - \frac{f_v}{6}}{f_d}$$

$$(91) \qquad f_s = T_{11} - f_d |\alpha|^2 - \frac{f_v}{2}.$$

Therefore, we can calculate the remaining parameters f_s, f_d, α, β for each of the volume scattering matrices, and assign the surface and dihedral powers,

$$(92) \qquad P_s = f_s \text{tr} \{T_s\} = f_s \left(1 + |\beta|^2 \right)$$

$$(93) \qquad P_d = f_d \text{tr} \{T_d\} = f_d \left(1 + |\alpha|^2 \right).$$

Similar to the Freeman-Durden decomposition, it is possible to end up with negative powers by overestimating the powers of scatter-types that are subtracted first, in this case the helical and the volume scatter-types. Therefore, certain checks were later placed in this decomposition to insure that nonnegative powers result and that the individual powers sum to the total power of the coherency matrix [4]:

$$\text{If} \quad P_v + P_c > TP,$$

$$(94) \qquad \text{set } P_s, P_d = 0, \text{ and } P_v = TP - P_c.$$

$$\text{If} \quad P_\text{v} + P_\text{c} \leq TP \text{ and } P_\text{s} < 0,$$

(95)
$$\text{set } P_\text{s} = 0, \text{ and } P_\text{d} = TP - P_\text{c} - P_\text{v}.$$

$$\text{If} \quad P_\text{v} + P_\text{c} \leq TP \text{ and } P_\text{d} < 0,$$

(96)
$$\text{set } P_\text{d} = 0, \text{ and } P_\text{s} = TP - P_\text{c} - P_\text{v}.$$

This decomposition improves on the Freeman-Durden decomposition by adding the helical model to account for asymmetrical coherency matrices where $\mathbf{Im}\{T_{23}\} \neq 0$. Therefore, six of the nine parameters of the measured coherency matrix are accounted for. The complex element T_{13} and the real part of element T_{23} remain unaccounted. Yamaguchi's decomposition also insures that all powers are nonnegative and that they sum to the total power, but it does so at the end of the decomposition without correcting for the overestimation of powers that caused the issue.

2.3. NONNEGATIVE EIGENVALUE DECOMPOSITION (NNED)

To address the problem of negative powers of both the Freeman-Durden and Yamaguchi decompositions, van Zyl, et al., propose a decomposition [15] that uses the eigenvalues of the coherency matrix to avoid negative powers. This decomposition also takes into consideration a residual term which contains the information in the measured coherency matrix that is not modeled by the chosen scatter-types:

(97)
$$\langle [\boldsymbol{T}] \rangle = a[\boldsymbol{T}_\text{model}] + [\boldsymbol{T}_\text{res}].$$

Each of the matrices in (97) must represent a physically realizable coherency matrix. This can be done by ensuring that the eigenvalues of each matrix are real and nonnegative.

To solve for a in (97), rearrange the equation in the form

$$(98) \qquad [\boldsymbol{T}_{\text{res}}] = \langle [\boldsymbol{T}] \rangle - a[\boldsymbol{T}_{\text{model}}].$$

This is similar to the subtraction of the volumetric model in the Freeman-Durden decomposition or the helical and volumetric models in the Yamaguchi decomposition with $a = 1$. Unlike those decompositions, van Zyl, et al., calculate the maximum value of a that ensures nonnegative real eigenvalues for the residual matrix. Assuming reflection symmetry, the model and the measured coherency matrices will have the form

$$(99) \qquad [\boldsymbol{T}_{\text{res}}] = \begin{bmatrix} \gamma & \delta & 0 \\ \delta^* & \zeta & 0 \\ 0 & 0 & \kappa \end{bmatrix} - a \begin{bmatrix} \gamma_a & \delta_a & 0 \\ \delta^* & \zeta_a & 0 \\ 0 & 0 & \kappa_a \end{bmatrix}.$$

The eigenvalues of the residual matrix are

$$
\lambda_1 = \frac{1}{2} \left(\gamma - \gamma_a + \zeta - a\zeta_a + \sqrt{(\gamma - a\gamma_a - \zeta + a\zeta_a)^2 + 4|\delta - a\delta_a|^2} \right)
$$

$$(100) \qquad \lambda_2 = \frac{1}{2} \left(\gamma - \gamma_a + \zeta - a\zeta_a - \sqrt{(\gamma - a\gamma_a - \zeta + a\zeta_a)^2 + 4|\delta - a\delta_a|^2} \right)$$

$$
\lambda_3 = \kappa - a\kappa_a.
$$

From (100), $\lambda_1 \geq \lambda_2$, and the maximum value for a is found when the smaller of λ_2 or λ_3 is zero. Any larger value of a will cause at least one eigenvalue to be negative. To find the largest value for a, find the minimum of the values that would make either λ_2 or λ_3 equal zero.

To make $\lambda_2 = 0$, set

(101)
$$\left(\gamma - a\gamma_a\right)\left(\zeta - a\zeta_a\right) - |\delta - a\delta_a|^2 = 0,$$

which gives the roots

(102)
$$a = \frac{Z \pm \sqrt{Z^2 - 4\left(\gamma_a\zeta_a - |\delta_a|^2\right)\left(\gamma\zeta - |\delta|^2\right)}}{2\left(\gamma_a\zeta_a - |\delta_a|^2\right)}.$$

For $\lambda_3 = 0$, $a = \frac{\kappa}{\kappa_a}$. Therefore, set

$$a_{\max} = \min \begin{cases} \dfrac{Z - \sqrt{Z^2 - 4\left(\gamma_a\zeta_a - |\delta_a|^2\right)\left(\gamma\zeta - |\delta|^2\right)}}{2\left(\gamma_a\zeta_a - |\delta_a|^2\right)} \\[2em] \dfrac{\kappa}{\kappa_a} \end{cases}.$$

In particular, van Zyl, et al., use this approach to separate the measured coherency matrix into three scatter-types: canopy, odd-bounce, and even-bounce (similar to the Freeman-Durden decomposition scatter-types: volumetric, surface, and dihedral) with a residual matrix to capture data that is not well represented by those models:

(103)
$$\langle \boldsymbol{T} \rangle = a[\boldsymbol{T}_{\text{canopy}}] + \lambda_{\text{odd}}[\boldsymbol{T}_{\text{odd}}] + \lambda_{\text{even}}[\boldsymbol{T}_{\text{even}}] + \lambda_{\text{res}}[\boldsymbol{T}_{\text{res}}].$$

The first step in the NNED is to subtract the canopy scatter-type from the measured coherency matrix and find the maximum value for a. The eigenvectors associated with the

eigenvalues from (100) are

$$(104) \qquad \mathbf{e}_1 = \begin{bmatrix} \frac{2\lambda_1 - 2(\zeta - a\zeta_a)}{2(\delta - a\delta_a)^*} \\ 1 \\ 0 \end{bmatrix} \qquad \mathbf{e}_2 = \begin{bmatrix} \frac{2\lambda_2 - 2(\zeta - a\zeta_a)}{2(\delta - a\delta_a)^*} \\ 1 \\ 0 \end{bmatrix} \qquad \mathbf{e}_3 = \begin{bmatrix} 0 \\ 0 \\ 1 \end{bmatrix}.$$

The eigenvectors of the surface and dihedral scatter-type models that are associated with nonzero eigenvalues are as follows:

$$(105) \qquad \mathrm{e}_\beta = \begin{bmatrix} \frac{1}{\beta} \\ 1 \\ 0 \end{bmatrix} \qquad \mathrm{e}_\alpha = \begin{bmatrix} \alpha \\ 1 \\ 0 \end{bmatrix}.$$

If $\gamma - a\gamma_a \geq \zeta - a\zeta_a$, then the matrix $\langle \boldsymbol{T} \rangle - a[\boldsymbol{T}_{\text{canopy}}]$ is surface dominant. Then associate the eigenvector $\boldsymbol{e}_1$ with surface scattering and the eigenvector $\boldsymbol{e}_1$ with dihedral scattering. Use this association to set values for β and α:

$$(106) \qquad \begin{aligned} \frac{1}{\beta} &= \frac{2\lambda_1 - 2(\zeta - a\zeta_a)}{2(\delta - a\delta_a)^*} \qquad & \lambda_{\text{odd}} = \lambda_1 \\[2mm] \alpha &= \frac{2\lambda_2 - 2(\zeta - a\zeta_a)}{2(\delta - a\delta_a)^*} \qquad & \lambda_{\text{even}} = \lambda_2. \end{aligned}$$

If $\gamma - a\gamma_a < \zeta - a\zeta_a$, then the matrix $\langle \boldsymbol{T} \rangle - a[\boldsymbol{T}_{\text{canopy}}]$ is dihedral dominant. Then associate the eigenvector $\boldsymbol{e}_1$ with dihedral scattering and the eigenvector $\boldsymbol{e}_1$ with surface scattering. Use this association to set values for β and α:

$$(107) \qquad \begin{aligned} \alpha &= \frac{2\lambda_1 - 2(\zeta - a\zeta_a)}{2(\delta - a\delta_a)^*} \qquad & \lambda_{\text{even}} = \lambda_1 \\[2mm] \frac{1}{\beta} &= \frac{2\lambda_2 - 2(\zeta - a\zeta_a)}{2(\delta - a\delta_a)^*} \qquad & \lambda_{\text{odd}} = \lambda_2. \end{aligned}$$

25

Now powers can be assigned:

$$(108) \qquad P_{\text{canopy}} = a\left(\text{tr}\left\{T_{\text{canopy}}\right\}\right)$$

$$(109) \qquad P_{\text{odd}} = \lambda_{\text{odd}}\left(1 + |\beta|^2\right)$$

$$(110) \qquad P_{\text{even}} = \lambda_{\text{even}}\left(1 + |\alpha|^2\right).$$

The NNED provides a solution to the negative power problem that exists in [11] and [14]. The NNED also provides a frame work of minimizing a residual matrix for an optimal decomposition. This method has been extended to include the full decomposition of the coherency matrix [16], as well as generalizing the volume scattering model [17].

2.4. ROTATION AROUND THE RADAR LINE OF SIGHT

Lee and Ainsworth proposed an orientation angle compensation [18] that Yamaguchi applied to his four component decomposition [19]. This rotation improves results by correctly identifying rotated dihedrals (double-bounce objects) as double-bounce instead of misclassifying them as volumetric.

2.4.1. **Line of Sight vs.** $S_{\text{HH}} + S_{\text{VV}}$ **Axis**. Throughout the literature of the following decompositions that rotate the coherency matrix, the claim is made that the rotation about the radar line of sight can be mathematically described by rotating the coherency matrix about the $S_{\text{HH}} + S_{\text{VV}}$ axis. In order to show that these two rotations are in fact equivalent, both rotations are analyzed.

The measured Sinclair scattering matrix can be rotated around the line of sight by matrix multiplication with

(111) $$[\boldsymbol{S}(\theta)] = [\boldsymbol{R}(\theta)]\,[\boldsymbol{S}]\,[\boldsymbol{R}(\theta)]^{*\mathrm{T}}$$

(112) $$[\boldsymbol{S}(\theta)] = \begin{bmatrix} \cos\theta & \sin\theta \\ -\sin\theta & \cos\theta \end{bmatrix} \begin{bmatrix} S_{\mathrm{HH}} & S_{\mathrm{HV}} \\ S_{\mathrm{VH}} & S_{\mathrm{VV}} \end{bmatrix} \begin{bmatrix} \cos\theta & -\sin\theta \\ \sin\theta & \cos\theta \end{bmatrix}$$

(113) $$S_{11}(\theta) = S_{\mathrm{HH}}\cos^2\theta + S_{\mathrm{VH}}\sin\theta\cos\theta + S_{\mathrm{HV}}\cos\theta\sin\theta + S_{\mathrm{VV}}\sin^2\theta$$

(114) $$S_{12}(\theta) = -S_{\mathrm{HH}}\sin\theta\cos\theta + S_{\mathrm{VH}}\cos^2\theta - S_{\mathrm{HV}}\sin^2\theta + S_{\mathrm{VV}}\sin\theta\cos\theta$$

(115) $$S_{21}(\theta) = -S_{\mathrm{HH}}\sin\theta\cos\theta - S_{\mathrm{VH}}\sin^2\theta + S_{\mathrm{HV}}\cos^2\theta + S_{\mathrm{VV}}\sin\theta\cos\theta$$

(116) $$S_{22}(\theta) = S_{\mathrm{HH}}\sin^2\theta - S_{\mathrm{VH}}\sin\theta\cos\theta - S_{\mathrm{HV}}\cos\theta\sin\theta + S_{\mathrm{VV}}\cos^2\theta$$

Assuming reciprocity, $S_{\mathrm{HV}} = S_{\mathrm{VH}}$, the Pauli feature vector associated with this rotated Sinclair matrix is

(117) $$\underline{\boldsymbol{k}}(\theta) = \frac{1}{\sqrt{2}} \begin{bmatrix} k_1 \\ k_2 \\ k_3 \end{bmatrix}$$

where

(118) $$k_1 = S_{11}(\theta) + S_{22}(\theta) = S_{\mathrm{HH}} + S_{\mathrm{VV}}$$

(119) $$k_2 = S_{11}(\theta) - S_{22}(\theta) = S_{\mathrm{HH}}\left(\cos^2\theta - \sin^2\theta\right) + 4S_{\mathrm{HV}}\sin\theta\cos\theta + S_{\mathrm{VV}}\left(\sin^2\theta - \cos^2\theta\right)$$

$$= (S_{\mathrm{HH}} - S_{\mathrm{VV}})\cos 2\theta + 2S_{\mathrm{HV}}\sin 2\theta$$

(120) $$k_3 = 2S_{12}(\theta) = -2S_{\mathrm{HH}}\sin\theta\cos\theta + 2S_{\mathrm{HV}}\left(\cos^2\theta - \sin^2\theta\right) + 2S_{\mathrm{VV}}\sin\theta\cos\theta$$

$$= -\left(S_{\mathrm{HH}} - S_{\mathrm{VV}}\right)\sin 2\theta + 2S_{\mathrm{HV}}\cos 2\theta.$$

The associated coherency matrix for this Pauli feature vector is

$$(121) \qquad \langle \boldsymbol{T}(\theta)\rangle = \left\langle \underline{\boldsymbol{k}}(\theta)\cdot\underline{\boldsymbol{k}}(\theta)^{*\mathrm{T}}\right\rangle = \frac{1}{2}\left\langle \begin{bmatrix} |k_1|^2 & k_1 k_2^* & k_1 k_3^* \\ k_2 k_1^* & |k_2|^2 & k_2 k_3^* \\ k_3 k_1^* & k_3 k_2^* & |k_3|^2 \end{bmatrix}\right\rangle,$$

with

$$(122) \qquad |k_1|^2 = |S_{\mathrm{HH}} + S_{\mathrm{VV}}|^2$$

$$(123) \qquad k_1 k_2^* = \left(S_{\mathrm{HH}} + S_{\mathrm{VV}}\right)\left(\left(S_{\mathrm{HH}} - S_{\mathrm{VV}}\right)\cos 2\theta + 2S_{\mathrm{HV}}\sin 2\theta\right)^*$$

$$= \left(|S_{\mathrm{HH}}|^2 - |S_{\mathrm{VV}}|^2 + 2\mathbf{Im}\left\{S_{\mathrm{VV}}S_{\mathrm{HH}}^*\right\}\right)\cos 2\theta$$

$$(124) \qquad k_1 k_3^* = \left(S_{\mathrm{HH}} + S_{\mathrm{VV}}\right)\left(-\left(S_{\mathrm{HH}} - S_{\mathrm{VV}}\right)\sin 2\theta + 2S_{\mathrm{HV}}\cos 2\theta\right)^*$$

$$= \left(|S_{\mathrm{VV}}|^2 - |S_{\mathrm{HH}}|^2 + 2\mathbf{Im}\left\{S_{\mathrm{HH}}S_{\mathrm{VV}}^*\right\}\right)\sin 2\theta$$

$$(125) \qquad |k_2|^2 = |\left(S_{\mathrm{HH}} - S_{\mathrm{VV}}\right)\cos 2\theta + 2S_{\mathrm{HV}}\sin 2\theta|^2$$

$$= |S_{\mathrm{HH}} - S_{\mathrm{VV}}|^2\cos^2 2\theta$$

$$(126) \qquad k_2 k_3^* = \left(\left(S_{\mathrm{HH}} - S_{\mathrm{VV}}\right)\cos 2\theta + 2S_{\mathrm{HV}}\sin 2\theta\right)\left(-\left(S_{\mathrm{HH}} - S_{\mathrm{VV}}\right)\sin 2\theta + 2S_{\mathrm{HV}}\cos 2\theta\right)^*$$

$$= -\frac{1}{2}|S_{\mathrm{HH}} - S_{\mathrm{VV}}|^2\sin 4\theta$$

$$(127) \qquad |k_3|^2 = |-\left(S_{\mathrm{HH}} - S_{\mathrm{VV}}\right)\sin 2\theta + 2S_{\mathrm{HV}}\cos 2\theta|^2$$

$$= |S_{\mathrm{HH}} - S_{\mathrm{VV}}|^2\sin 4\theta.$$

A rotation of the coherency matrix around the $S_{\mathrm{HH}} + S_{\mathrm{VV}}$ axis is described by

$$(128) \qquad \langle \boldsymbol{T}(\theta)\rangle = \boldsymbol{R}(\theta)\,\langle \boldsymbol{T}\rangle\,\boldsymbol{R}(\theta)^{*\mathrm{T}},$$

with

$$
(129) \qquad \mathbf{R}(\theta) = \begin{bmatrix} 1 & 0 & 0 \\ 0 & \cos 2\theta & \sin 2\theta \\ 0 & -\sin 2\theta & \cos 2\theta \end{bmatrix}.
$$

The elements of this rotated coherency matrix about the $S_{\mathrm{HH}} + S_{\mathrm{VV}}$ axis are

$$
(130) \qquad T_{11}(\theta) = |S_{\mathrm{HH}} + S_{\mathrm{VV}}|^2 = T_{11} = |k_1|^2
$$

$$
(131) \qquad T_{12}(\theta) = (S_{\mathrm{HH}} + S_{\mathrm{VV}})\left((S_{\mathrm{HH}} - S_{\mathrm{VV}})\cos 2\theta + 2S_{\mathrm{HV}}\sin 2\theta\right)^* = k_1 k_2^*
$$

$$
= T_{12}\cos 2\theta + T_{13}\sin 2\theta
$$

$$
T_{21}(\theta) = T_{12}(\theta)^*
$$

$$
(132) \qquad T_{13}(\theta) = (S_{\mathrm{HH}} + S_{\mathrm{VV}})\left(-(S_{\mathrm{HH}} - S_{\mathrm{VV}})\sin 2\theta + 2S_{\mathrm{HV}}\cos 2\theta\right)^* = k_1 k_3^*
$$

$$
= -T_{12}\sin 2\theta + T_{13}\cos 2\theta
$$

$$
T_{31}(\theta) = T_{13}(\theta)^*
$$

$$
(133) \qquad T_{22}(\theta) = |(S_{\mathrm{HH}} - S_{\mathrm{VV}})\cos 2\theta + 2S_{\mathrm{HV}}\sin 2\theta|^2 = |k_2|^2
$$

$$
= T_{22}\cos^2 2\theta + \mathbf{Re}\{T_{23}\}\sin 4\theta + T_{33}\sin^2 2\theta
$$

$$
T_{23}(\theta) = \left((S_{\mathrm{HH}} - S_{\mathrm{VV}})\cos 2\theta + 2S_{\mathrm{HV}}\sin 2\theta\right)\ldots
$$

$$
(134) \qquad \left(-(S_{\mathrm{HH}} - S_{\mathrm{VV}})\sin 2\theta + 2S_{\mathrm{HV}}\cos 2\theta\right)^* = k_2 k_3^*
$$

$$
= j\mathbf{Im}\{T_{23}\}
$$

$$
T_{32}(\theta) = T_{23}(\theta)^* = -j\mathbf{Im}\{T_{23}\}
$$

$$
(135) \qquad T_{33}(\theta) = |-(S_{\mathrm{HH}} - S_{\mathrm{VV}})\sin 2\theta + 2S_{\mathrm{HV}}\cos 2\theta|^2 = |k_3|^2
$$

$$
= T_{22}\sin^2 2\theta - \mathbf{Re}\{T_{23}\}\sin 4\theta + T_{33}\cos^2 2\theta.
$$

Therefore, a rotation of the Sinclair scattering matrix about the radar line of sight is equivalent to a rotation of the coherency matrix about the $S_{HH} + S_{VV}$ axis.

2.4.2. **Finding** θ. The misclassification of rotated dihedrals as volumetric can be reduced by rotating the coherency matrix in order to minimize the $T_{33}(\theta)$ term. The derivative of $T_{33}(\theta)$ with respect to θ is

$$T_{33}(\theta)' = |S_{HH} - S_{VV}|^2 \, 2 \sin 4\theta - 4\mathbf{Re}\left\{(S_{HH} - S_{VV})(2S_{HV})^*\right\} \cos 4\theta - 8\,|S_{HV}|^2 \sin 4\theta$$

(136)
$$= \left(2\,|S_{HH} - S_{VV}|^2 - 8\,|S_{HV}|^2\right) \sin 4\theta - 4\mathbf{Re}\left\{(S_{HH} - S_{VV})(2S_{HV})^*\right\} \cos 4\theta.$$

By setting $T_{33}(\theta)' = 0$ we find the θ that minimizes the $T_{33}(\theta)$ element:

(137)
$$0 = \left(2\,|S_{HH} - S_{VV}|^2 - 8\,|S_{HV}|^2\right) \sin 4\theta - 4\mathbf{Re}\left\{(S_{HH} - S_{VV})(2S_{HV})^*\right\} \cos 4\theta.$$

Solving this equation for 2θ:

(138)
$$\tan 4\theta = \frac{4\mathbf{Re}\left\{(S_{HH} - S_{VV})S_{HV}^*\right\}}{|S_{HH} - S_{VV}|^2 - 4\,|S_{HV}|^2}$$

and

$$2\theta = \frac{1}{2}\tan^{-1}\left(\frac{2\mathbf{Re}\left\{(S_{HH} - S_{VV})S_{HV}^*\right\}}{|S_{HH} - S_{VV}|^2 - 4\,|S_{HV}|^2}\right)$$

(139)
$$= \frac{1}{2}\tan^{-1}\left(\frac{2\mathbf{Im}\left\{T_{23}\right\}}{T_{22} - T_{33}} \pm n\pi\right) \qquad n = 0, 1,$$

with $\theta \in \left[-\frac{\pi}{4}, \frac{\pi}{4}\right]$.

After this rotation of the coherency matrix, (134) shows that $T_{23}(\theta) = j\mathbf{Im}\left\{T_{23}\right\}$. So the only contribution to $T_{23}(\theta)$ is the imaginary part of T_{23}. This rotation reduces the number of parameters of the coherency matrix from nine to eight by eliminating the real part of element T_{23} which was previously unaccounted for. The only canonical scatterer to contribute to the element $T_{23}(\theta)$ is the

helical scatterer. Therefore, similar to the Yamaguchi decomposition without rotation, the helical scattering power is defined first with (61) (62). The rest of the powers are assigned as before using the rotated coherency matrix and (63), (64), (94), (95), and (96).

2.5. G4U

The rotation of the coherency matrix eliminates the real part of the T_{23} element. Singh, et al., introduce an additional unitary transformation that eliminates the element altogether in the General Four-Component Scattering Power Decomposition with Unitary Transformation of Coherency Matrix (G4U) [20].

After the first real unitary rotation (129) about the radar line of sight, the second complex unitary transformation (141) is

$$(140) \qquad \langle \boldsymbol{T}(\varphi) \rangle = \boldsymbol{U}(\varphi) \langle \boldsymbol{T} \rangle \boldsymbol{U}(\varphi)^{*\mathrm{T}},$$

where $\boldsymbol{U}(\varphi)$ is defined as

$$(141) \qquad \boldsymbol{U}(\varphi) = \begin{bmatrix} 1 & 0 & 0 \\ 0 & \cos 2\varphi & j\sin 2\varphi \\ 0 & j\sin 2\varphi & \cos 2\varphi \end{bmatrix}.$$

After this second unitary transformation, the elements of the twice-rotated matrix are

$$(142) \qquad T_{11}(\varphi) = T_{11}(\theta) = T_{11}$$

$$(143) \qquad T_{12}(\varphi) = T_{21}^*(\varphi) = T_{12}(\theta)\cos 2\varphi - jT_{13}(\theta)\sin 2\varphi$$

$$(144) \qquad T_{13}(\varphi) = T_{31}^*(\varphi) = T_{13}(\theta)\cos 2\varphi - jT_{12}(\theta)\sin 2\varphi$$

$$(145) \qquad T_{22}(\varphi) = T_{22}(\theta)\cos^2 2\varphi + \mathbf{Im}\,\{T_{23}(\theta)\}\sin 4\varphi + T_{33}(\theta)\sin^2 2\varphi$$

$$(146) \qquad T_{23}(\varphi) = T_{32}^*(\varphi) = \mathbf{Re}\,\{T_{23}(\theta)\} = 0$$

31

$$(147) \qquad T_{33}(\varphi) = T_{22}(\theta)\sin^2 2\varphi - \mathbf{Im}\left\{T_{23}(\theta)\right\}\sin 4\varphi + T_{33}(\theta)\cos^2 2\varphi.$$

Note that $T_{23}(\varphi) = 0$. After this second transformation, both the real and imaginary components of the T_{23} are eliminated. Therefore, the total number of parameters of the coherency matrix is reduced to seven. Also, the twice-rotated coherency matrix makes use of both the real and imaginary parts of the complex element T_{13}. So this decomposition is able to make use of all the elements of the measured coherency matrix.

The angle φ is calculated, similar to θ, by minimizing the $T_{33}(\theta)$ element.

$$(148) \qquad 2\varphi = \frac{1}{2}\tan^{-1}\left(\frac{2\mathbf{Im}\left\{T_{23}(\theta)\right\}}{T_{22}(\theta) - T_{33}(\theta)} \pm n\pi\right) \qquad n = 0, 1,$$

with $\varphi \in \left[-\frac{\pi}{4}, \frac{\pi}{4}\right]$.

Singh also implements another volumetric scattering matrix for volume scattering caused by oriented dihedrals from Sato's paper [**21**]:

$$(149) \qquad \boldsymbol{T}_{\mathrm{v}} = \frac{1}{15}\begin{bmatrix} 0 & 0 & 0 \\ 0 & 7 & 0 \\ 0 & 0 & 8 \end{bmatrix}.$$

This matrix accounts for the HV component for dihedral structures.

The decision of whether to use a volumetric scattering matrix with oriented dipoles or one with oriented dihedrals is made with the expression

$$C_1 = 2\mathbf{Re}\left\{f_{\mathrm{s}}\beta + f_{\mathrm{d}}\alpha^*\right\}$$

$$(150) \qquad\qquad = T_{11}(\theta) - T_{22}(\theta) + \frac{1}{2}f_{\mathrm{c}}.$$

According to the sign of C_1 the volume scattering from the HV component is assigned to surface scattering (vegetation) or double bounce scattering (oriented dihedral structure).

(151) $\qquad C_1 < 0:\qquad\qquad\qquad$ volume scattering by vegetation.

(152) $\qquad C_1 \geq 0:\qquad\qquad\qquad$ volume scattering by dihedral.

The powers are assigned similarly to the Yamaguchi decomposition. A comprehensive flowchart can be found in Singh's paper [20]. After the coherency matrix is rotated around the radar line of sight, the helical power is set $P_c = 2|\mathbf{Im}\{T_{23}\}|$. Next, the volumetric power is set depending on the volumetric scattering matrix (from (57)-(59), (149)) that is selected using (54), (150)-(152). A system of equations is constructed for each of the four volumetric matrices that are used in this decomposition. Each of the systems contain three equations with four unknowns and has the form

$$f_s + f_d|\alpha|^2 = S$$

(153) $$f_s|\beta|^2 + f_d = D$$

$$f_s\beta^* + f_d\alpha = C.$$

where S, D, and C depend on the volumetric scattering matrix that is used. For the volumetric scattering matrix using a cosine distribution, (57),

$$S = T_{11}(\theta) - \frac{1}{2}P_v$$

(154) $$D = TP - P_v - P_c - S$$

$$C = T_{12}(\theta) + T_{13}(\theta) + \frac{1}{6}P_c,$$

$$\text{with}$$

(155) $$P_v = \frac{15}{8}(2T_{33}(\theta) - P_c).$$

33

For the volumetric scattering matrix using a uniform distribution (58),

$$S = T_{11}(\theta) - \frac{1}{2}P_{\mathrm{v}}$$

(156)
$$D = TP - P_{\mathrm{v}} - P_{\mathrm{c}} - S$$

$$C = T_{12}(\theta) + T_{13}(\theta),$$

with

(157)
$$P_{\mathrm{v}} = 2\left(2T_{33}(\theta) - P_{\mathrm{c}}\right).$$

For the volumetric scattering matrix using a sine distribution (59),

$$S = T_{11}(\theta) - \frac{1}{2}P_{\mathrm{v}}$$

(158)
$$D = TP - P_{\mathrm{v}} - P_{\mathrm{c}} - S$$

$$C = T_{12}(\theta) + T_{13}(\theta) - \frac{1}{6}P_{\mathrm{c}},$$

with

(159)
$$P_{\mathrm{v}} = \frac{15}{8}\left(2T_{33}(\theta) - P_{\mathrm{c}}\right).$$

For the volumetric scattering matrix caused by oriented dihedral scattering (149),

$$S = T_{11}(\theta)$$

(160)
$$D = TP - P_{\mathrm{v}} - P_{\mathrm{c}} - S$$

$$C = T_{12}(\theta) + T_{13}(\theta),$$

with

(161)
$$P_{\mathrm{v}} = \frac{15}{16}\left(2T_{33}(\theta) - P_{\mathrm{c}}\right).$$

Similar to the Freeman-Durden and Yamaguchi decompositions, to solve the system of equations, a decision is made on whether the coherency matrix is dominated by surface or dihedral scattering. The decision made by looking at the quantity C_0 defined by

$$(162) \qquad C_0 = 2T_{11} + P_{\mathrm{c}} - TP.$$

If $C_0 > 0$, then the coherency matrix is dominated by surface scattering and α is set to zero. Therefore, the quantities f_{s}, β, and f_{d} can be obtained as follows:

$$(163) \qquad \begin{aligned} f_{\mathrm{s}} &= S \\ \beta^* &= \frac{C}{S} \\ f_{\mathrm{d}} &= D - \frac{|C|^2}{S}. \end{aligned}$$

If $C_0 \leq 0$, then the coherency matrix is dominated by surface scattering and β is set to zero. Therefore, the quantities f_{s}, α, and f_{d} can be solved:

$$(164) \qquad \begin{aligned} f_{\mathrm{s}} &= S - \frac{|C|^2}{D} \\ \alpha &= \frac{C}{D} \\ f_{\mathrm{d}} &= D. \end{aligned}$$

The remaining surface and dihedral powers, P_{s} and P_{d}, are calculated in the same way as Freeman-Durden and Yamaguchi, $P_{\mathrm{s}} = f_{\mathrm{s}} \left(1 + |\beta|^2 \right)$ and $P_{\mathrm{d}} = f_{\mathrm{d}} \left(1 + |\alpha|^2 \right)$.

2.6. FREEMAN II

Freeman extends the Freeman-Durden decomposition to a 2-component decomposition [22] that divides the measured coherency matrix, that is assumed to be reflection-symmetric, into a canopy

scattering component and a ground scattering component:

$$(165) \qquad \langle \boldsymbol{T} \rangle = f_{\mathrm{g}} \boldsymbol{T}_{\mathrm{g}} + f_{\mathrm{can}} \boldsymbol{T}_{\mathrm{can}}.$$

The canopy scattering model assumes randomly oriented scatterers with azimuthal symmetry (a scatterer that exhibits azimuthal symmetry is one that exhibits both reflection symmetry and rotational symmetry):

$$(166) \qquad T_{\mathrm{can}} = \begin{bmatrix} 1 + \rho & 0 & 0 \\ 0 & 1 - \rho & 0 \\ 0 & 0 & 1 - \rho \end{bmatrix},$$

with $\rho \in \mathbf{Re}$ and $0 \leq \rho \leq 1$. The second scattering mechanism combines the surface and dihedral scattering mechanisms from the original Freeman-Durden decomposition [11] into one scattering model to describe the ground:

$$(167) \qquad T_{\mathrm{g}} = \begin{bmatrix} |\alpha_{\mathrm{g}}|^2 & \alpha_{\mathrm{g}} & 0 \\ \alpha_{\mathrm{g}}^* & 1 & 0 \\ 0 & 0 & 0 \end{bmatrix},$$

where $|\alpha_{\mathrm{g}}|$ is allowed to take on any positive value. In the case where $|\alpha| \leq 1$, this ground matrix represents the dihedral matrix from before in (22). In the case where $|\alpha_{\mathrm{g}}| \geq 1$, this ground matrix represents a direct surface scatterer, and takes the form of the surface scattering matrix in (17). In this second case, α_{g} is assumed to be real.

Along with the assumption of reflection symmetry, this parameterization gives the following equation:

$$(168) \qquad \langle \boldsymbol{T} \rangle = \begin{bmatrix} T_{11} & T_{12} & 0 \\ T_{21} & T_{22} & 0 \\ 0 & 0 & T_{33} \end{bmatrix} = f_{\mathrm{g}} \begin{bmatrix} |\alpha_{\mathrm{g}}|^2 & \alpha_{\mathrm{g}} & 0 \\ \alpha_{\mathrm{g}}^* & 1 & 0 \\ 0 & 0 & 0 \end{bmatrix} + f_{\mathrm{can}} \begin{bmatrix} 1+\rho & 0 & 0 \\ 0 & 1-\rho & 0 \\ 0 & 0 & 1-\rho \end{bmatrix}.$$

Equation (168) yields the following system of four equations with four unknowns:

$$(169) \qquad T_{11} = f_{\mathrm{g}} |\alpha_{\mathrm{g}}|^2 + f_{\mathrm{can}} (1 + \rho)$$

$$(170) \qquad T_{22} = f_{\mathrm{g}} + f_{\mathrm{can}} (1 - \rho)$$

$$(171) \qquad T_{33} = f_{\mathrm{can}} (1 - \rho)$$

$$(172) \qquad T_{12} = f_{\mathrm{g}} \alpha_{\mathrm{g}}.$$

To solve this system of equations, note that combining (170) and (171) yields:

$$(173) \qquad T_{22} - T_{33} = f_{\mathrm{g}}.$$

Then α_{g} can be solved for using (172):

$$(174) \qquad \alpha_{\mathrm{g}} = \frac{T_{12}}{f_{\mathrm{g}}} = \frac{T_{12}}{T_{22} - T_{33}}.$$

f_{can} can now be solved by using (169) and (171):

$$T_{11} + T_{33} = f_{\mathrm{g}} |\alpha_{\mathrm{g}}|^2 + f_{\mathrm{can}} (1 + \rho) + f_{\mathrm{can}} (1 - \rho) = f_{\mathrm{g}} |\alpha_{\mathrm{g}}|^2 + 2 f_{\mathrm{can}}$$

$$(175) \qquad \rightarrow f_{\mathrm{can}} = \frac{T_{11} + T_{33} - f_{\mathrm{g}} |\alpha_{\mathrm{g}}|^2}{2}.$$

Lastly, ρ can be solved for using (171):

$$(176) \qquad \rho = \frac{f_{\text{can}} - T_{33}}{f_{\text{can}}}.$$

Now the powers of the scatter-types can be solved:

$$(177) \qquad P_{\text{g}} = f_{\text{g}} \left(1 + |\alpha_{\text{g}}|^2\right)$$

$$(178) \qquad P_{\text{can}} = f_{\text{can}} \left(3 - \rho\right).$$

If the solution to the parameters are not within the constraints $f_{\text{g}} \geq 0, f_{\text{can}} \geq 0, 0 \leq \rho \leq 1$, then they are not acceptable. To get around this issue, Freeman averaged over more and more pixels, by increasing the size of the box-filter, until the negative values were eliminated. It is important to note that this particular decomposition is specifically designed to measure the polSAR return from natural terrain containing mostly forested regions. Therefore, it is not ideal to be used to describe other terrain.

2.7. EXTENDED BRAGG SURFACE MODEL

The surface model used in the Freeman-Durden decomposition, subsequently other model-based decompositions, is based on the small perturbation model (SPM), which makes some assumptions that one must consider.

Some of the limitations of the SPM are as follows:

- Small roughness validity range $\frac{2\pi s}{\lambda} \ll 0.3$

- Inability to describe depolarization effects,

where s is the surface rms height and λ is the wavelength. This means with $\frac{0.3}{2\pi} \approx 0.048$ that $s \ll 0.048\lambda$. So for X-band systems, where $\lambda \approx 3\text{cm}$, that the surface rms height must be small, $s \ll 0.15\text{cm}$. Many natural surface do not fit this limitation.

The robustness of SPM inside its validity range and its relevant physical background lead to several investigations to use it as a valuable starting point for an extended model. Hanjsek, et. al., extend the Bragg surface model to address these limitations by modeling the surface as a reflection-symmetric depolarizer by rotating the Bragg coherency matrix $[T]$ about an angle θ in the plane perpendicular to the scattering plane [23]

$$
(179) \qquad [T(\theta)] = \begin{bmatrix} 1 & 0 & 0 \\ 0 & \cos 2\theta & \sin 2\theta \\ 0 & -\sin 2\theta & \cos 2\theta \end{bmatrix} [T] \begin{bmatrix} 1 & 0 & 0 \\ 0 & \cos 2\theta & -\sin 2\theta \\ 0 & \sin 2\theta & \cos 2\theta \end{bmatrix},
$$

and performing a configurational average over a given distribution $P(\theta)$ of θ:

$$
(180) \qquad [T] = \int_0^{2\pi} [T(\theta)] P(\theta) \mathrm{d}\theta.
$$

Assuming $P(\theta)$ to be a uniform distribution about zero with width θ_1

$$
(181) \qquad P(\theta) = \begin{cases} \frac{1}{2\theta_1} & |\theta| \leq \theta_1 \\ 0 & \text{otherwise} \end{cases} \qquad \text{with} \quad 0 \leq \theta_1 \leq \frac{\pi}{2},
$$

and the coherency matrix becomes

$$
(182) \qquad T_{\mathrm{X-Bragg}} = \begin{bmatrix} C_1 & C_2\mathrm{sinc}(2\theta_1) & 0 \\ C_2\mathrm{sinc}(2\theta_1) & C_3(1 + \mathrm{sinc}(4\theta_1)) & 0 \\ 0 & 0 & C_3(1 - \mathrm{sinc}(4\theta_1)) \end{bmatrix},
$$

with

$$
C_1 = |R_s + R_p|^2 \quad C_2 = (R_s + R_p)(R_s^* - R_p^*)
$$

$$
(183) \qquad C_3 = \frac{1}{2}|R_s - R_p|^2.
$$

Recall

$$(184) \qquad \beta = \frac{(R_s + R_p)^* \, (R_s - R_p)}{|R_s + R_p|^2}.$$

Then

$$(185) \qquad T_{\text{X–Bragg}} = \begin{bmatrix} 1 & \beta^* \text{sinc}(2\theta_1) & 0 \\ \beta \text{sinc}(2\theta_1) & \frac{|\beta|^2}{2}(1 + \text{sinc}(4\theta_1)) & 0 \\ 0 & 0 & \frac{|\beta|^2}{2}(1 - \text{sinc}(4\theta_1)) \end{bmatrix},$$

with $|\beta| \leq 1$.

Equation (185) descibes the coherency matrix of a surface model that loosens the constraints of the SPM (17) in order to model a slightly rougher surface.

2.8. ADAPTIVE TWO-COMPONENT DECOMPOSITION

This decomposition extends FreemanII to have an X-Bragg surface model and an improved volume scattering model. Therefore, it will take on a similar form to (165). If the PDF in (181) is assumed to have a zero-mean Gaussian distribution [**24**], [**25**] with standard deviation, σ^2, instead of a uniform distribution, the ground scattering model becomes

$$(186) \qquad T_{\text{g}} = f_{\text{g}} \begin{bmatrix} 1 & \beta^* \text{e}^{-2\sigma^2} & 0 \\ \beta \text{e}^{-2\sigma^2} & \frac{|\beta|^2}{2}\left(1 + \text{e}^{-8\sigma^2}\right) & 0 \\ 0 & 0 & \frac{|\beta|^2}{2}\left(1 - \text{e}^{-8\sigma^2}\right) \end{bmatrix},$$

again with $|\beta| \leq 1$.

The improved volume scattering model builds on the volume matrices based on the first order sine function in Yamaguchi's decomposition [**14**]. The nth sine and cosine PDFs are used here with the corresponding coherency matrices:

$$(187) \qquad T_{\text{v}}^{\sin} = \frac{1}{A} \begin{bmatrix} T_{\text{v}11} & T_{\text{v}12} & 0 \\ T_{\text{v}12} & T_{\text{v}22} & 0 \\ 0 & 0 & T_{\text{v}33} \end{bmatrix} \qquad T_{\text{v}}^{\cos} = \frac{1}{A} \begin{bmatrix} T_{\text{v}11} & -T_{\text{v}12} & 0 \\ -T_{\text{v}12} & T_{\text{v}22} & 0 \\ 0 & 0 & T_{\text{v}33} \end{bmatrix},$$

with

$$(188) \qquad T_{\text{v}11} = \frac{\sqrt{\pi}\Gamma\left(\frac{n+1}{2}\right)}{2\Gamma\left(\frac{n}{2}+1\right)}$$

$$(189) \qquad T_{\text{v}12} = -\frac{n\sqrt{\pi}\Gamma\left(\frac{n+1}{2}\right)}{4\Gamma\left(\frac{n}{2}+2\right)}$$

$$(190) \qquad T_{\text{v}22} = \frac{\left(n^2 + 2n + 4\right)\sqrt{\pi}\Gamma\left(\frac{n+1}{2}\right)}{8\Gamma\left(\frac{n}{2}+3\right)}$$

$$(191) \qquad T_{\text{v}33} = \frac{\sqrt{\pi}\Gamma\left(\frac{n+3}{2}\right)}{\Gamma\left(\frac{n}{2}+3\right)}$$

$$(192) \qquad A = \int_0^\pi \sin^n\theta\,d\theta = \int_{-\frac{\pi}{2}}^{\frac{\pi}{2}} \cos^n\theta\,d\theta = \frac{\sqrt{\pi}\Gamma\left(\frac{n+1}{2}\right)}{\Gamma\left(\frac{n}{2}+1\right)}$$

$$(193) \qquad \Gamma\left(a\right) = \int_0^\infty e^{-t}t^{a-1}\,dt.$$

The parameter n is solved for first by way of the NNED [15]. The matrix $\langle T \rangle - T_{\text{v}}$,

$$(194) \qquad \begin{bmatrix} T_{11} - f_{\text{v}}T_{\text{v}11} & T_{12} - f_{\text{v}}T_{\text{v}12} & 0 \\ T_{12} - f_{\text{v}}T_{\text{v}12} & T_{22} - f_{\text{v}}T_{\text{v}22} & 0 \\ 0 & 0 & T_{33} - f_{\text{v}}T_{\text{v}33} \end{bmatrix}$$

is minimized while holding to the constraint that its eigenvalues are nonnegative. Once this solved,

it gives the system of equations

$$(195) \qquad T_{11} - f_{\text{v}}T_{\text{v}11} = f_{\text{g}}$$

$$(196) \qquad T_{12} - f_{\text{v}}T_{\text{v}12} = f_{\text{g}}\beta^* e^{-2\sigma^2}$$

$$(197) \qquad T_{22} - f_{\mathrm{v}}T_{\mathrm{v}22} = \frac{f_{\mathrm{g}}}{2}|\beta|^2\left(1 + \mathrm{e}^{-8\sigma^2}\right)$$

$$(198) \qquad T_{33} - f_{\mathrm{v}}T_{\mathrm{v}33} = \frac{f_{\mathrm{g}}}{2}|\beta|^2\left(1 - \mathrm{e}^{-8\sigma^2}\right).$$

The parameter, f_{g}, is defined by (195). Adding (197) and (198) allows $|\beta|^2$ to be solved. Subtracting (198) from (197) then allows σ to be solved. Once sigma is solved, use (196) to solve for β^*.

This decomposition is an example of inserting improved scatter-types into an existing decomposition. Though the models theoretically handle cases that are more general than the previously used ones, we still need a way to verify that the newer scatter-types really do a better job of modeling the backscatter.

2.9. CHEN DECOMPOSITION

Model-based decompositions [14], [19], and [20] continue to improve on the Freeman-Durden decomposition [11] by continuing to address issues of negative power, reflection symmetry assumption, orientation angle compensation, etc. Even with these improvements, additional issues still remain to be addressed such as

- scattering model priority,
- overestimation of parameters α and β,
- model adaptability,
- having a way to assess how well the canonical scattering models describe the measured data.

Model-based decompositions such as [14], [19], and [20] all solve for P_{c} first, then solve for P_{v}, then solve for the rest of the powers. This order of solving for powers leads to overestimations of P_{c} and P_{v} and therefore underestimations of P_{s} and P_{d}. The parameters α and β should both have a magnitude less than 1 for every pixel. With the α and β values from the model-based decompositions mentioned in the previous chapters, these magnitude values are routinely greater

than 1, sometimes greater than 10^5. A surface scattering coherency matrix with $|\beta| > 1$ acts like a dihedral matrix with $\tilde{\alpha} = \frac{1}{\beta^*}$.

Model adaptability refers to how easily different scattering models can be added into the decomposition. There is not an easy way to swap out a scattering model for another with the aforementioned model-based decompositions. The previous model-based decompositions force the total response to equal the contributions from the scattering models, but does not assess whether or not the contributions accurately represent the measured data. These issues are addressed in a general model-based decomposition proposed by Chen, et al. [26]

Model-based decompositions assume that each pixel in a polarimetric SAR image is composed of contributions of specific scattering models. How do we know that we are using models that accurately represent what is measured? Chen, et al., propose a general model-based decomposition [26] that decomposes the coherency matrix into the same four scatter-types as the Yamaguchi and G4U decompositions [14, 20], and includes a residual coherency matrix that captures all the contribution that is not modeled with the chosen canonical scatter-types [17, 15]:

$$(199) \qquad \boldsymbol{T} = \boldsymbol{T}_\mathrm{s}(\theta_\mathrm{odd}) + \boldsymbol{T}_\mathrm{d}(\theta_\mathrm{dbl}) + \langle \boldsymbol{T}_\mathrm{v} \rangle + \boldsymbol{T}_\mathrm{c} + \boldsymbol{T}_\mathrm{res},$$

where $T_\mathrm{s}(\theta_\mathrm{odd})$ represents the rotation of the odd-bounce coherency matrix by angle θ_odd. Similarly, the double-bounce coherency matrix is rotated by θ_dbl. The T_res is the residual coherency matrix. Note that there are two different θ rotations for odd-bounce and double-bounce. This accounts for the case where the surface scattering and the dihedral scattering take place at different orientations.

The goal of this decomposition is to solve for the unknown parameters by minimizing the residual matrix. Using the scattering models from the *G4U* decomposition, with different rotations about the line of sight for the odd-bounce and double-bounce scattering matrices, (199) becomes

$$(200) \quad \begin{bmatrix} T_{11} & T_{12} & T_{13} \\ T_{21} & T_{22} & T_{23} \\ T_{31} & T_{23} & T_{33} \end{bmatrix} = f_{\mathrm{s}} \begin{bmatrix} 1 & \beta^* \cos 2\theta_{\mathrm{odd}} & -\beta^* \sin 2\theta_{\mathrm{odd}} \\ \beta \cos 2\theta_{\mathrm{odd}} & |\beta|^2 \cos^2 2\theta_{\mathrm{odd}} & -\frac{1}{2}|\beta|^2 \sin 4\theta_{\mathrm{odd}} \\ -\beta \sin 2\theta_{\mathrm{odd}} & -\frac{1}{2}|\beta|^2 \sin 4\theta_{\mathrm{odd}} & |\beta|^2 \sin^2 2\theta_{\mathrm{odd}} \end{bmatrix} + \cdots$$

$$f_{\mathrm{d}} \begin{bmatrix} |\alpha|^2 & \alpha \cos 2\theta_{\mathrm{dbl}} & -\alpha \sin 2\theta_{\mathrm{dbl}} \\ \alpha^* \cos 2\theta_{\mathrm{dbl}} & \cos^2 2\theta_{\mathrm{dbl}} & -\frac{1}{2} \sin 4\theta_{\mathrm{dbl}} \\ -\alpha^* \sin 2\theta_{\mathrm{dbl}} & -\frac{1}{2} \sin 4\theta_{\mathrm{dbl}} & \sin^2 2\theta_{\mathrm{dbl}} \end{bmatrix} + \cdots$$

$$f_{\mathrm{v}} \begin{bmatrix} a & d & e \\ d^* & b & f \\ e^* & f^* & c \end{bmatrix} + f_{\mathrm{c}} \begin{bmatrix} 0 & 0 & 0 \\ 0 & 1 & \pm j \\ 0 & \mp j & 1 \end{bmatrix} + \begin{bmatrix} T_{\mathrm{res}11} & T_{\mathrm{res}12} & T_{\mathrm{res}13} \\ T_{\mathrm{res}21} & T_{\mathrm{res}22} & T_{\mathrm{res}23} \\ T_{\mathrm{res}31} & T_{\mathrm{res}23} & T_{\mathrm{res}33} \end{bmatrix}.$$

The values of a through f for the volumetric coherency matrix are set depending on the volumetric model that is used for a particular iteration, from (57)-(59), (149), or other volumetric models. Here, Chen, et al., introduces another volumetric scattering model which produces the highest entropy:

$$(201) \quad \boldsymbol{T}_{\mathrm{v}} = \frac{1}{3} \begin{bmatrix} 1 & 0 & 0 \\ 0 & 1 & 0 \\ 0 & 0 & 1 \end{bmatrix}.$$

Chen, et al., also make the assumption that $\beta \approx \mathbf{Re}\{\beta\}$ and set $\mathbf{Im}\{\beta\} = 0$. Equation (200) yields nine equations with nine unknown parameters. Solving for the residual terms gives

$$(202) \quad T_{\mathrm{res}11} = T_{11} - f_{\mathrm{s}} - f_{\mathrm{d}}|\alpha|^2 - af_{\mathrm{v}}$$

$$(203) \quad T_{\mathrm{res}22} = T_{22} - f_{\mathrm{s}}|\beta|^2 \cos^2 2\theta_{\mathrm{odd}} - f_{\mathrm{d}} \cos^2 2\theta_{\mathrm{dbl}} - bf_{\mathrm{v}} - \frac{f_{\mathrm{c}}}{2}$$

$$(204) \quad T_{\mathrm{res}33} = T_{33} - f_{\mathrm{s}}|\beta|^2 \sin^2 2\theta_{\mathrm{odd}} - f_{\mathrm{d}} \sin^2 2\theta_{\mathrm{dbl}} - cf_{\mathrm{v}} - \frac{f_{\mathrm{c}}}{2}$$

(205) $\quad \mathbf{Re}\left\{T_{\mathrm{res}12}\right\} = \mathbf{Re}\left\{T_{12}\right\} - f_{\mathrm{s}}\beta\cos 2\theta_{\mathrm{odd}} - f_{\mathrm{d}}\mathbf{Re}\left\{\alpha\right\}\cos 2\theta_{\mathrm{dbl}} - f_{\mathrm{v}}\mathbf{Re}\left\{d\right\}$

(206) $\quad \mathbf{Re}\left\{T_{\mathrm{res}13}\right\} = \mathbf{Re}\left\{T_{13}\right\} + f_{\mathrm{s}}\beta\sin 2\theta_{\mathrm{odd}} + f_{\mathrm{d}}\mathbf{Re}\left\{\alpha\right\}\sin 2\theta_{\mathrm{dbl}} - f_{\mathrm{v}}\mathbf{Re}\left\{e\right\}$

(207) $\quad \mathbf{Re}\left\{T_{\mathrm{res}23}\right\} = \mathbf{Re}\left\{T_{23}\right\} + \dfrac{f_{\mathrm{s}}}{2}|\beta|^2\sin 4\theta_{\mathrm{odd}} + \dfrac{f_{\mathrm{d}}}{2}\sin 4\theta_{\mathrm{dbl}} - f_{\mathrm{v}}\mathbf{Re}\left\{f\right\}$

(208) $\quad \mathbf{Im}\left\{T_{\mathrm{res}12}\right\} = \mathbf{Im}\left\{T_{12}\right\} - f_{\mathrm{d}}\mathbf{Im}\left\{\alpha\right\}\cos 2\theta_{\mathrm{dbl}} - f_{\mathrm{v}}\mathbf{Im}\left\{d\right\}$

(209) $\quad \mathbf{Im}\left\{T_{\mathrm{res}13}\right\} = \mathbf{Im}\left\{T_{13}\right\} + f_{\mathrm{d}}\mathbf{Im}\left\{\alpha\right\}\sin 2\theta_{\mathrm{dbl}} - f_{\mathrm{v}}\mathbf{Im}\left\{e\right\}$

(210) $\quad \mathbf{Im}\left\{T_{\mathrm{res}23}\right\} = \mathbf{Im}\left\{T_{23}\right\} - f_{\mathrm{v}}\mathbf{Im}\left\{f\right\} \mp \dfrac{f_{\mathrm{c}}}{2}.$

The parameters, $\{f_{\mathrm{s}}, f_{\mathrm{d}}, f_{\mathrm{v}}, f_{\mathrm{c}}, \theta_{\mathrm{odd}}, \theta_{\mathrm{dbl}}, \alpha, \beta\}$, have the following constraints [26]:

$$0 \le f_{\mathrm{v}}, f_{\mathrm{d}}, f_{\mathrm{s}} \le \mathrm{tr}\left\{\boldsymbol{T}\right\} \quad 0 \le f_{\mathrm{c}} \le 2|\mathbf{Im}\left(T_{23}\right)|$$

(211) $$-\frac{\pi}{4} \le \theta_{\mathrm{dbl}}, \theta_{\mathrm{odd}} \le \frac{\pi}{4} \quad |\beta|, |\alpha| < 1,$$

where $\mathrm{tr}\left\{\boldsymbol{T}\right\}$ is the trace of the coherency matrix and $\mathrm{tr}\left\{\boldsymbol{T}\right\} = T_{11} + T_{22} + T_{33}$.

Let $\underline{\boldsymbol{T}}_{\mathrm{r}}$ represent a vector that contains the real and imaginary elements that define $\boldsymbol{T}_{\mathrm{res}}$. For model inversion, the optimization criterion is to minimize the square of the L^2 norm of $\underline{\boldsymbol{T}}_{\mathrm{r}}$:

(212)
$$\underline{\boldsymbol{T}}_{\mathrm{r}} = \begin{bmatrix} T_{\mathrm{res}11} \\ T_{\mathrm{res}22} \\ T_{\mathrm{res}33} \\ \mathbf{Re}\left\{T_{\mathrm{res}12}\right\} \\ \mathbf{Re}\left\{T_{\mathrm{res}13}\right\} \\ \mathbf{Re}\left\{T_{\mathrm{res}23}\right\} \\ \mathbf{Im}\left\{T_{\mathrm{res}12}\right\} \\ \mathbf{Im}\left\{T_{\mathrm{res}13}\right\} \\ \mathbf{Im}\left\{T_{\mathrm{res}23}\right\} \end{bmatrix} \qquad ||\underline{\boldsymbol{T}}_{\mathrm{r}}||_2^2 = \sum_{i=1}^{9} |\underline{\boldsymbol{T}}_{\mathrm{r}(i)}|^2.$$

Therefore, with $\beta \approx \mathbf{Re}\{\beta\}$, the objective function that is to be minimized is $F = \sum\limits_{i=1}^{9} |T_{\mathrm{r}(i)}|^2$:

$$F = \left(T_{11} - f_{\mathrm{s}} - f_{\mathrm{d}}|\alpha|^2 - af_{\mathrm{v}}\right)^2$$

$$+ \left(T_{22} - f_{\mathrm{s}}\beta^2 \cos^2 2\theta_{\mathrm{odd}} - f_{\mathrm{d}} \cos^2 2\theta_{\mathrm{dbl}} - bf_{\mathrm{v}} - \frac{f_{\mathrm{c}}}{2}\right)^2$$

$$+ \left(T_{33} - f_{\mathrm{s}}\beta^2 \sin^2 2\theta_{\mathrm{odd}} - f_{\mathrm{d}} \sin^2 2\theta_{\mathrm{dbl}} - cf_{\mathrm{v}} - \frac{f_{\mathrm{c}}}{2}\right)^2$$

$$+ \left(\mathbf{Re}\{T_{12}\} - f_{\mathrm{s}}\beta \cos 2\theta_{\mathrm{odd}} - f_{\mathrm{d}}\mathbf{Re}\{\alpha\} \cos 2\theta_{\mathrm{dbl}} - f_{\mathrm{v}}\mathbf{Re}\{d\}\right)^2$$

$$+ \left(\mathbf{Re}\{T_{13}\} + f_{\mathrm{s}}\beta \sin 2\theta_{\mathrm{odd}} + f_{\mathrm{d}}\mathbf{Re}\{\alpha\} \sin 2\theta_{\mathrm{dbl}} - f_{\mathrm{v}}\mathbf{Re}\{e\}\right)^2$$

$$+ \left(\mathbf{Re}\{T_{23}\} + \frac{f_{\mathrm{s}}}{2}\beta^2 \sin 4\theta_{\mathrm{odd}} + \frac{f_{\mathrm{d}}}{2} \sin 4\theta_{\mathrm{dbl}} - f_{\mathrm{v}}\mathbf{Re}\{f\}\right)^2$$

$$+ \left(\mathbf{Im}\{T_{12}\} - f_{\mathrm{d}}\mathbf{Im}\{\alpha\} \cos 2\theta_{\mathrm{dbl}} - f_{\mathrm{v}}\mathbf{Im}\{d\}\right)^2$$

$$+ \left(\mathbf{Im}\{T_{13}\} + f_{\mathrm{d}}\mathbf{Im}\{\alpha\} \sin 2\theta_{\mathrm{dbl}} - f_{\mathrm{v}}\mathbf{Im}\{e\}\right)^2$$

(213)
$$+ \left(\mathbf{Im}\{T_{23}\} - f_{\mathrm{v}}\mathbf{Im}\{f\} - \frac{f_{\mathrm{c}}}{2}\right)^2.$$

The solution provided by the "conventional model-based decomposition" [**26**] is used as an initial value for this nonlinear least squares optimization. This minimization is repeated for each volumetric coherency matrix, $\langle \boldsymbol{T}_{\mathrm{v}} \rangle$, that is to be considered. Chen sites five such volumetric coherency matrices in [**26**] and are found in (57)-(59),(149), and (201), but mentions that others could be used as well. The set of parameters with the smallest residual is selected, and the four powers are calculated as in (61).

IMPLEMENTATION OF EXISTING METHODS

In order to analyze these two methods of modeling the backscatter, I created working algorithms in MATLAB. The HH, HV, VH, VV channels of the polarimetric SAR image are loaded in to the script. I implemented and ran the G4U decomposition on the polarimetric data to set initial points. From this, the averaged coherency matrix values, $T_{11}, T_{22}, T_{33}, T_{12}, T_{13}, T_{23}$, the volume coherency matrix values a, b, c, d, e, f from the volume coherency matrices in Chen's paper, and the parameter values $f_s, f_d, f_v, f_c, \theta, \alpha, \beta$ are recorded for each pixel in image.

3.1. CONVEXITY OF THE OBJECTIVE FUNCTION

Many minimization techniques assume that the objective function is convex. This means that for every pair of points $(\underline{x}_1, \underline{x}_2)$ within the convex domain, D, set up by the upper and lower bounds, then [27]

$$(214) \qquad \forall t \in [0,1], \forall \underline{x}_1, \underline{x}_2 \in D \qquad F\left(t\underline{x}_1 + (1-t)\,\underline{x}_2\right) \le tF\left(\underline{x}_1\right) + (1-t)\,F\left(\underline{x}_2\right)$$

The benefits of optimizing a convex function are that there exist many efficient solvers that are publicly available, and that every local minimum is also a global minimum [27]. If a function is nonconvex, optimization techniques are generally slower and only find a local minimum.

To show that a function is nonconvex is to show that there exists a counterexample to (214), which is to show

$$\exists t \in [0,1] \ \ \underline{x}_1, \underline{x}_2 \in D, \ \ D \,\text{a convex domain}$$

$$(215) \qquad \text{such that} \ \ F\left(t\underline{x}_1 + (1-t)\,\underline{x}_2\right) > tF\left(\underline{x}_1\right) + (1-t)\,F\left(\underline{x}_2\right)$$

Define $\underline{\boldsymbol{x}}_1$ and $\underline{\boldsymbol{x}}_2$ as follows:

$$
(216) \qquad \underline{\boldsymbol{x}}_1 = \begin{bmatrix} f_{\mathrm{s}} \\ f_{\mathrm{d}} \\ f_{\mathrm{v}} \\ f_{\mathrm{c}} \\ \theta_{\mathrm{odd}} \\ \theta_{\mathrm{dbl}} \\ \mathbf{Re}\{\alpha\} \\ \mathbf{Im}\{\alpha\} \\ \mathbf{Re}\{\beta\} \\ \mathbf{Im}\{\beta\} \end{bmatrix} = \begin{bmatrix} 200.9667 \\ 0 \\ 0 \\ 0 \\ 0.5620 \\ 0 \\ 0 \\ 0 \\ -0.2550 \\ 0 \end{bmatrix} \qquad \underline{\boldsymbol{x}}_2 = \begin{bmatrix} f_{\mathrm{s}} \\ f_{\mathrm{d}} \\ f_{\mathrm{v}} \\ f_{\mathrm{c}} \\ \theta_{\mathrm{odd}} \\ \theta_{\mathrm{dbl}} \\ \mathbf{Re}\{\alpha\} \\ \mathbf{Im}\{\alpha\} \\ \mathbf{Re}\{\beta\} \\ \mathbf{Im}\{\beta\} \end{bmatrix} = \begin{bmatrix} 211.5955 \\ 0 \\ 0 \\ 0 \\ -0.7021 \\ 0 \\ 0 \\ 0 \\ -0.5247 \\ 0 \end{bmatrix}.
$$

These values for $\underline{\boldsymbol{x}}_1$ and $\underline{\boldsymbol{x}}_2$ represent two different points within the bounds from (211). Therefore, their residual can be formed with the same objective function with the measured coherency values

$$
(217) \qquad \langle \boldsymbol{T} \rangle = \begin{bmatrix} 690.86 & 734.16 + 97.64i & 120.17 + 83.50i \\ 734.16 - 97.64i & 814.94 & 141.11 + 80.19i \\ 120.17 - 83.50i & 141.11 - 80.19i & 35.11 \end{bmatrix}.
$$

Both sides of the inequality in (214) are plotted in Figure 3.1 for $t \in [0,1]$ with the vertical axis represented the value of each side of the inequality. Clearly, the blue line that represents the left side of the inequality (214) is greater that the red line that represents the right side of (214). Note: The blue line only had to be greater than the red for some $t \in [0,1]$ to be a valid counterexample. This one counterexample shows that the objective function is not convex across all $\underline{\boldsymbol{x}}_1, \underline{\boldsymbol{x}}_2 \in D, t \in [0,1]$, and therefore the function is nonconvex. An optimization method must
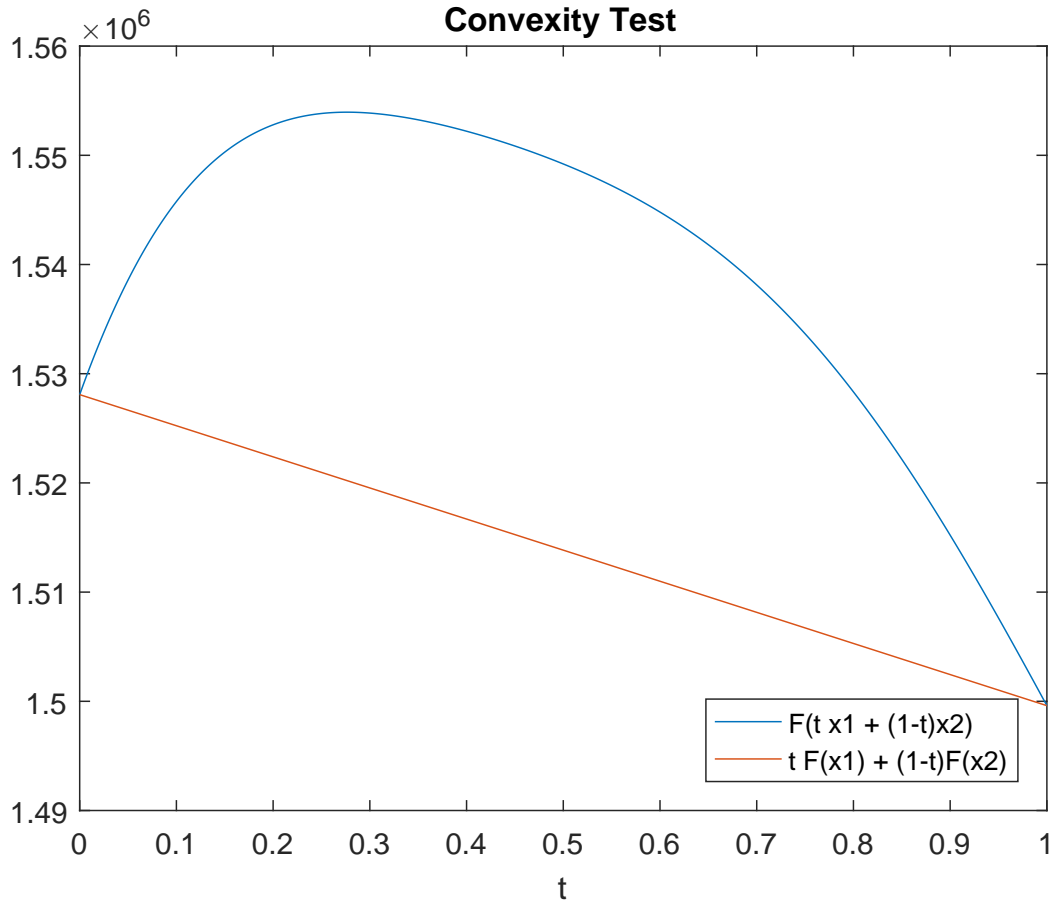
FIGURE 3.1. Plot showing that the objective function is nonconvex

be carefully considered to minimize the objective function, and it must be recognized that many

methods may only converge to a local minimum.

3.2. STEEPEST DESCENT

In an effort to try the most straightforward method to optimize the nonconvex objective function, I implemented the method of steepest descent with a variable step size and two conditions. The method of steepest descent begins by calculating the value of the objective function at an initial value $\underline{x}_0$, then take a step in the direction of the negative gradient, which gives a new value $\underline{x}_1$. Repeat this process to iteratively "walk downhill" until a local minimum is reached. The gradient

has already been computed analytically and can be found in Appendix B.

$$(218) \qquad \underline{x}_{n+1} = \underline{x}_n - \gamma_n \nabla F(\underline{x}_n)$$

There is a variable step size γ that can be adjusted with each iteration. It is important to note that at each step in the iteration, two conditions must be met. First, the $\underline{x}_{n+1}$ that results after taking a step must be within the domain D of possible values. If a step results in a point outside the domain, the step was too large. Adjust the step size and try again. Also, if the value of the objective function evaluated at the new step results in a greater residual than the previous value, the step was too large and overshot the local minimum. Adjust the step size and try again.

Step 1: Perform the $G4U$ decomposition across an image to serve as the initial values.

Step 2: Correct any results from the $G4U$ decomposition by forcing them within the bounds in (211).

Step 3: Evaluate the objective function and the gradient at these initial values

Step 4: Begin iteration sequence.

    Step 4a: Calculate $\underline{x}_{n+1}$ using (218)

    Step 4b: Correct any results that stepped outside of the bounds from (211).

    Step 4c: Evaluate the objective function at $\underline{x}_{n+1}$.

    Step 4d: If $F(\underline{x}_{n+1}) \geq F(\underline{x}_n)$ then the minimum has been overshot. Reduce the step size and try again.

    Step 4e: Set $\underline{x}_n = x_{n+1}$ and evaluate using the objective function and the gradient.

    Step 4f: Repeat the iterative sequence until a minimum is reached.

Step 5: From the solution, calculate the scatter-type powers with (61)

This method succeeds at finding a local minimum and lowering the average and total residual across the image. The time for the code to run on an image with 13.8 million pixels is less than ten minutes. Further coding efforts could very likely reduce the run time further.

The Chen framework is very useful, not only in decomposing the coherency matrix into meaningful canonical scatter-types, but also providing a means of comparing how well different scatter-types model the polSAR images by way of comparing the sum of squares of the residual terms. The limitation of the number of unknown parameters to nine forces one to select only a few scatter-types at a time.

3.3. CONCLUSION OF CURRENT MODEL-BASED DECOMPOSITIONS

Model-based decompositions of polarimetric SAR images attempt to model the image with physically meaningful canonical scatter-types. Since the Freeman-Durden decomposition [11] there have been many additions to correct the negative power issues [15, 16, 17, 20, 26, 28, 29, 30, 31, 32], as well as additional scatter-type models [14, 15, 16, 17, 20, 22, 23, 24, 25, 26, 28, 29, 30, 31, 32, 33, 34]. Typically, the new scatter-types are either specific to a particular scene or a generalization of previous models that were too specific.

Chen's decomposition framework allows for the comparison between decompositions by comparing their residual if the number of unknown parameters is limited to nine.

CHAPTER 4

GENERAL MODEL-BASED DECOMPOSITION

FRAMEWORK (GMBDF)

The framework of the Chen decomposition [26] allows for the flexibility of interchanging different canonical scatter-types. Decompositions with different sets of canonical scatter-types can be inserted into the Chen decomposition and their residuals calculated. The set of canonical scatter-types with the lowest residual is selected as the best model of the backscatter for that pixel. In this way, model-based decompositions can be compared with each other. The model-based decomposition with the lower residual is the better model for a given pixel. This framework also allows for new scatter-type models. This includes new parameterizations of currently used scatter-type and new models altogether.

4.1. LINEAR INDEPENDENCE OF CANONICAL SCATTER-TYPE MODELS

It should be noted that the coherency matrices of the canonical scatter-types must be linearly independent in order to get a solution to the minimization of the objective function. The flexibility of the framework will not support linearly dependent scatter-types. For the coherency matrices of the scatter-types, $\langle \boldsymbol{T} \rangle_i$, to be linearly independent is to say

$$(219) \qquad \sum_{i=1}^{n} c_i \langle \boldsymbol{T} \rangle_i = 0 \quad \implies \quad c_i = 0, \, \forall i \in \{1, ..., n\}.$$

If the coherency matrices of the canonical scatter-types are linearly *dependent*, then without loss of generality, there exists scalars c_i, not all zero, such that

$$(220) \qquad \langle \boldsymbol{T} \rangle_1 = \sum_{i=2}^{n} c_i \langle \boldsymbol{T} \rangle_i.$$

52

Assume that the canonical scatter-types are not linearly independent and (220) holds for scalars c_i which are not all zero. Let the minimum of the objective function be defined by the coefficients $\{f_1, ..., f_n\}$. Then the coefficients $\{0, c_2 f_2, ..., c_n f_n\}$ would also minimize the objective function. Therefore, you would have two different solution sets of parameters that achieve the minimum residual. One solution would have a nonzero power for the scatter-type $\langle \boldsymbol{T} \rangle_1$, and another solution where the power for the same scatter-type is zero. Therefore, the scatter-type models must be linearly independent in order for the solution set of parameters with a minimum residual to be unique.

4.2. ADDING MORE PARAMETERS TO THE CHEN DECOMPOSITION FRAMEWORK

Chen, et al., limit the number of unknown parameters to nine in an effort to avoid having an underdetermined system of nine equations [26]; see (202)-(210). This system of nine equations actually has 18 unknowns since the values of the residual matrix are also not known. In addition, the goal is not to solve a system of equations, but to minimize the objective function comprised of the square of the L^2 norm of the residual values. Minimizing a multivariable function does not inherently require a limit to the number of parameters. Therefore, in order to better fit the data, additional parameters are permitted.

With this in mind, one can choose which scatter-types to use in the framework. For instance, one could try the decomposition composed of a rotated X-Bragg surface model [23] which has parameters $\{\theta_{\mathrm{odd}}, \theta_1, \gamma\}$, the rotated dihedral [26] $\{\theta_{\mathrm{dbl}}, \alpha\}$, the volume model from Freeman II [22] with parameter $\{\rho\}$ and a helical model [14].

$$\langle \boldsymbol{T} \rangle = f_{\mathrm{s}} T_{\mathrm{X-Bragg}}\left(\theta_{\mathrm{odd}}\right) + f_{\mathrm{d}} T_{\mathrm{d}}\left(\theta_{\mathrm{dbl}}\right) + f_{\mathrm{can}} T_{\mathrm{can}} + f_{\mathrm{c}} T_{\mathrm{c}} \tag{221}$$

With real coefficients f_s, f_d, f_{can}, f_c, real parameters $\theta_{odd}, \theta_1, \theta_{dbl}, \rho$, and complex parameters γ, α, the total number of unknown parameters is 12. These scatter-types are linearly independent and can be used in the GMBDF.

Therefore, the GMBDF accommodates a whole family of new and existing decompositions with interchangeable scatter-types. These decompositions can be compared with each other with their residuals.

4.3. ADDITIONAL PARAMETER EXAMPLE: GMBDF WITH COMPLEX β

Model-based decompositions from Freeman-Durden's to Chen's have made the assumption that $\beta \approx \mathbf{Re}\{\beta\}$. The reasoning from Chen's paper [26], "For most natural surfaces, $\mathbf{Re}\{\varepsilon_r\} \gg \mathbf{Im}\{\varepsilon_r\}$. Therefore, ε_r, R_H, and R_V are approximated as real-valued." Chen cites Von Hippel's text [35], which contains charts of the relative permittivity of many natural substances, as justification for the statement. Most of the materials' relative permittivities from these charts have imaginary components that are relatively small compared to their real components. If $\varepsilon_r \approx \mathbf{Re}\{\varepsilon_r\}$, then $R_H \approx \mathbf{Re}\{R_H\}$ and $R_V \approx \mathbf{Re}\{R_V\}$. Then it follows that $\beta \approx \mathbf{Re}\{\beta\}$. With this reasoning, Chen continues with the Freeman-Durden approximation that β is considered to be real. This approximation reduces the number of unknown parameters from ten to nine.

Although the imaginary components of the relative permittivities in [35] are small, for some materials the ratio of the imaginary component to magnitude increases as the wavelength decreases. Also, Mead, et al., claim that $\mathbf{Im}\{VV\,HH^*\}$ is not negligible in describing natural surfaces [36].

(222)
$$\mathbf{Im}\{VV\,HH^*\} = -\mathbf{Im}\left\{\frac{f_s}{2}\beta\right\}$$

Therefore, according to Mead, et al., the imaginary component of $f_s\beta$ is not negligible.

What if the scope of the analysis is not constrained to natural surfaces where one can assume $\beta \approx \mathbf{Re}\{\beta\}$? The GMBDF allows the surface parameter, β, to be complex. This increases the number of unknowns from nine to ten, which, as stated above, is permitted. Both Chen's

decomposition and the GMBDF with complex β are run on polarimetric SAR image data and the residual term is analyzed. If the GMBDF with complex β has the lower residual, then it can be concluded that the surface model which includes the imaginary part of β models the measured backscatter better than the surface model which assumes that β is real. Allowing for a complex β parameter, the equations for the residual matrix elements are as follows:

(223)
$$T_{\mathrm{res}11} = T_{11} - f_{\mathrm{s}} - f_{\mathrm{d}}|\alpha|^2 - af_{\mathrm{v}}$$

(224)
$$T_{\mathrm{res}22} = T_{22} - f_{\mathrm{s}}|\beta|^2 \cos^2 2\theta_{\mathrm{odd}} - f_{\mathrm{d}} \cos^2 2\theta_{\mathrm{dbl}} - bf_{\mathrm{v}} - \frac{f_{\mathrm{c}}}{2}$$

(225)
$$T_{\mathrm{res}33} = T_{33} - f_{\mathrm{s}}|\beta|^2 \sin^2 2\theta_{\mathrm{odd}} - f_{\mathrm{d}} \sin^2 2\theta_{\mathrm{dbl}} - cf_{\mathrm{v}} - \frac{f_{\mathrm{c}}}{2}$$

(226)
$$\mathbf{Re}\left\{T_{\mathrm{res}12}\right\} = \mathbf{Re}\left\{T_{12}\right\} - f_{\mathrm{s}}\mathbf{Re}\left\{\beta\right\} \cos 2\theta_{\mathrm{odd}} - f_{\mathrm{d}}\mathbf{Re}\left\{\alpha\right\} \cos 2\theta_{\mathrm{dbl}} - f_{\mathrm{v}}\mathbf{Re}\left\{d\right\}$$

(227)
$$\mathbf{Re}\left\{T_{\mathrm{res}13}\right\} = \mathbf{Re}\left\{T_{13}\right\} + f_{\mathrm{s}}\mathbf{Re}\left\{\beta\right\} \sin 2\theta_{\mathrm{odd}} + f_{\mathrm{d}}\mathbf{Re}\left\{\alpha\right\} \sin 2\theta_{\mathrm{dbl}} - f_{\mathrm{v}}\mathbf{Re}\left\{e\right\}$$

(228)
$$\mathbf{Re}\left\{T_{\mathrm{res}23}\right\} = \mathbf{Re}\left\{T_{23}\right\} + \frac{f_{\mathrm{s}}}{2}|\beta|^2 \sin 4\theta_{\mathrm{odd}} + \frac{f_{\mathrm{d}}}{2} \sin 4\theta_{\mathrm{dbl}} - f_{\mathrm{v}}\mathbf{Re}\left\{f\right\}$$

(229)
$$\mathbf{Im}\left\{T_{\mathrm{res}12}\right\} = \mathbf{Im}\left\{T_{12}\right\} + f_{\mathrm{s}}\mathbf{Im}\left\{\beta\right\} \cos 2\theta_{\mathrm{odd}} - f_{\mathrm{d}}\mathbf{Im}\left\{\alpha\right\} \cos 2\theta_{\mathrm{dbl}} - f_{\mathrm{v}}\mathbf{Im}\left\{d\right\}$$

(230)
$$\mathbf{Im}\left\{T_{\mathrm{res}13}\right\} = \mathbf{Im}\left\{T_{13}\right\} - f_{\mathrm{s}}\mathbf{Im}\left\{\beta\right\} \sin 2\theta_{\mathrm{odd}} + f_{\mathrm{d}}\mathbf{Im}\left\{\alpha\right\} \sin 2\theta_{\mathrm{dbl}} - f_{\mathrm{v}}\mathbf{Im}\left\{e\right\}$$

(231)
$$\mathbf{Im}\left\{T_{\mathrm{res}23}\right\} = \mathbf{Im}\left\{T_{23}\right\} - f_{\mathrm{v}}\mathbf{Im}\left\{f\right\} \mp \frac{f_{\mathrm{c}}}{2}.$$

The objection function for the new decomposition becomes

$$F = \left(T_{11} - f_{\mathrm{s}} - f_{\mathrm{d}}|\alpha|^2 - af_{\mathrm{v}}\right)^2$$

$$+ \left(T_{22} - f_{\mathrm{s}}|\beta|^2 \cos^2 2\theta_{\mathrm{odd}} - f_{\mathrm{d}} \cos^2 2\theta_{\mathrm{dbl}} - bf_{\mathrm{v}} - \frac{f_{\mathrm{c}}}{2}\right)^2$$

$$+ \left(T_{33} - f_{\mathrm{s}}|\beta|^2 \sin^2 2\theta_{\mathrm{odd}} - f_{\mathrm{d}} \sin^2 2\theta_{\mathrm{dbl}} - cf_{\mathrm{v}} - \frac{f_{\mathrm{c}}}{2}\right)^2$$

$$+ \left(\mathbf{Re}\left\{T_{12}\right\} - f_{\mathrm{s}}\mathbf{Re}\left\{\beta\right\} \cos 2\theta_{\mathrm{odd}} - f_{\mathrm{d}}\mathbf{Re}\left\{\alpha\right\} \cos 2\theta_{\mathrm{dbl}} - f_{\mathrm{v}}\mathbf{Re}\left\{d\right\}\right)^2$$

$$+ \left(\mathbf{Re}\left\{T_{13}\right\} + f_{\mathrm{s}}\mathbf{Re}\left\{\beta\right\} \sin 2\theta_{\mathrm{odd}} + f_{\mathrm{d}}\mathbf{Re}\left\{\alpha\right\} \sin 2\theta_{\mathrm{dbl}} - f_{\mathrm{v}}\mathbf{Re}\left\{e\right\}\right)^2$$

$$+ \left(\mathbf{Re}\left\{ T_{23} \right\} + \frac{f_\mathrm{s}}{2}|\beta|^2 \sin 4\theta_\mathrm{odd} + \frac{f_\mathrm{d}}{2}\sin 4\theta_\mathrm{dbl} - f_\mathrm{v}\mathbf{Re}\left\{ f \right\} \right)^2$$

$$+ \left(\mathbf{Im}\left\{ T_{12} \right\} + f_\mathrm{s}\mathbf{Im}\left\{ \beta \right\} \cos 2\theta_\mathrm{odd} - f_\mathrm{d}\mathbf{Im}\left\{ \alpha \right\} \cos 2\theta_\mathrm{dbl} - f_\mathrm{v}\mathbf{Im}\left\{ d \right\} \right)^2$$

$$+ \left(\mathbf{Im}\left\{ T_{13} \right\} - f_\mathrm{s}\mathbf{Im}\left\{ \beta \right\} \sin 2\theta_\mathrm{odd} + f_\mathrm{d}\mathbf{Im}\left\{ \alpha \right\} \sin 2\theta_\mathrm{dbl} - f_\mathrm{v}\mathbf{Im}\left\{ e \right\} \right)^2$$

(232) $$+ \left(\mathbf{Im}\left\{ T_{23} \right\} - f_\mathrm{v}\mathbf{Im}\left\{ f \right\} \mp \frac{f_\mathrm{c}}{2} \right)^2.$$

Now we can compare the minimums of the objective functions and see which has the smaller residual.

4.4. COLOR SCHEME

Before the results of these decompositions are shown, there should be something said about the color scheme used to display these images. The purpose of the false-color displays is to accurately represent the reflectivity of the scene and characterize the scattering model(s) in the scene. Typically, each scattering mechanism power is assigned a color channel in the RGB (red, green, blue) color space. This is fine for 3 or fewer scattering models since the RGB color space has three channels, but for four or more, care needs to be taken to clearly define the color scheme. The color scheme used here will represent surface power, P_s, with red, the volumetric power, P_v, with green, the double-bounce or dihedral power, P_d with blue, and the helical power will be split across the red and blue channels evenly. Describing contributions of more than three scattering mechanisms will inevitably lead to ambiguity. For instance, a magenta colored pixel could represent equal parts P_s and P_d, it could represent P_c alone, or it could be a combination of the three. The minimum and maximum radar cross sections (minRCS and maxRCS) of the display are set and represent black and white pixels respectively. Scatter-type powers that are less than the minRCS are set to the minRCS and powers greater than the maxRCS are set to the maxRCS. This gives control over the dynamic range of the image to be displayed. For this dissertation, these values are $RCS_{min} = -57dB$ and $RCS_{max} = -9dB$, each pixel can then be described by their combination

of scatter-type powers. The RGB color space is then converted to the HSV (hue, saturation, value) color space. The V of the HSV color space represents the value or the brightness of the pixel. This channel is then set to equal the trace of the coherency matrix, which represents the total power of the response for that pixel. The HSV color space is then converted back to RGB and is ready to be displayed. Special thanks to Derek West and Robert Riley at Sandia National Laboratories for this approach and permission to use their code.

4.5. DECOMPOSITION RESULTS

A comparison of three decomposition results is in 4.1. With an optical image of the scene for reference, the results from the Freeman-Durden, Yamaguchi, G4U, Chen, and GMBDF with complex beta decompositions can be analyzed. The color of the three polarimetric decompositions represent the scattering mechanisms present: Red for surface scattering, blue for dihedral, green for volumetric, and magenta for helical. The brightness of the pixel is set by the trace of the coherency matrix for that pixel. The dynamic range of the brightness of the polarimetric decomposition displays is set to $[-57dB, -9dB]$. Thus a pixel with a trace of the coherency matrix less than $-57dB$ will appear black. Likewise, pixels with a trace of the coherency matrix larger than $-9dB$ will have full value (or brightness). These polarimetric results are on images that are 1500 pixels by 2000 pixels. Note that the optical image was taken at a different time and therefore is only a reference to permanent objects (the optical image does not contain the same number of cars, etc.). The polarimetric data that the images represent was collected and formed by Sandia National Laboratories FARAD fully polarimetric airborne SAR X-Band (9.6 GHz) system. These images have a 6-inch spatial resolution.

4.5.1. SOME GENERAL OBSERVATIONS REGARDING 4.1. The radar used to form these images was on a plane flying along the bottom of the image. The radar is a self-illuminating imaging system, which is why there are shadows in the direction away from the radar. Horizontal streaks represent moving objects; the one around row 1300 from column 900 to column 1200 is a car driving

along the road. The structure of the playgrounds under the two canopies in the middle of the image are visible, which is due to the signal penetrating the canopies and scattering off the structures. Similarly, the structures underneath the covered picnic tables along the curved path in the middle of the image are visible. In all the images, the volumetric scatter-type does a good job of modeling the vegetation in the image. The roads and parking lots have a low return, but noticeably a surface return. The dirt around the track in the upper right and the warning track around the baseball field in the upper left have an evident surface response. The main double-bounce scattering occurs on the playground structures, the roof of the building, and the three light poles along the center of the road (around pixels (row 1150, column 500), (row 1200, column 1100), and (row 1200, column 1750)). The main helical scatterer is the roof of the building. The return from the cement walk paths is extremely low and noticeably lower than the asphalt of the road and parking lots.

The Freeman-Durden decomposition is colored with the most green due to overestimating the volume scattering component. The white on the roof in the Freeman-Durden decomposition shows that all three scatter-type powers are greater than -9dB. As the decompositions become more intricate, the volume scatter-type on the roof is reduced and is displayed by the white on the roof changing to magenta (white minus green equals magenta). The $G4U$ decomposition colors the trees with more red than the other decompositions, which is due to how it reduces the volume scattering power by rotating the coherency matrix. The GMBDF with complex β has the most scatter-type contrast and has the lowest residual across the image. The Chen decomposition did the best along the roads, the sand volleyball court, and the track. The areas where the two decompositions had approximately the same residual corresponds well with the shadow regions. The GMBDF with complex β did very well especially in the area of the roof, the dirt areas around the track and the warning track of the baseball field.

Fig. 4.2 compares the residuals of the GMBDF with complex β and Chen decompositions. The yellow pixels are locations where the GMBDF with complex β has a lower residual, 59% of the

image. The blue pixels are locations where the Chen decomposition has a lower residual, 30% of the image. The green pixels are locations where they had equal residuals, 11% of the image.

(A) Optical image   (B) Freeman-Durden image
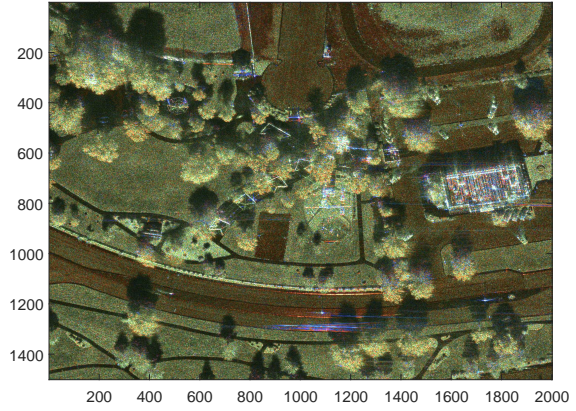
(C) Yamaguchi Image   (D) G4U image
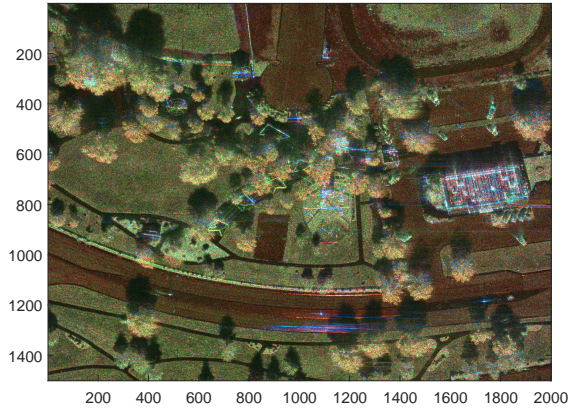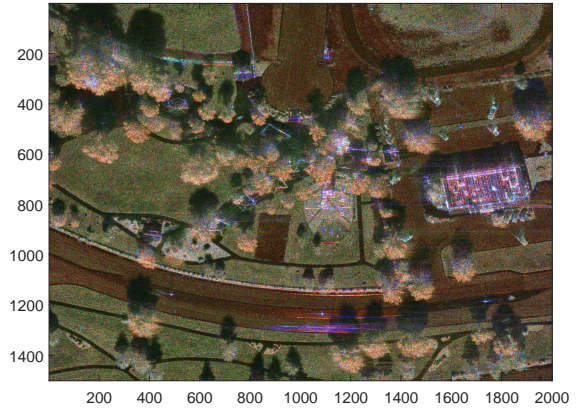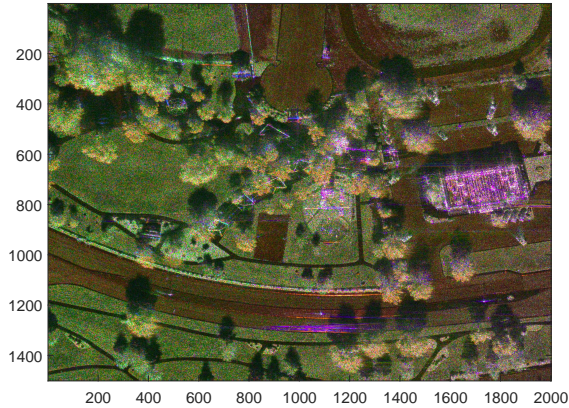
(E) Chen image with $\beta \approx \mathbf{Re}\{\beta\}$ (F) GMBDF with complex β
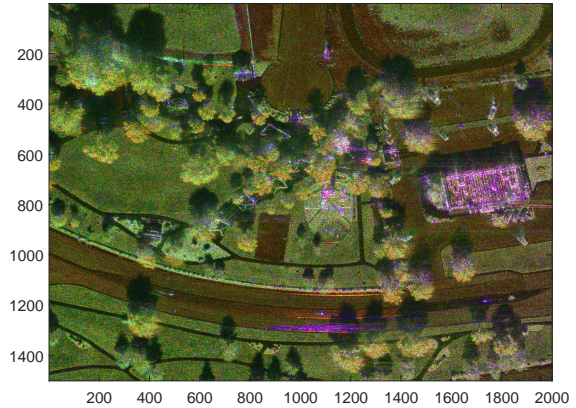
FIGURE 4.1. Decomposition results

60
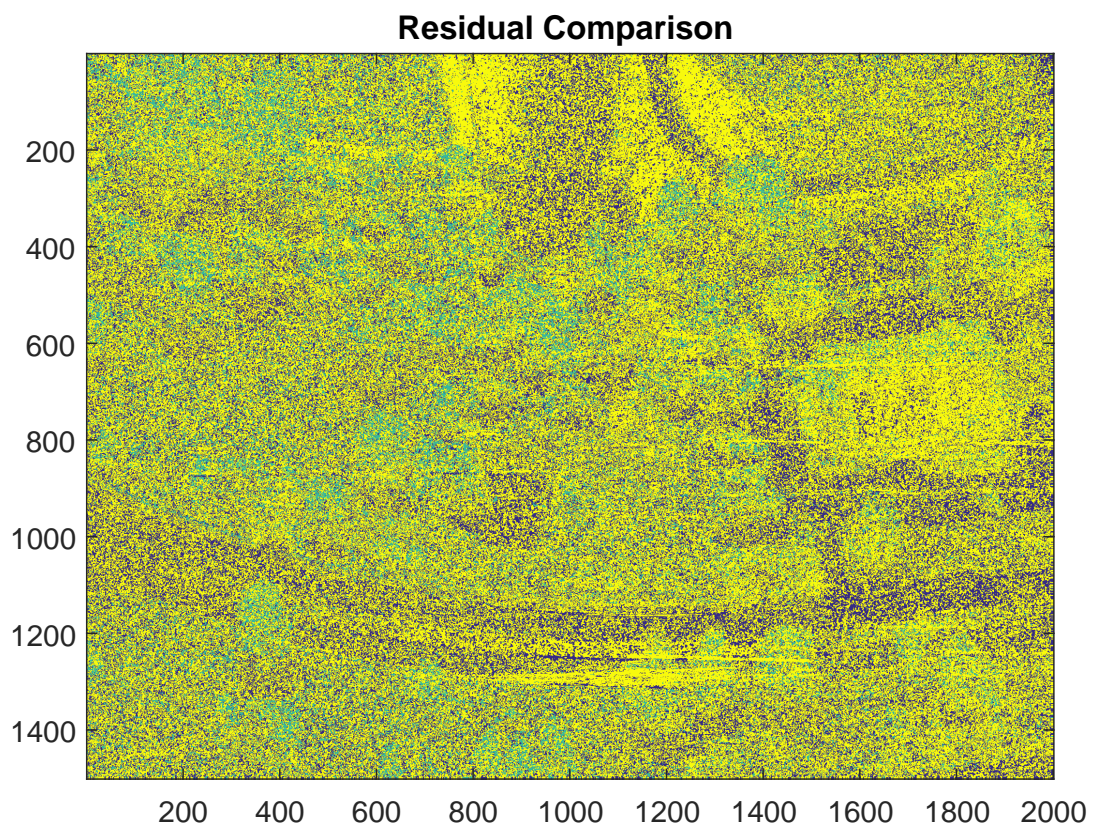
FIGURE 4.2. Comparison of residuals from the Chen and Imaginary Beta decompositions

CHAPTER 5

APPLICATIONS

An important application to the outputs of polarimetric decompositions is the ability to classify the terrain in meaningful categories. In this chapter, I introduce a novel semi-supervised terrain classification framework for polarimetric SAR imagery [37]. The training consists of selecting small regions of homogeneous terrain for each terrain category of interest from a training image. Probabilistic models are generated from these homogeneous regions: in the test image each pixel in the image (or stack of images) is labeled with one of the training categories. This classification approach uses eight parameters from two well-known polarimetric decompositions which describe the physical nature of the scatterers within each pixel. The probabilistic modeling, which occurs during training, fits probability density functions (pdfs) to each of the eight parameters for each region. The eight parameters of every pixel in the test images are each compared with the corresponding pdf, and assigned a p-value. The eight p-values for each pixel are fused together to give each pixel a probability value for fitting each terrain region. This probability determines the terrain region label it is assigned to. If the probability is below a set threshold (which corresponds directly to the desired probability of detection), the pixel is labeled unclassified.

5.1. EIGEN-BASED DECOMPOSITIONS

The $H/A/\bar{\alpha}$ decomposition is an eigenvalue-based decomposition [9] which uses the eigenvalues and eigenvectors of the coherency matrix $\boldsymbol{T}$ to compute polarimetric parameters that represent the physical nature of the scatterers. Namely the scatter-type entropy H, the scatter-type A, and the weighted average of the scattering mechanisms $\bar{\alpha}$. In order to calculate these values, the eigenvalues of the coherency matrix are used to create pseudoprobabilities:

$$\text{(233)} \qquad\qquad p_k = \frac{\lambda_k}{\lambda_1 + \lambda_2 + \lambda_3} \qquad \text{for } k = 1, 2, 3$$

The entropy, H, is defined as

$$(234) \qquad H = \sum_{k=1}^{3} -p_k \log_3 p_k$$

This entropy parameter represents the scatter-type entropy. If the scatterer exhibits the properties of one scatter-type, then $\lambda_1 \approx 1$ and $\lambda_2, \lambda_3 \approx 0$ and $H \approx 0$. If the scatterer exhibits the superposition of three different orthogonal scatter-types, then $\lambda_1, \lambda_2, \lambda_3 \approx \frac{1}{3}$ and $H \approx 1$.

The anisotropy, A, is defined with the second and third eigenvalues as

$$(235) \qquad A = \frac{\lambda_2 - \lambda_3}{\lambda_2 + \lambda_3}.$$

The anisotropy can tell us about the type of symmetry. A scatterer which exhibits both reflection and rotation symmetry (this combination of symmetries is also referred to as azimuthal symmetry) will have $\lambda_2 \approx \lambda_3$ which gives $A \approx 0$. A scatterer that does not have reflection or rotation symmetry will have $\lambda_3 \approx 0$ which gives $A \approx 1$.

The eigenvectors can be parameterized by

$$(236) \qquad \underline{e}_k = \begin{bmatrix} \cos \alpha_k \\ \sin \alpha_k \cos \beta_k e^{i\delta_k} \\ \sin \alpha_k \sin \beta_k e^{i\gamma_k} \end{bmatrix} \qquad \text{with } k = 1, 2, 3$$

and $\bar{\alpha}$ can be defined as the weighted average

$$(237) \qquad \bar{\alpha} = \sum_{k=1}^{3} \alpha_k p_k \qquad \text{with} \quad 0 \leq \bar{\alpha} \leq \frac{\pi}{4}$$

The value for $\bar{\alpha}$ represents a smooth change of scattering mechanism. Values close to zero, $\bar{\alpha} \approx 0$, represent surface scattering. For $\bar{\alpha} \approx \pi/4$, dipole scatterers are represented. For $\bar{\alpha} \approx \pi/2$, dihedral scatterers are represented.

The two decompositions, $G4U$ and $H/A/\bar{\alpha}$, are run on the set of complex-valued images. From the results of these decompositions, each pixel has the following eight parameters associated with it: $P_s, P_d, P_v, P_c, H, A, \bar{\alpha}$ values along with total power TP. At this point, the SLIC superpixel segmentation algorithm [**38**] is used as a method to quickly and easily select homogeneous (or *nearly* homogeneous) pixels of interest for training. Each parameter of the selected pixels are fit to parametric probability density functions using method of moments parameter estimation. For this approach, Gamma distributions are fit to the parameters P_s, P_d, P_v, P_c, and TP. Beta distributions are fit to the parameters H, A, and $\bar{\alpha}$ (normalized). From the entire image, each pixel's parameters are given p-values that correspond to how well a parameter fits the distribution of that parameter for the given class. The process of selecting pixels to represent a class, fitting distributions to each of the eight parameters, and assigning p-values to every pixel's parameters based on the distributions is repeated for each class that is desired. Therefore, every pixel parameter is assigned N p-values, where N represents the number of classes.

The following probabilistic fusion framework [**39**] is used to combine a pixel's eight p-value scores (for each class) into one value that represents the probability that the pixel belongs to the distributions of the selected pixels and therefore belongs to the class the selected pixels represent. Let F_i be the pdf of the ith polarimetric parameter, and let $P_i(x)$ be the probability that the ith parameter of a pixel, x, fits the distribution. As long as F_i is continuous (or well approximated by a continuous function), then the random variable P_i of the selected pixels has a distribution that is uniform on $[0, 1]$. The P_i of pixels that do not belong to the distribution will not be uniform.

Let $Y_i = -\log(P_i)$. The *log* of a uniform distribution is the standard exponential. Y_i will be very large for pixels with at least one characteristic that has low probability of fitting the distribution of the selected pixels.

Let

$$(238) \qquad S_f = \sum_{i=1}^{N} Y_i$$

where N represents the number of characteristics to combine. For the example in this dissertation, $N = 8$. The sum of N independent standard exponentials is represented by a gamma distribution with $r = N$ and $\lambda = 1$. Therefore, if the Y_i values are independent, the sum is represented with a gamma distribution with the theoretical parameters stated above. If the Y_i values are not independent, as with the parameters used in this approach, their sum is still gamma distributed, but the parameters need to be computed with the correlation taken into account. Let $\hat{\rho}_{ij}$ be the estimated correlation between Y_i and Y_j. Then

$$(239) \qquad C = \sum_{i=1}^{N} \sum_{j \neq i} \hat{\rho}_{ij}$$

is the correlation correction factor that can be used to account for correlations between the parameters. Accounting for correlation, the distribution of S_f is gamma distributed with parameters:

$$(240) \qquad \hat{r} = \frac{N^2}{N + C} \qquad \hat{\lambda} = \frac{N}{N + C}$$

A threshold S_f^* can be selected so that the probability that a gamma random variable with the above parameters in (240) is less than S_f^*, matches the desired probability of detection. A pixel is labeled with a category if the pixel's S_f parameter is less than or equal to the category's S_f^* threshold; otherwise, the pixel remains unclassified. If a pixel is labeled with two or more categories, the pixel is labeled with the category that yields the lowest $\frac{S_f}{S_f^*}$ ratio. This classification scheme is illustrated with the flow chart in Figure 5.3.

5.3. EXPERIMENTAL RESULTS

The data for this example were collected along the Rio Grande River in Albuquerque, New Mexico, with the Sandia National Laboratories fully-polarimetric X-band development radar.

The histograms shown in figure 5.1 are of the eight parameters of the hand-selected pixels for the category of vegetation shadow. Overlaid on the histograms are the estimated distributions computed using the method of moments parameter estimation from the hand-selected pixels. The eight parameters of each pixel in the image are compared to these distributions and are each given a p-value representing the probability that the pixel's parameters fit the corresponding distributions of the category's hand-selected pixels.

The three images shown in figure 5.2 are the $G4U$-colored PolSAR image 5.2(a), the hand-selected pixels representing the categories are represented in image 5.2(b), and the classification result in image 5.2(c). The $G4U$ is a false-color PolSAR image with the color representing each pixel's scattering mechanism contributions represented by the percentage of P_s blue, P_d red, P_v green, P_c yellow, and the power of the return represented by pixel brightness. Image 5.2(b) illustrates the hand-selected pixels that generate the categories. The number of pixels selected per category has an order of magnitude of 10^2 compared to the number of pixels in the image 4.5×10^6. The different colors represent different categories. The legend for the colors of the categories is shown in table 5.3. Image 5.2(c) is the resulting pixel-by-pixel classified image.
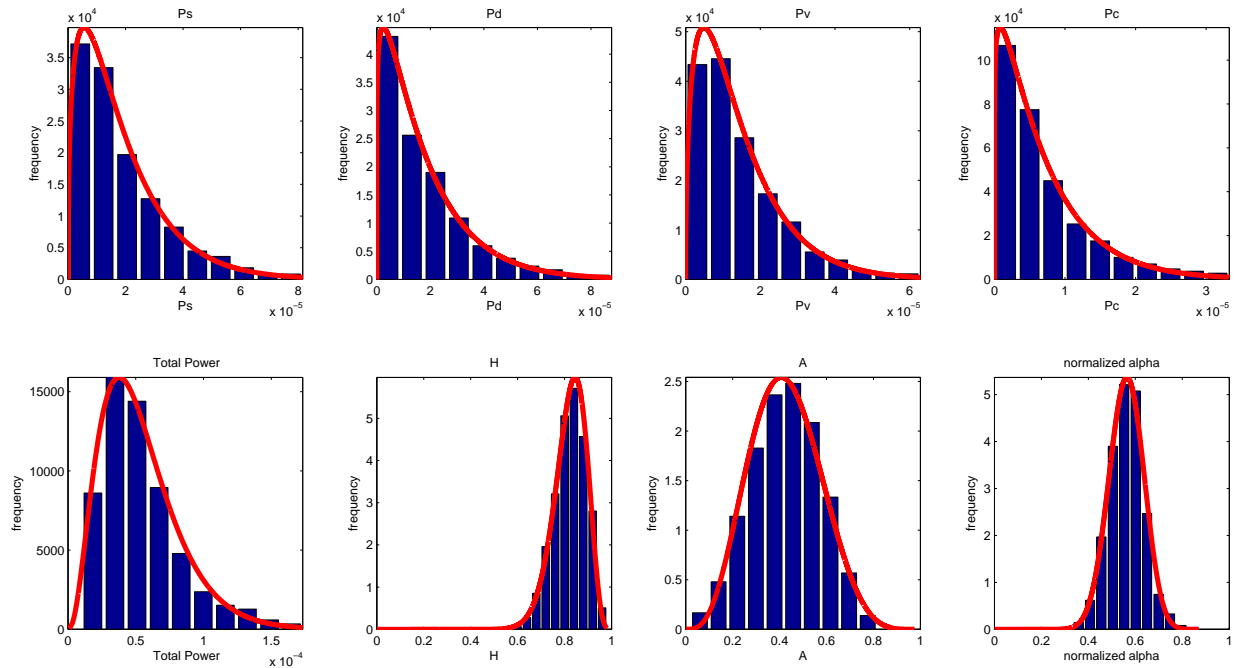
FIGURE 5.1. Histograms of the eight parameters of selected pixels for one category. The red plot represents the distribution that is fit to the data

Legend	
Ground Vegetation	
Vegetation Shadow	
Tree Tops	
Shallow Water	
Deeper Water	
Hard-packed Dirt	
Sand/Loose Dirt	
Unclassified	
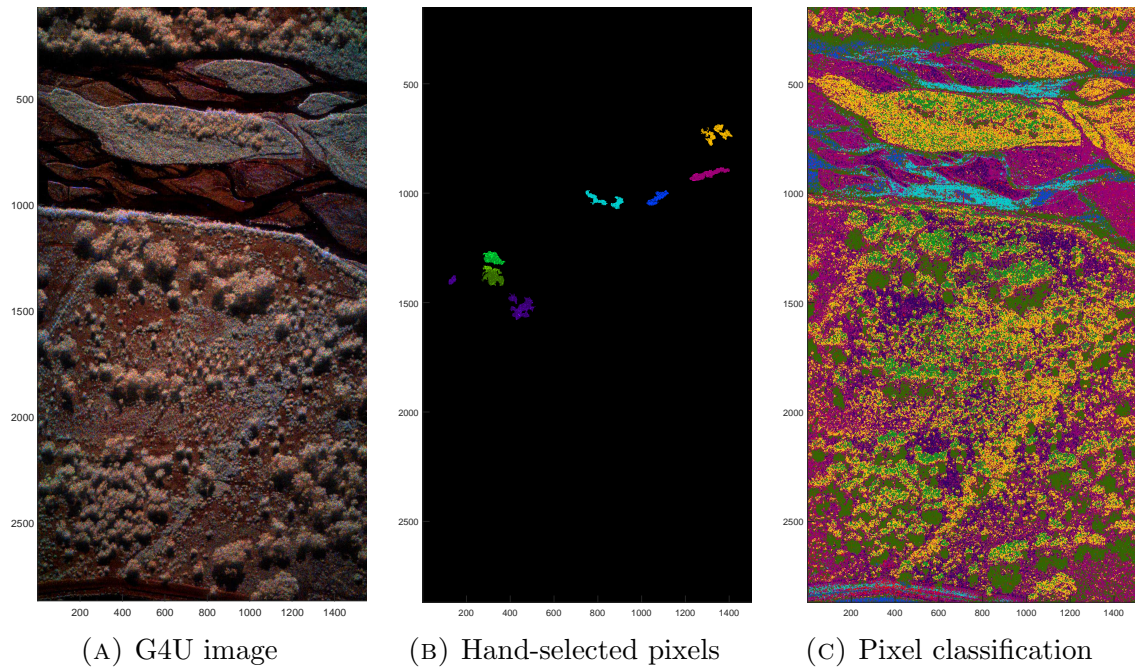
(A) G4U image   (B) Hand-selected pixels   (C) Pixel classification

FIGURE 5.2. Classification results
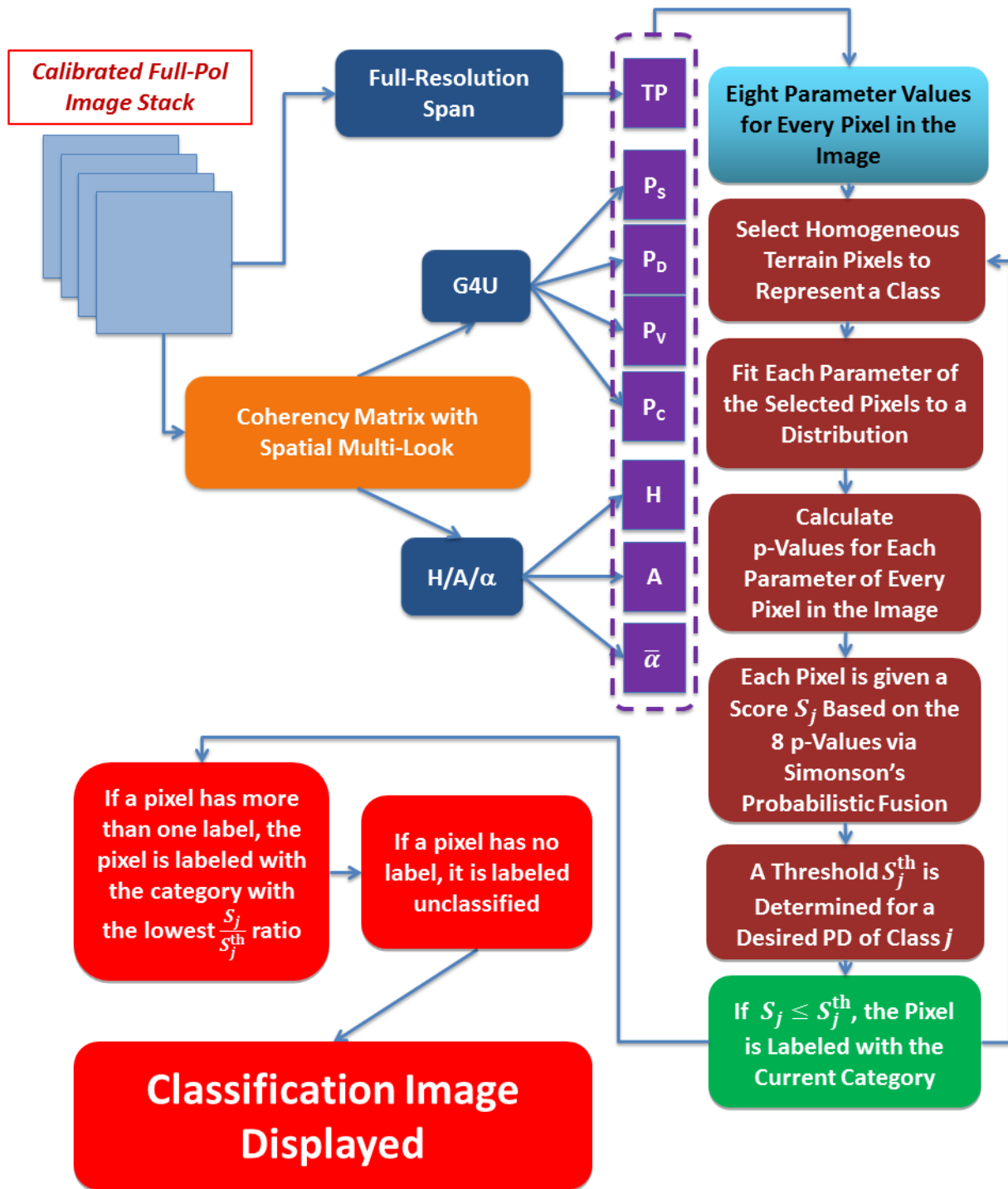
FIGURE 5.3. Flow chart illustrating the proposed classification method

CHAPTER 6

CONCLUSION

With all the model-based decompositions that have come out in the last two decades since the Freeman-Durden decomposition [11], there is a growing need to be able to evaluate how well the different scatter-types model the polarimetric data. The GMBDF provides this framework to evaluate and compare these various decompositions and their scatter-types by comparing their residual terms. The GMBDF extends the Chen decomposition [26] by allowing more than nine unknown parameters within the scatter-types. The scatter-types must be linearly independent to achieve a reasonable result. Attention must be paid to the convexity of the objective function. Minimizing the residual must be done with a method that is valid for nonconvex functions (unless the scatter-types are specifically chosen to create a convex objective function). In this dissertation, the method of steepest descent is used to find a local minimum of the objective function. The values of the parameters at this local minimum are used to calculate scatter-type powers. These scatter-type powers are displayed in a false-color image that assigns a specific color to each scatter-type power.

The worked out example in this dissertation demonstrates how the GMBDF can evaluate and compare the Chen decomposition with a similar decomposition with a surface model that includes the imaginary part of the surface parameter β. This example shows that for a majority of the pixels in the image that was used, using the decomposition with the complex β term reduced the residual term lower than the Chen decomposition and therefore better modeled the data.

An application of polarimetric decompositions is to use the results to classify terrain. A novel terrain classification scheme is presented to show the power of decomposed polarimetric data to classify natural terrain in physically meaningful categories.

BIBLIOGRAPHY

[1] C. V. Jakowatz, Jr., D. E. Wahl, P. E. Eichel, D. C. Ghiglia, and P. A. Thompson, *Spotlight-mode Synthetic Aperture Radar: A Signal Processing Approach.* Springer, 1996.

[2] M. Cheney and B. Borden, *Fundamentals of radar imaging.* Siam, 2009, vol. 79.

[3] A. Moreira, P. Prats-Iraola, M. Younis, G. Krieger, I. Hajnsek, and K. P. Papathanassiou, "A tutorial on synthetic aperture radar," *IEEE Geoscience and Remote Sensing Magazine*, vol. 1, no. 1, pp. 6–43, March 2013.

[4] J. Lee and E. Pottier, *Polarimetric Radar Imaging: From Basics to Applications.* CRC Press, 2002.

[5] S. Cloude, *Polarisation: Applications in Remote Sensing.* Oxford University Press, 2010.

[6] J. van Zyl and Y. Kim, *Synthetic Aperture Radar Polarimetry.* CRC John Wiley & Sons, 2011.

[7] J.-S. Lee, M. Grunes, and G. De Grandi, "Polarimetric sar speckle filtering and its implication for classification," *Geoscience and Remote Sensing, IEEE Transactions on*, vol. 37, no. 5, pp. 2363–2373, Sep 1999.

[8] J.-S. Lee, T. Ainsworth, Y. Wang, and K.-S. Chen, "Polarimetric sar speckle filtering and the extended sigma filter," *Geoscience and Remote Sensing, IEEE Transactions on*, vol. 53, no. 3, pp. 1150–1160, March 2015.

[9] S. Cloude and E. Pottier, "An entropy based classification scheme for land applications of polarimetric SAR," *Geoscience and Remote Sensing, IEEE Transactions on*, vol. 35, no. 1, pp. 68–78, 1997.

[10] G. Golub and C. Van Loan, *Matrix Computations*, 2nd ed. Baltimore: Johns Hopkins University Press, 1989.

[11] A. Freeman and S. Durden, "A three-component scattering model for polarimetric SAR data," *Geoscience and Remote Sensing, IEEE Transactions on*, vol. 36, no. 3, pp. 963–973, May 1998.

[12] J. A. Ogilvy, *Theory of Wave Scattering from Random Surfaces.* Institute of Physics Publishing, 1992.

[13] J. J. van Zyl, "Unsupervised classification of scattering behavior using radar polarimetry data," *IEEE Transactions on Geoscience and Remote Sensing*, vol. 27, no. 1, pp. 36–45, Jan 1989.

[14] Y. Yamaguchi, T. Moriyama, M. Ishido, and H. Yamada, "Four-component scattering model for polarimetric SAR image decomposition," *Geoscience and Remote Sensing, IEEE Transactions on*, vol. 43, no. 8, pp. 1699–1706, 2005.

[15] J. J. van Zyl, M. Arii, and Y. Kim, "Model-based decomposition of polarimetric sar covariance matrices constrained for nonnegative eigenvalues," *IEEE Transactions on Geoscience and Remote Sensing*, vol. 49, no. 9, pp. 3452–3459, Sept 2011.

[16] C. Wang, W. Yu, R. Wang, Y. Deng, and F. Zhao, "Comparison of nonnegative eigenvalue decompositions with and without reflection symmetry assumptions," *IEEE Transactions on Geoscience and Remote Sensing*, vol. 52, no. 4, pp. 2278–2287, April 2014.

[17] M. Arii, J. J. van Zyl, and Y. Kim, "Adaptive model-based decomposition of polarimetric sar covariance matrices," *IEEE Transactions on Geoscience and Remote Sensing*, vol. 49, no. 3, pp. 1104–1113, March 2011.

[18] J.-S. Lee and T. Ainsworth, "The effect of orientation angle compensation on coherency matrix and polarimetric target decompositions," *Geoscience and Remote Sensing, IEEE Transactions on*, vol. 49, no. 1, pp. 53–64, Jan 2011.

[19] Y. Yamaguchi, A. Sato, W.-M. Boerner, R. Sato, and H. Yamada, "Four-component scattering power decomposition with rotation of coherency matrix," *Geoscience and Remote Sensing, IEEE Transactions on*, vol. 49, no. 6, pp. 2251–2258, June 2011.

[20] G. Singh, Y. Yamaguchi, and S.-E. Park, "General four-component scattering power decomposition with unitary transformation of coherency matrix," *Geoscience and Remote Sensing, IEEE Transactions on*, vol. 51, no. 5, pp. 3014–3022, May 2013.

[21] A. Sato, Y. Yamaguchi, G. Singh, and S. E. Park, "Four-component scattering power decomposition with extended volume scattering model," *IEEE Geoscience and Remote Sensing Letters*, vol. 9, no. 2, pp. 166–170, March 2012.

[22] A. Freeman, "Fitting a two-component scattering model to polarimetric sar data from forests," *IEEE Transactions on Geoscience and Remote Sensing*, vol. 45, no. 8, pp. 2583–2592, Aug 2007.

[23] I. Hajnsek, E. Pottier, and S. Cloude, "Inversion of surface parameters from polarimetric sar," *Geoscience and Remote Sensing, IEEE Transactions on*, vol. 41, no. 4, pp. 727–744, April 2003.

[24] D. L. Schuler, J.-S. Lee, D. Kasilingam, and G. Nesti, "Surface roughness and slope measurements using polarimetric sar data," *IEEE Transactions on Geoscience and Remote Sensing*, vol. 40, no. 3, pp. 687–698, Mar 2002.

[25] X. Huang, J. Wang, and J. Shang, "An adaptive two-component model-based decomposition on soil moisture estimation for c-band radarsat-2 imagery over wheat fields at early growing stages," *IEEE Geoscience and Remote Sensing Letters*, vol. 13, no. 3, pp. 414–418, March 2016.

[26] S.-W. Chen, X. song Wang, S.-P. Xiao, and M. Sato, "General polarimetric model-based decomposition for coherency matrix," *IEEE Transactions on Geoscience and Remote Sensing*, vol. 52, no. 3, pp. 1843–1855, March 2014.

[27] S. Boyd and L. Vandenberghe, *Convex Optimization*. Cambridge University Press, 2004.

[28] J. S. Lee, T. L. Ainsworth, and Y. Wang, "Generalized polarimetric model-based decompositions using extended incoherent scattering models," in *2012 IEEE International Geoscience and Remote Sensing Symposium*, July 2012, pp. 1421–1424.

[29] B. Chen, L. Jiao, and S. Zhang, "An improved three-component model-based decomposition for polarimetric sar data," in *2014 International Conference on Audio, Language and Image Processing*, July 2014, pp. 419–422.

[30] A. Bhattacharya, G. Singh, S. Manickam, and Y. Yamaguchi, "An adaptive general four-component scattering power decomposition with unitary transformation of coherency matrix (ag4u)," *IEEE Geoscience and Remote Sensing Letters*, vol. 12, no. 10, pp. 2110–2114, Oct 2015.

[31] Y. Cui, Y. Yamaguchi, J. Yang, H. Kobayashi, S.-E. Park, and G. Singh, "On complete model-based decomposition of polarimetric sar coherency matrix data," *IEEE Transactions on Geoscience and Remote Sensing*, vol. 52, no. 4, pp. 1991–2001, April 2014.

[32] A. Bhattacharya, A. Muhuri, S. De, S. Manickam, and A. C. Frery, "Modifying the yamaguchi four-component decomposition scattering powers using a stochastic distance," *IEEE Journal of Selected Topics in Applied Earth Observations and Remote Sensing*, vol. 8, no. 7, pp. 3497–3506, July 2015.

[33] B. Zou, Y. Zhang, N. Cao, and N. P. Minh, "A four-component decomposition model for polsar data using asymmetric scattering component," *IEEE Journal of Selected Topics in Applied Earth Observations and Remote Sensing*, vol. 8, no. 3, pp. 1051–1061, March 2015.

[34] O. Antropov, Y. Rauste, and T. Hame, "Volume scattering modeling in polsar decompositions: Study of alos palsar data over boreal forest," *IEEE Transactions on Geoscience and Remote Sensing*, vol. 49, no. 10, pp. 3838–3848, Oct 2011.

[35] A. Von Hippel, *Dielectric materials and applications*, ser. Artech House microwave library. Artech House, 1954. [Online]. Available: https://books.google.com/books?id=2ywbAQAAIAAJ

[36] J. Mead, P. Langlois, P. Chang, and R. McIntosh, "Polarimetric scattering from natural surfaces at 225 ghz," in *Antennas and Propagation Society Symposium 1991 Digest*, June 1991, pp. 756–759 vol.2.

[37] S. Dauphin, R. Derek West, R. Riley, and K. M. Simonson, "Semi-supervised classification of terrain features in polarimetric sar images using h/a/alpha; and the general four-component scattering power decompositions," in *Signals, Systems and Computers, 2014 48th Asilomar Conference on*, Nov 2014, pp. 167–171.

[38] R. Achanta, A. Shaji, K. Smith, A. Lucchi, P. Fua, and S. Süsstrunk, "SLIC superpixels compared to state-of-the-art superpixel methods," *Pattern Analysis and Machine Intelligence, IEEE Transactions on*, vol. 34, no. 11, pp. 2274–2282, Nov 2012.

[39] K. M. Simonson, "Probabilistic fusion of ATR results," Sandia National Laboratories, Albuquerque, New Mexico 87185 and Livermore, California 94550, Technical report SAND98-1699, August 1998.

A DESCRIPTION OF A WAVE'S POLARIZATION

FROM MAXWELL'S EQUATIONS

Using notation similar to [**4**], electromagnetic waves are described in time and space by the famous Maxwell equations.

$$(241) \qquad \vec{\boldsymbol{\nabla}} \times \vec{\boldsymbol{E}}\left(\vec{\boldsymbol{r}}, t\right) = -\frac{\partial \vec{\boldsymbol{B}}\left(\vec{\boldsymbol{r}}, t\right)}{\partial t}$$

$$(242) \qquad \vec{\boldsymbol{\nabla}} \times \vec{\boldsymbol{H}}\left(\vec{\boldsymbol{r}}, t\right) = \vec{\boldsymbol{J}}\left(\vec{\boldsymbol{r}}, t\right) + \frac{\partial \vec{\boldsymbol{D}}\left(\vec{\boldsymbol{r}}, t\right)}{\partial t}$$

$$(243) \qquad \vec{\boldsymbol{\nabla}} \cdot \vec{\boldsymbol{D}}\left(\vec{\boldsymbol{r}}, t\right) = \rho\left(\vec{\boldsymbol{r}}, t\right)$$

$$(244) \qquad \vec{\boldsymbol{\nabla}} \cdot \vec{\boldsymbol{B}}\left(\vec{\boldsymbol{r}}, t\right) = 0$$

$\vec{\boldsymbol{E}}\left(\vec{\boldsymbol{r}}, t\right)$ is the electric field.

$\vec{\boldsymbol{H}}\left(\vec{\boldsymbol{r}}, t\right)$ is the magnetic field.

$\vec{\boldsymbol{D}}\left(\vec{\boldsymbol{r}}, t\right)$ is the electric induction.

$\vec{\boldsymbol{B}}\left(\vec{\boldsymbol{r}}, t\right)$ is the magnetic induction.

$\vec{\boldsymbol{J}}\left(\vec{\boldsymbol{r}}, t\right)$ is the total current density.

$\rho\left(\vec{\boldsymbol{r}}, t\right)$ is the volume density of free charges.

Assuming that the wave is propagating through a linear medium that is free of saturation, hysteresis, or any source term, then

$$(245) \qquad \vec{\boldsymbol{J}}\left(\vec{\boldsymbol{r}}, t\right) = \sigma \vec{\boldsymbol{E}}\left(\vec{\boldsymbol{r}}, t\right)$$

$$(246) \qquad \vec{\boldsymbol{D}}\left(\vec{\boldsymbol{r}}, t\right) = \varepsilon \vec{\boldsymbol{E}}\left(\vec{\boldsymbol{r}}, t\right)$$

$$(247) \qquad \vec{\boldsymbol{B}}\left(\vec{\boldsymbol{r}}, t\right) = \mu \vec{\boldsymbol{H}}\left(\vec{\boldsymbol{r}}, t\right)$$

$$(248) \qquad \rho\left(\vec{\boldsymbol{r}}, t\right) = 0$$

where σ, ε and μ are the conductivity, permittivity and the permeability of the medium.

Taking the curl of both sides of (241), the vector identity $\vec{\nabla} \times \left(\vec{\nabla} \times \vec{E} \right) = \vec{\nabla} \left(\vec{\nabla} \cdot \vec{E} \right) - \nabla^2 \vec{E}$, and substituting in equations (245) - (248) we have

$$
(249) \qquad \vec{\nabla} \times \left(\vec{\nabla} \times \vec{E}\left(\vec{r}, t\right) \right) = \vec{\nabla} \times \left(-\frac{\partial \vec{B}\left(\vec{r}, t\right)}{\partial t} \right)
$$

$$
(250) \qquad \vec{\nabla} \left(\vec{\nabla} \cdot \vec{E}\left(\vec{r}, t\right) \right) - \nabla^2 \vec{E}\left(\vec{r}, t\right) = -\frac{\partial \left(\vec{\nabla} \times \vec{B}\left(\vec{r}, t\right) \right)}{\partial t}
$$

$$
(251) \qquad 0 - \nabla^2 \vec{E}\left(\vec{r}, t\right) = -\frac{\partial \left(\vec{\nabla} \times \mu \vec{H}\left(\vec{r}, t\right) \right)}{\partial t}
$$

$$
(252) \qquad \nabla^2 \vec{E}\left(\vec{r}, t\right) = \mu \frac{\partial \left(\vec{\nabla} \times \vec{H}\left(\vec{r}, t\right) \right)}{\partial t}
$$

$$
(253) \qquad \nabla^2 \vec{E}\left(\vec{r}, t\right) = \mu \frac{\partial \left(\vec{J}\left(\vec{r}, t\right) + \frac{\partial \vec{D}\left(\vec{r}, t\right)}{\partial t} \right)}{\partial t}
$$

$$
(254) \qquad \nabla^2 \vec{E}\left(\vec{r}, t\right) = \mu \frac{\partial \left(\sigma \vec{E}\left(\vec{r}, t\right) + \frac{\partial \left(\varepsilon \vec{E}\left(\vec{r}, t\right) \right)}{\partial t} \right)}{\partial t}
$$

$$
(255) \qquad \nabla^2 \vec{E}\left(\vec{r}, t\right) = \mu \left(\frac{\partial \left(\sigma \vec{E}\left(\vec{r}, t\right) \right)}{\partial t} + \frac{\partial^2 \left(\varepsilon \vec{E}\left(\vec{r}, t\right) \right)}{\partial t^2} \right)
$$

$$
(256) \qquad \nabla^2 \vec{E}\left(\vec{r}, t\right) = \mu \sigma \frac{\partial \vec{E}\left(\vec{r}, t\right)}{\partial t} + \mu \varepsilon \frac{\partial^2 \vec{E}\left(\vec{r}, t\right)}{\partial t^2}
$$

Continuing the reasoning from [4], a simplification can be made by considering the complex expression $\vec{E}\left(\vec{r}\right)$ of the monochromatic time-space electric field $\vec{E}\left(\vec{r}, t\right)$, defined as

$$
(257) \qquad \vec{E}\left(\vec{r}, t\right) = \mathbf{Re} \left\{ \vec{E}\left(\vec{r}\right) e^{j\omega t} \right\}
$$

With (257), (256) can be written as

$$
(258) \qquad \nabla^2 \vec{E}\left(\vec{r}\right) + k^2 \vec{E}\left(\vec{r}\right) = 0
$$

where

$$(259) \qquad k = \omega \sqrt{\mu \varepsilon \left(1 + j \frac{\mathbf{Im}\,\{\varepsilon\}}{\mathbf{Re}\,\{\varepsilon\}} \right)}$$

Let the electric field be defined on a 3-dimensional Cartesian space $(\hat{x}, \hat{y}, \hat{z})$ so that the direction of propagation is in the positive $\hat{z}$ direction.

Therefore,

$$(260) \qquad \vec{E}(\vec{r}) = \vec{E_0} \mathrm{e}^{-j\hat{z}\cdot\vec{r}} \qquad \text{with} \quad \vec{E}(\vec{r}) \cdot \hat{z} = 0$$

where $\vec{E_0}$ is the constant complex amplitude of the monochromatic plane wave. The parameter k is complex and can be separated into its real and imaginary parts with $k = \beta - j\alpha$. (As a side note, k is defined this way to remain consistent with other literature that uses the expression $\nabla^2 \vec{E}(\vec{r}) = \gamma^2 \vec{E}(\vec{r})$ instead of (258), with $\gamma^2 = -k^2$. Therefore, defining the complex components of k like this aligns with complex components of γ with $\gamma = \alpha + j\beta$)

The electric field can now be expressed as

$$(261) \qquad \vec{E}(z) = \vec{E_0} \mathrm{e}^{-\alpha z} \mathrm{e}^{-j\beta z}$$

Inserting the expression from (261) into (257) we have

$$(262) \qquad \vec{E}(\vec{z}, t) = \mathbf{Re}\left\{ \vec{E}(z)\, \mathrm{e}^{j\omega t} \right\}$$

$$(263) \qquad \vec{E}(\vec{z}, t) = \mathbf{Re}\left\{ \left(\vec{E_0} \mathrm{e}^{-\alpha z} \mathrm{e}^{-j\beta z} \right) \mathrm{e}^{j\omega t} \right\}$$

$$(264) \qquad \vec{E}(\vec{z}, t) = \begin{bmatrix} \mathbf{Re}\left\{ E_{0x} \mathrm{e}^{j\delta_x} \mathrm{e}^{-\alpha z} \mathrm{e}^{-j\beta z} \mathrm{e}^{j\omega t} \right\} \\ \mathbf{Re}\left\{ E_{0y} \mathrm{e}^{j\delta_x} \mathrm{e}^{-\alpha z} \mathrm{e}^{-j\beta z} \mathrm{e}^{j\omega t} \right\} \\ 0 \end{bmatrix}$$

$$(265) \qquad \vec{E}\left(\vec{z}, t\right) = \begin{bmatrix} E_{0x}\mathrm{e}^{-\alpha z}\cos\left(\omega t - \beta z + \delta_x\right) \\ E_{0y}\mathrm{e}^{-\alpha z}\cos\left(\omega t - \beta z + \delta_y\right) \\ 0 \end{bmatrix}$$

where E_{0x} and δ_x represent the magnitude and phase of the electric field in the $\hat{x}$ direction.

The attenuation term $\mathrm{e}^{-\alpha z}$ is common to all elements of the electric field and, therefore, does not describe the wave's polarization, which is what we are interested in. Therefore, the medium can be assumed to be loss free, $\alpha = 0$, and

$$(266) \qquad \vec{E}\left(\vec{z}, t\right) = \begin{bmatrix} E_{0x}\cos\left(\omega t - \beta z + \delta_x\right) \\ E_{0y}\cos\left(\omega t - \beta z + \delta_y\right) \\ 0 \end{bmatrix}.$$

The Jones vector $\underline{E}$ is used to describe a wave's polarization and is defined as

$$(267) \qquad \underline{E} = \vec{E}\left(z\right)\big|_{z=0} = \vec{E}\left(0\right) = \begin{bmatrix} E_{0x}\mathrm{e}^{j\delta_x} \\ E_{0y}\mathrm{e}^{j\delta_y} \end{bmatrix}.$$

For a given Jones vector, there exists an orthogonal Jones vector that forms a polarization basis that can be used to represent the polarization of an arbitrary wave. The benefit of this structure is that one only needs to collect measurements in one polarization basis to have all the information to represent the response in any polarization basis. For instance, if a measurement is made using horizontally and vertically polarization, a simple mathematical transformation can give the response as if it has been collect with a different basis, say left-circular and right-circular.

The electric field of a general propagating electromagnetic wave carves out an ellipse in the plane that is perpendicular to the direction of propagation (see Figure (A.1). Therefore,the Jones vector description of a wave's polarization also defines the wave's polarization ellipse.

We can also define an ellipse with the ellipse's amplitude, orientation, and ellipticity. From the diagram of ellipse parameters (Fig A.1), A represents the amplitude of the ellipse

$$(268) \qquad A = \sqrt{E_{0x}^2 + E_{0y}^2}$$

$\phi \in \left[-\frac{\pi}{2}, \frac{\pi}{2}\right]$ represents the orientation of the ellipse and is the angle between the major axis of the ellipse and $\hat{s}$. ϕ can be found with the equation

$$(269) \qquad \tan 2\phi = 2\frac{E_{0x}E_{0y}}{E_{0x}^2 - E_{0y}^2} \cos\left(\delta_y - \delta_x\right).$$

The ellipticity, $\tau \in \left[-\frac{\pi}{4}, \frac{\pi}{4}\right]$, can be found with

$$(270) \qquad \sin 2\tau = 2\frac{E_{0x}E_{0y}}{E_{0x}^2 + E_{0y}^2} \sin\left(\delta_y - \delta_x\right).$$

Now, a Jones vector can be defined by these parameters as follows:

$$(271) \qquad \underline{\boldsymbol{E}} = A\mathrm{e}^{+j\alpha} \begin{bmatrix} \cos\phi\cos\tau - j\sin\phi\sin\tau \\ \sin\phi\cos\tau + j\cos\phi\sin\tau \end{bmatrix},$$

where α is the absolute phase term. The three ellipse parameters do not need α to be defined, they only need E_{0x}, E_{0y}, and the phase difference $\delta_y - \delta_x$.

The ϕ and τ parameters can be separated

$$(272) \qquad \underline{\boldsymbol{E}} = A\mathrm{e}^{+j\alpha} \begin{bmatrix} \cos\phi & -\sin\phi \\ \sin\phi & \cos\phi \end{bmatrix} \begin{bmatrix} \cos\tau \\ j\sin\tau \end{bmatrix}$$

$$(273) \qquad = A\mathrm{e}^{+j\alpha} \begin{bmatrix} \cos\phi & -\sin\phi \\ \sin\phi & \cos\phi \end{bmatrix} \begin{bmatrix} \cos\tau & j\sin\tau \\ j\sin\tau & \cos\tau \end{bmatrix} \begin{bmatrix} 1 \\ 0 \end{bmatrix}$$

$$(274) \qquad = A \begin{bmatrix} \cos\phi & -\sin\phi \\ \sin\phi & \cos\phi \end{bmatrix} \begin{bmatrix} \cos\tau & j\sin\tau \\ j\sin\tau & \cos\tau \end{bmatrix} \begin{bmatrix} A\mathrm{e}^{+j\alpha} & 0 \\ 0 & A\mathrm{e}^{-j\alpha} \end{bmatrix} \begin{bmatrix} 1 \\ 0 \end{bmatrix}$$

The 2×2 matrices in (274) form a group of special unitary matrices. To show that, a connection to the unitary Pauli matrices is shown. The Pauli matrices are defined as

$$(275) \qquad \boldsymbol{\sigma}_0 = \begin{bmatrix} 1 & 0 \\ 0 & 1 \end{bmatrix} \quad \boldsymbol{\sigma}_1 = \begin{bmatrix} 1 & 0 \\ 0 & -1 \end{bmatrix} \quad \boldsymbol{\sigma}_2 = \begin{bmatrix} 0 & 1 \\ 1 & 0 \end{bmatrix} \quad \boldsymbol{\sigma}_3 = \begin{bmatrix} 0 & -j \\ j & 0 \end{bmatrix}$$

These matrices have the qualities $\boldsymbol{\sigma}_i^{-1} = \boldsymbol{\sigma}_i^{*\mathrm{T}}$ and $|\det(\boldsymbol{\sigma}_i)| = 1$ and represent the quaternion group with the following multiplicative table:

$\vec{\otimes}$	$\boldsymbol{\sigma}_0$	$\boldsymbol{\sigma}_1$	$\boldsymbol{\sigma}_2$	$\boldsymbol{\sigma}_3$
$\boldsymbol{\sigma}_0$	$\boldsymbol{\sigma}_0$	$\boldsymbol{\sigma}_1$	$\boldsymbol{\sigma}_2$	$\boldsymbol{\sigma}_3$
$\boldsymbol{\sigma}_1$	$\boldsymbol{\sigma}_1$	$\boldsymbol{\sigma}_0$	$j\boldsymbol{\sigma}_3$	$-j\boldsymbol{\sigma}_2$
$\boldsymbol{\sigma}_2$	$\boldsymbol{\sigma}_2$	$-j\boldsymbol{\sigma}_3$	$\boldsymbol{\sigma}_0$	$j\boldsymbol{\sigma}_1$
$\boldsymbol{\sigma}_3$	$\boldsymbol{\sigma}_3$	$j\boldsymbol{\sigma}_2$	$-j\boldsymbol{\sigma}_1$	$\boldsymbol{\sigma}_0$

These matrices therefore have the following commutative properties: $\boldsymbol{\sigma}_i\boldsymbol{\sigma}_j = -\boldsymbol{\sigma}_j\boldsymbol{\sigma}_i$ and $\boldsymbol{\sigma}_i\boldsymbol{\sigma}_i = \boldsymbol{\sigma}_0$.

The group of special unitary matrices, SU(2), is defined as

$$(276) \qquad \mathrm{e}^{+j\psi\boldsymbol{\sigma}_p} = \boldsymbol{\sigma}_0 \cos\psi + j\boldsymbol{\sigma}_p \sin\psi$$

Now, the three 2×2 matrices from (274) correspond with the three special unitary groups:

$$(277) \qquad U_{2\phi}(\phi) = \begin{bmatrix} \cos\phi & -\sin\phi \\ \sin\phi & \cos\phi \end{bmatrix} = \boldsymbol{\sigma}_0 \cos\phi - j\boldsymbol{\sigma}_3 \sin\phi = \mathrm{e}^{-j\phi\boldsymbol{\sigma}_3}$$

$$(278) \qquad U_{2\tau}(\tau) = \begin{bmatrix} \cos\tau & j\sin\tau \\ j\sin\tau & \cos\tau \end{bmatrix} = \boldsymbol{\sigma}_0 \cos\tau + j\boldsymbol{\sigma}_2 \sin\tau = \mathrm{e}^{+j\tau\boldsymbol{\sigma}_2}$$

$$(279) \qquad U_{2\alpha}(\alpha) = \begin{bmatrix} A\mathrm{e}^{+j\alpha} & 0 \\ 0 & A\mathrm{e}^{-j\alpha} \end{bmatrix} = \boldsymbol{\sigma}_0 \cos\alpha + j\boldsymbol{\sigma}_1 \sin\alpha = \mathrm{e}^{+j\alpha\boldsymbol{\sigma}_1}.$$

The inverse of each of these matrices is its conjugate transpose, $U_2^{-1} = U_2^{*\mathrm{T}}$, and each has a determinant of 1. From this, we can rewrite (274) as

$$\underline{\boldsymbol{E}} = A \begin{bmatrix} \cos\phi & -\sin\phi \\ \sin\phi & \cos\phi \end{bmatrix} \begin{bmatrix} \cos\tau & j\sin\tau \\ j\sin\tau & \cos\tau \end{bmatrix} \begin{bmatrix} A\mathrm{e}^{+j\alpha} & 0 \\ 0 & A\mathrm{e}^{-j\alpha} \end{bmatrix} \begin{bmatrix} 1 \\ 0 \end{bmatrix}$$

$$(280) \qquad = A U_{2\phi}(\phi) U_{2\tau}(\tau) U_{2\alpha}(\alpha)\, \hat{x}$$

$$= A U_2(\phi, \tau, \alpha)\, \hat{x}$$

$$(281) \qquad = A\mathrm{e}^{-j\phi\boldsymbol{\sigma}_3}\mathrm{e}^{+j\tau\boldsymbol{\sigma}_2}\mathrm{e}^{+j\alpha\boldsymbol{\sigma}_1}\, \hat{x}$$

with

$$(282) \qquad\qquad \hat{x} = \hat{\boldsymbol{u}}_\mathrm{H} = \begin{bmatrix} 1 \\ 0 \end{bmatrix}$$

where $\hat{\boldsymbol{u}}_\mathrm{H}$ is the unit Jones vector that represents a horizontally polarized state.

Two complex vectors are orthogonal if their Hermitian scalar product is 0. Therefore, the orthogonal Jones vectors $\underline{\boldsymbol{E}}_1$ and $\underline{\boldsymbol{E}}_2$ exhibit the property

$$(283) \qquad\qquad \langle \underline{\boldsymbol{E}}_1 | \underline{\boldsymbol{E}}_2 \rangle = \underline{\boldsymbol{E}}_1^{\mathrm{T}} \cdot \underline{\boldsymbol{E}}_2^* = 0$$

Consider the general Jones vector, $\underline{\boldsymbol{E}}$ from (281) that takes the horizontal Jones vector, $\hat{x}$, and transforms it by three rotations defined by ϕ, τ, and α. To find the Jones vector, $\underline{\boldsymbol{E}}_\perp$, that is orthogonal to $\underline{\boldsymbol{E}}$, simply perform the same unitary transformations to the vertical Jones vector $\hat{y}$.

$$\underline{\boldsymbol{E}}_\perp = A U_2(\phi, \tau, \alpha)\, \hat{y}$$

$$(284) \qquad = A \begin{bmatrix} \cos\phi & -\sin\phi \\ \sin\phi & \cos\phi \end{bmatrix} \begin{bmatrix} \cos\tau & j\sin\tau \\ j\sin\tau & \cos\tau \end{bmatrix} \begin{bmatrix} \mathrm{e}^{+j\alpha} & 0 \\ 0 & \mathrm{e}^{-j\alpha} \end{bmatrix} \hat{y}$$

This equation can be rearranged to be a transformation of the horizontal Jones vector $\hat{x}$:

$$\underline{E}_{\perp} = A U_2 \left(\phi, \tau, \alpha\right) \hat{y}$$

$$= A \begin{bmatrix} \cos\phi & -\sin\phi \\ \sin\phi & \cos\phi \end{bmatrix} \begin{bmatrix} \cos\tau & j\sin\tau \\ j\sin\tau & \cos\tau \end{bmatrix} \begin{bmatrix} e^{+j\alpha} & 0 \\ 0 & e^{-j\alpha} \end{bmatrix} \hat{y}$$

$$= A \begin{bmatrix} \cos\phi\cos\tau - j\sin\phi\sin\tau & j\cos\phi\sin\tau - \sin\phi\cos\tau \\ \sin\phi\cos\tau + j\cos\phi\sin\tau & j\sin\phi\sin\tau + \cos\phi\cos\tau \end{bmatrix} \begin{bmatrix} e^{+j\alpha} & 0 \\ 0 & e^{-j\alpha} \end{bmatrix} \hat{y}$$

$$= A \begin{bmatrix} \left(\cos\phi\cos\tau - j\sin\phi\sin\tau\right)e^{+j\alpha} & \left(j\cos\phi\sin\tau - \sin\phi\cos\tau\right)e^{-j\alpha} \\ \left(\sin\phi\cos\tau + j\cos\phi\sin\tau\right)e^{+j\alpha} & \left(j\sin\phi\sin\tau + \cos\phi\cos\tau\right)e^{-j\alpha} \end{bmatrix} \hat{y}$$

$$= A \begin{bmatrix} \left(j\cos\phi\sin\tau - \sin\phi\cos\tau\right)e^{-j\alpha} \\ \left(j\sin\phi\sin\tau + \cos\phi\cos\tau\right)e^{-j\alpha} \end{bmatrix}$$

$$= A \begin{bmatrix} \left(j\cos\phi\sin\tau - \sin\phi\cos\tau\right)e^{-j\alpha} & -\left(\cos\phi\cos\tau - j\sin\phi\sin\tau\right)e^{+j\alpha} \\ \left(j\sin\phi\sin\tau + \cos\phi\cos\tau\right)e^{-j\alpha} & -\left(\sin\phi\cos\tau + j\cos\phi\sin\tau\right)e^{+j\alpha} \end{bmatrix} \hat{x}$$

$$= A \begin{bmatrix} j\cos\phi\sin\tau - \sin\phi\cos\tau & -\cos\phi\cos\tau + j\sin\phi\sin\tau \\ j\sin\phi\sin\tau + \cos\phi\cos\tau & -\sin\phi\cos\tau - j\cos\phi\sin\tau \end{bmatrix} \begin{bmatrix} e^{-j\alpha} & 0 \\ 0 & e^{+j\alpha} \end{bmatrix} \hat{x}$$

$$= A \begin{bmatrix} -\sin\phi & -\cos\phi \\ \cos\phi & -\sin\phi \end{bmatrix} \begin{bmatrix} \cos\tau & -j\sin\tau \\ -j\sin\tau & \cos\tau \end{bmatrix} \begin{bmatrix} e^{-j\alpha} & 0 \\ 0 & e^{+j\alpha} \end{bmatrix} \hat{x}$$

$$= A \begin{bmatrix} \cos\left(\phi + \frac{\pi}{2}\right) & -\sin\left(\phi + \frac{\pi}{2}\right) \\ \sin\left(\phi + \frac{\pi}{2}\right) & \cos\left(\phi + \frac{\pi}{2}\right) \end{bmatrix} \begin{bmatrix} \cos\left(-\tau\right) & j\sin\left(-\tau\right) \\ j\sin\left(-\tau\right) & \cos\left(-\tau\right) \end{bmatrix} \begin{bmatrix} e^{+j(-\alpha)} & 0 \\ 0 & e^{-j(-\alpha)} \end{bmatrix} \hat{x}$$

$$= A U_{2\phi}\left(\phi + \frac{\pi}{2}\right) U_{2\tau}\left(-\tau\right) U_{2\alpha}\left(-\alpha\right) \hat{x}$$

$$\text{(285)} \qquad = A U_2 \left(\phi + \frac{\pi}{2}, -\tau, -\alpha\right) \hat{x}$$

Two unit Jones vectors $\underline{\boldsymbol{u}}$ and $\underline{\boldsymbol{u}}_{\perp}$ form an elliptical polarization basis if they result from the transformation of the Cartesian $(\hat{x}, \hat{y})$ basis with

$$\underline{\boldsymbol{u}} = U_2\left(\phi, \tau, \alpha\right)\hat{x} \quad \text{and} \quad \underline{\boldsymbol{u}}_{\perp} = U_2\left(\phi, \tau, \alpha\right)\hat{y}$$

(286)   or similarly

$$\underline{\boldsymbol{u}} = U_2\left(\phi, \tau, \alpha\right)\hat{x} \quad \text{and} \quad \underline{\boldsymbol{u}}_{\perp} = U_2\left(\phi + \frac{\pi}{2}, -\tau, -\alpha\right)\hat{x}$$

We now have a framework to transform the polarization of a return, say collected at horizontal and vertical polarization states, to any desired polarization basis.

Any general return can be interpreted in the general orthogonal Jones vector basis $(\hat{\boldsymbol{u}}, \hat{\boldsymbol{u}}_{\perp})$.

(287) $$\underline{\boldsymbol{E}}_{(\hat{\boldsymbol{u}}, \hat{\boldsymbol{u}}_{\perp})} = E_u\hat{\boldsymbol{u}} + E_{u_{\perp}}\hat{\boldsymbol{u}}_{\perp}$$

We know that any unit Jones vector is some $U_2\left(\phi, \tau, \alpha\right)$ transformation of the horizontal unit Jones vector $\hat{x}$. Therefore, the transformation from the general Jones vector basis $(\hat{\boldsymbol{u}}, \hat{\boldsymbol{u}}_{\perp})$ into the Cartesian basis $(\hat{x}, \hat{y})$ is as follows:

$$\underline{\boldsymbol{E}}_{(\hat{\boldsymbol{u}}, \hat{\boldsymbol{u}}_{\perp})} = E_u\hat{\boldsymbol{u}} + E_{u_{\perp}}\hat{\boldsymbol{u}}_{\perp} = E_u\underbrace{U_2\left(\phi, \tau, \alpha\right)\hat{x}}_{\hat{\boldsymbol{u}}} + E_{u_{\perp}}\underbrace{U_2\left(\phi, \tau, \alpha\right)\hat{y}}_{\hat{\boldsymbol{u}}_{\perp}}$$

$$= \underbrace{E_uU_2\left(\phi, \tau, \alpha\right)}_{E_x}\hat{x} + \underbrace{E_{u_{\perp}}U_2\left(\phi, \tau, \alpha\right)}_{E_y}\hat{y}$$

(288) $$= E_x\hat{x} + E_y\hat{y} = \underline{\boldsymbol{E}}_{(\hat{x}, \hat{y})}$$

From (288) we see that

$$E_uU_2\left(\phi, \tau, \alpha\right) = E_x$$

(289) $$E_{u_{\perp}}U_2\left(\phi, \tau, \alpha\right) = E_y$$

83

Which can be written as

$$(290) \qquad \begin{bmatrix} E_u \\ E_{u_\perp} \end{bmatrix} U_2\left(\phi, \tau, \alpha\right) = \begin{bmatrix} E_x \\ E_y \end{bmatrix}$$

and

$$(291) \qquad \begin{bmatrix} E_u \\ E_{u_\perp} \end{bmatrix} = U_2\left(\phi, \tau, \alpha\right)^{-1} \begin{bmatrix} E_x \\ E_y \end{bmatrix}$$

$$U_2\left(\phi, \tau, \alpha\right)^{-1} = \left(U_{2\phi}\left(\phi\right) U_{2\tau}\left(\tau\right) U_{2\alpha}\left(\alpha\right)\right)^{-1}$$

$$= U_{2\alpha}\left(\alpha\right)^{-1} U_{2\tau}\left(\tau\right)^{-1} U_{2\phi}\left(\phi\right)^{-1}$$

$$= \begin{bmatrix} e^{+j\alpha} & 0 \\ 0 & e^{-j\alpha} \end{bmatrix}^{-1} \begin{bmatrix} \cos\tau & j\sin\tau \\ j\sin\tau & \cos\tau \end{bmatrix}^{-1} \begin{bmatrix} \cos\phi & -\sin\phi \\ \sin\phi & \cos\phi \end{bmatrix}^{-1}$$

$$= \begin{bmatrix} e^{-j\alpha} & 0 \\ 0 & e^{+j\alpha} \end{bmatrix} \begin{bmatrix} \cos\tau & -j\sin\tau \\ -j\sin\tau & \cos\tau \end{bmatrix} \begin{bmatrix} \cos\phi & \sin\phi \\ -\sin\phi & \cos\phi \end{bmatrix}$$

$$= \begin{bmatrix} e^{+j(-\alpha)} & 0 \\ 0 & e^{-j(-\alpha)} \end{bmatrix} \begin{bmatrix} \cos\left(-\tau\right) & j\sin\left(-\tau\right) \\ j\sin\left(-\tau\right) & \cos\left(-\tau\right) \end{bmatrix} \begin{bmatrix} \cos\left(-\phi\right) & -\sin\left(-\phi\right) \\ \sin\left(-\phi\right) & \cos\left(-\phi\right) \end{bmatrix}$$

$$= \begin{bmatrix} \cos\left(-\phi\right) & -\sin\left(-\phi\right) \\ \sin\left(-\phi\right) & \cos\left(-\phi\right) \end{bmatrix} \begin{bmatrix} \cos\left(-\tau\right) & j\sin\left(-\tau\right) \\ j\sin\left(-\tau\right) & \cos\left(-\tau\right) \end{bmatrix} \begin{bmatrix} e^{+j(-\alpha)} & 0 \\ 0 & e^{-j(-\alpha)} \end{bmatrix}$$

$$= U_{2\phi}\left(-\phi\right) U_{2\tau}\left(-\tau\right) U_{2\alpha}\left(-\alpha\right)$$

$$(292) \qquad = U_2\left(-\phi, -\tau, -\alpha\right)$$

Therefore, to change a Jones vector's polarization basis from $(\hat{x}, \hat{y})$ to a general basis $(\hat{u}, \hat{u}_{\perp})$ defined by elliptical parameters ϕ, τ, and α is as follows:

$$(293) \qquad \begin{bmatrix} E_u \\ E_{u_{\perp}} \end{bmatrix} = U_2 \left(-\phi, -\tau, -\alpha \right) \begin{bmatrix} E_x \\ E_y \end{bmatrix}.$$
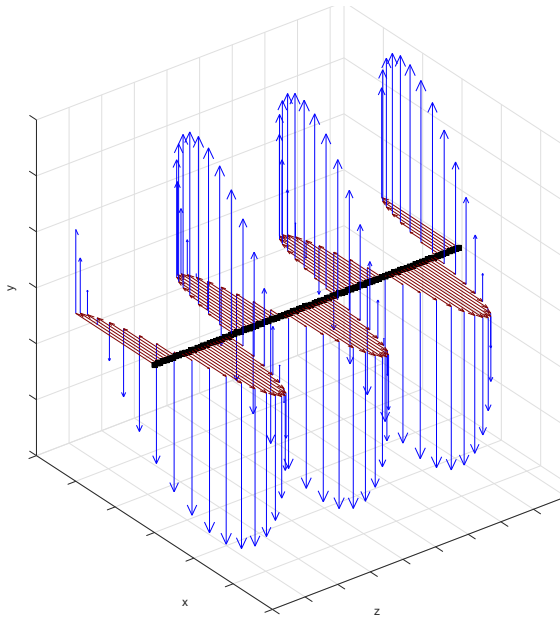
(A) E_{0x} (red) and E_{0y} (blue)
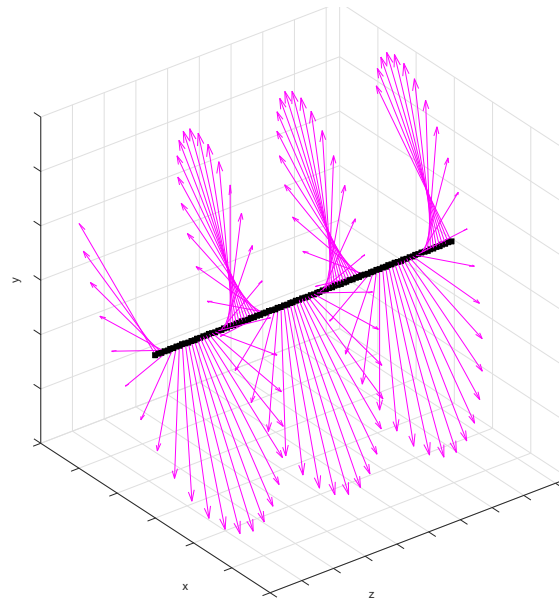
(B) $\sqrt{(E_{0x})^2 + (E_{0y})^2}$
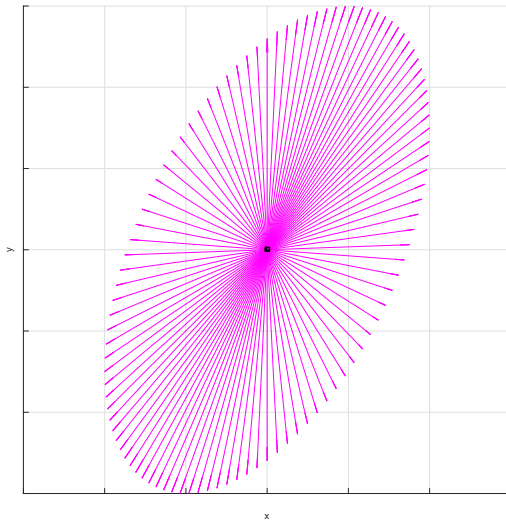
(C) $\sqrt{(E_{0x})^2 + (E_{0y})^2}$ along the $\hat{z}$ direction
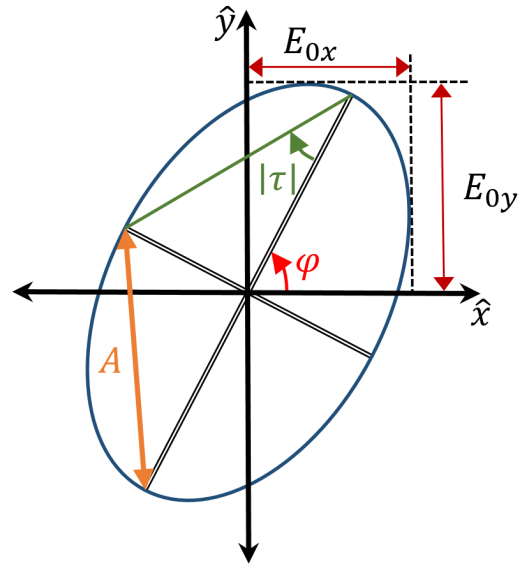
(D) Diagram of ellipse parameters

FIGURE A.1. Polarization Ellipse

PARTIAL DERIVATIVES

The following are the first and second partial derivatives of Chen's objective function as well as the proposed objective function that includes $\mathbf{Im}\{\beta\}$, in order to analyze the Hessian. The values of the coherency matrix, $T_{11}, T_{12}, T_{13}, T_{22}, T_{23}, T_{33}$, are determined by the data, and the values for the volumetric scattering matrix, a, b, c, d, e, f, are set according to the scattering models in (57)-(59), (149), and (201). The Chen partial derivatives will be in black and the additions due to $\mathbf{Im}\{\beta\}$ will be in blue. Also, note that the Hessian is symmetric, which is to say $\frac{\partial^2 F}{\partial A \partial B} = \frac{\partial^2 F}{\partial B \partial A}$. So there is only a need to solve for the upper triangular portion of the Hessian. The notation $\frac{\partial^2 F}{\partial f_{\mathrm{s}} \partial []}$ refers to the family of second partial derivatives where the first partial derivative is with respect to f_{s}.

B.1. PARTIAL DERIVATIVES OF $\frac{\partial F}{\partial FS}$

The first partial derivative of the objective function with respect to f_{s} is

$$
\begin{aligned}
\frac{\partial F}{\partial fs} = &-2\left(T_{11} - f_{\mathrm{s}} - f_{\mathrm{d}}|\alpha|^2 - a\,f_{\mathrm{v}}\right) \dots \\
&- 2|\beta|^2 \cos^2\left(2\theta_{\mathrm{odd}}\right)\left(T_{22} - f_{\mathrm{s}}|\beta|^2 \cos^2\left(2\theta_{\mathrm{odd}}\right) - f_{\mathrm{d}} \cos^2\left(2\theta_{\mathrm{dbl}}\right) - b\,f_{\mathrm{v}} - \frac{f_{\mathrm{c}}}{2}\right)\dots \\
&- 2|\beta|^2 \sin^2\left(2\theta_{\mathrm{odd}}\right)\left(T_{33} - f_{\mathrm{s}}|\beta|^2 \sin^2\left(2\theta_{\mathrm{odd}}\right) - f_{\mathrm{d}} \sin^2\left(2\theta_{\mathrm{dbl}}\right) - c\,f_{\mathrm{v}} - \frac{f_{\mathrm{c}}}{2}\right)\dots \\
&- 2\mathbf{Re}\{\beta\}\cos\left(2\theta_{\mathrm{odd}}\right)\Bigg(\mathbf{Re}\{T_{12}\} - f_{\mathrm{s}}\mathbf{Re}\{\beta\}\cos\left(2\theta_{\mathrm{odd}}\right) - \dots \\
&\qquad f_{\mathrm{d}}\mathbf{Re}\{\alpha\}\cos\left(2\theta_{\mathrm{dbl}}\right) - \mathbf{Re}\{d\}\,f_{\mathrm{v}}\Bigg)\dots \\
&+ 2\mathbf{Re}\{\beta\}\sin\left(2\theta_{\mathrm{odd}}\right)\Bigg(\mathbf{Re}\{T_{13}\} + f_{\mathrm{s}}\mathbf{Re}\{\beta\}\sin\left(2\theta_{\mathrm{odd}}\right) \dots \\
&\qquad + f_{\mathrm{d}}\mathbf{Re}\{\alpha\}\sin\left(2\theta_{\mathrm{dbl}}\right) - \mathbf{Re}\{e\}\,f_{\mathrm{v}}\Bigg)\dots \\
&+ |\beta|^2 \sin\left(4\theta_{\mathrm{odd}}\right)\left(\mathbf{Re}\{T_{23}\} + \frac{f_{\mathrm{s}}}{2}|\beta|^2 \sin\left(4\theta_{\mathrm{odd}}\right) + \frac{f_{\mathrm{d}}}{2}\sin\left(4\theta_{\mathrm{dbl}}\right) - \mathbf{Re}\{f\}\,f_{\mathrm{v}}\right)\dots \\
&+ 2\mathbf{Im}\{\beta\}\cos\left(2\theta_{\mathrm{odd}}\right)\Bigg(\mathbf{Im}\{T_{12}\} + f_{\mathrm{s}}\mathbf{Im}\{\beta\}\cos\left(2\theta_{\mathrm{odd}}\right) - \dots
\end{aligned}
$$

$$f_{\mathrm{d}}\mathbf{Im}\left\{\alpha\right\}\cos\left(2\theta_{\mathrm{dbl}}\right) - \mathbf{Im}\left\{d\right\}f_{\mathrm{v}}\Bigg) \ldots$$

$$-2\mathbf{Im}\left\{\beta\right\}\sin\left(2\theta_{\mathrm{odd}}\right)\left(\mathbf{Im}\left\{T_{13}\right\} - f_{\mathrm{s}}\mathbf{Im}\left\{\beta\right\}\sin\left(2\theta_{\mathrm{odd}}\right) + \ldots\right.$$

$$(294) \qquad\qquad f_{\mathrm{d}}\mathbf{Im}\left\{\alpha\right\}\sin\left(2\theta_{\mathrm{dbl}}\right) - \mathbf{Im}\left\{e\right\}f_{\mathrm{v}}).$$

The second partial derivatives of the form $\frac{\partial^2 F}{\partial f_{\mathrm{s}}\partial []}$ that form the first row of the Hessian are as follows:

$$(295) \qquad\qquad \frac{\partial^2 F}{\partial f_{\mathrm{s}}^2} = \frac{1}{4}\left(|\beta|^4\left(7 + \cos\left(8\theta_{\mathrm{odd}}\right)\right) + 8\left(1 + |\beta|^2\right)\right)$$

$$\frac{\partial^2 F}{\partial f_{\mathrm{s}}\partial f_{\mathrm{d}}} = 2|\alpha|^2 + \frac{|\beta|^2}{4}\left(4 + 3\cos\left(4\left(\theta_{\mathrm{dbl}} - \theta_{\mathrm{odd}}\right)\right) + \cos\left(4\left(\theta_{\mathrm{dbl}} + \theta_{\mathrm{odd}}\right)\right)\right) \ldots$$

$$(296) \qquad\qquad + 2\cos\left(2\left(\theta_{\mathrm{dbl}} - \theta_{\mathrm{odd}}\right)\right)\left(-\mathbf{Im}\left\{\alpha\right\}\mathbf{Im}\left\{\beta\right\} + \mathbf{Re}\left\{\alpha\right\}\mathbf{Re}\left\{\beta\right\}\right)$$

$$\frac{\partial^2 F}{\partial f_{\mathrm{s}}\partial f_{\mathrm{v}}} = 2\left(a + \mathbf{Im}\left\{\beta\right\}\left(-\cos\left(2\theta_{\mathrm{odd}}\right)\mathbf{Im}\left\{d\right\} + \mathbf{Im}\left\{e\right\}\sin\left(2\theta_{\mathrm{odd}}\right)\right)\right) \ldots$$

$$+ \mathbf{Re}\left\{\beta\right\}\left(\cos\left(2\theta_{\mathrm{odd}}\right)\mathbf{Re}\left\{d\right\} - \mathbf{Re}\left\{e\right\}\sin\left(2\theta_{\mathrm{odd}}\right)\right)\Bigg) \ldots$$

$$(297) \qquad\qquad + |\beta|^2\left(b + c + (b - c)\cos\left(4\theta_{\mathrm{odd}}\right) - \mathbf{Re}\left\{f\right\}\sin\left(4\theta_{\mathrm{odd}}\right)\right)$$

$$(298) \qquad\qquad\qquad \frac{\partial^2 F}{\partial f_{\mathrm{s}}\partial f_{\mathrm{c}}} = |\beta|^2$$

$$\frac{\partial^2 F}{\partial f_{\mathrm{s}}\partial \theta_{\mathrm{odd}}} = 4\mathbf{Im}\left\{\beta\right\}\left(f_{\mathrm{v}}\cos\left(2\theta_{\mathrm{odd}}\right)\mathbf{Im}\left\{e\right\} - \cos\left(2\theta_{\mathrm{odd}}\right)\mathbf{Im}\left\{T_{13}\right\} \ldots\right.$$

$$-f_{\mathrm{d}}\mathbf{Im}\left\{\alpha\right\}\sin\left(2\left(\theta_{\mathrm{dbl}}-\theta_{\mathrm{odd}}\right)\right)+f_{\mathrm{v}}\mathbf{Im}\left\{d\right\}\sin\left(2\theta_{\mathrm{odd}}\right)-\mathbf{Im}\left\{T_{12}\right\}\sin\left(2\theta_{\mathrm{odd}}\right)\Bigg)\dots$$

$$+4\mathbf{Re}\left\{\beta\right\}\Bigg(-f_{\mathrm{v}}\cos\left(2\theta_{\mathrm{odd}}\right)\mathbf{Re}\left\{e\right\}+\cos\left(2\theta_{\mathrm{odd}}\right)\mathbf{Re}\left\{T_{13}\right\}\dots$$

$$+f_{\mathrm{d}}\mathbf{Re}\left\{\alpha\right\}\sin\left(2\left(\theta_{\mathrm{dbl}}-\theta_{\mathrm{odd}}\right)\right)-f_{\mathrm{v}}\mathbf{Re}\left\{d\right\}\sin\left(2\theta_{\mathrm{odd}}\right)+\mathbf{Re}\left\{T_{12}\right\}\sin\left(2\theta_{\mathrm{odd}}\right)\Bigg)\dots$$

$$-|\beta|^{2}\Bigg(4f_{\mathrm{v}}\cos\left(4\theta_{\mathrm{odd}}\right)\mathbf{Re}\left\{f\right\}-4\cos\left(4\theta_{\mathrm{odd}}\right)\mathbf{Re}\left\{T_{23}\right\}\dots$$

$$-3f_{\mathrm{d}}\sin\left(4\left(\theta_{\mathrm{dbl}}-\theta_{odd}\right)\right)+4bf_{\mathrm{v}}\sin\left(4\theta_{\mathrm{odd}}\right)-4cf_{\mathrm{v}}\sin\left(4\theta_{\mathrm{odd}}\right)\dots$$

$$(299)\qquad-4T_{22}\sin\left(4\theta_{\mathrm{odd}}\right)+4T_{33}\sin\left(4\theta_{\mathrm{odd}}\right)+2f_{\mathrm{s}}|\beta|^{2}\sin\left(8\theta_{\mathrm{odd}}\right)+f_{\mathrm{d}}\sin\left(4\left(\theta_{\mathrm{dbl}}+\theta_{\mathrm{odd}}\right)\right)\Bigg)$$

$$(300)\qquad
\begin{aligned}
\frac{\partial^{2}F}{\partial f_{\mathrm{s}}\partial\theta_{\mathrm{dbl}}} &= -f_{\mathrm{d}}\Bigg(4\left(-\mathbf{Im}\left\{\alpha\right\}\mathbf{Im}\left\{\beta\right\}+\mathbf{Re}\left\{\alpha\right\}\mathbf{Re}\left\{\beta\right\}\right)\sin\left(2\left(\theta_{\mathrm{dbl}}-\theta_{\mathrm{odd}}\right)\right)\dots\\
&\quad+|\beta|^{2}\left(3\sin\left(4\left(\theta_{\mathrm{dbl}}-\theta_{\mathrm{odd}}\right)\right)+\sin\left(4\left(\theta_{\mathrm{dbl}}+\theta_{\mathrm{odd}}\right)\right)\right)\Bigg)
\end{aligned}$$

$$(301)\qquad\frac{\partial^{2}F}{\partial f_{\mathrm{s}}\partial\mathbf{Re}\left\{\alpha\right\}}=2f_{\mathrm{d}}\Bigg(2\mathbf{Re}\left\{\alpha\right\}+\mathbf{Re}\left\{\beta\right\}\cos\left(2\left(\theta_{\mathrm{dbl}}-\theta_{\mathrm{odd}}\right)\right)\Bigg)$$

$$(302)\qquad\frac{\partial^{2}F}{\partial f_{\mathrm{s}}\partial\mathbf{Im}\left\{\alpha\right\}}=4\mathbf{Im}\left\{\alpha\right\}f_{\mathrm{d}}-2\mathbf{Im}\left\{\beta\right\}f_{\mathrm{d}}\cos\left(2\left(\theta_{\mathrm{dbl}}-\theta_{\mathrm{odd}}\right)\right)$$

$$
\begin{aligned}
\frac{\partial^{2}F}{\partial f_{\mathrm{s}}\partial\mathbf{Re}\left\{\beta\right\}} &= 2\mathbf{Re}\left\{\beta\right\}f_{\mathrm{c}}+2\mathbf{Re}\left\{\beta\right\}f_{\mathrm{d}}+4\mathbf{Re}\left\{\beta\right\}f_{\mathrm{s}}+7\left(\mathbf{Im}\left\{\beta\right\}\right)^{2}\mathbf{Re}\left\{\beta\right\}f_{\mathrm{s}}\dots\\
&\quad+7\left(\mathbf{Re}\left\{\beta\right\}\right)^{3}f_{\mathrm{s}}+2b\mathbf{Re}\left\{\beta\right\}f_{\mathrm{v}}+2c\mathbf{Re}\left\{\beta\right\}f_{\mathrm{v}}-2\mathbf{Re}\left\{\beta\right\}T_{22}\dots\\
&\quad-2\mathbf{Re}\left\{\beta\right\}T_{33}+\frac{3}{2}\mathbf{Re}\left\{\beta\right\}f_{\mathrm{d}}\cos\left(4\left(\theta_{\mathrm{dbl}}-\theta_{\mathrm{odd}}\right)\right)\dots
\end{aligned}$$

$$+ 2\mathbf{Re}\left\{\alpha\right\} f_\mathrm{d} \cos\left(2\left(\theta_\mathrm{dbl} - \theta_\mathrm{odd}\right)\right) + 2b\mathbf{Re}\left\{\beta\right\} f_\mathrm{v} \cos\left(4\theta_\mathrm{odd}\right)\ldots$$

$$- 2c\mathbf{Re}\left\{\beta\right\} f_\mathrm{v} \cos\left(4\theta_\mathrm{odd}\right) + \left(\mathbf{Im}\left\{\beta\right\}\right)^2 \mathbf{Re}\left\{\beta\right\} f_\mathrm{s} \cos\left(8\theta_\mathrm{odd}\right)\ldots$$

$$+ \left(\mathbf{Re}\left\{\beta\right\}\right)^3 f_\mathrm{s} \cos\left(8\theta_\mathrm{odd}\right) + \frac{1}{2}\mathbf{Re}\left\{\beta\right\} f_\mathrm{d} \cos\left(4\left(\theta_\mathrm{dbl} - \theta_\mathrm{odd}\right)\right)\ldots$$

$$+ 2 f_\mathrm{v} \cos\left(2\theta_\mathrm{odd}\right) \mathbf{Re}\left\{d\right\} - 2\cos\left(2\theta_\mathrm{odd}\right) \mathbf{Re}\left\{T_{12}\right\}\ldots$$

$$- 2 f_\mathrm{v} \mathbf{Re}\left\{e\right\} \sin\left(2\theta_\mathrm{odd}\right) + 2\mathbf{Re}\left\{T_{13}\right\} \sin\left(2\theta_\mathrm{odd}\right)\ldots$$

(303)
$$- 2\mathbf{Re}\left\{\beta\right\} f_\mathrm{v} \mathbf{Re}\left\{f\right\} \sin\left(4\theta_\mathrm{odd}\right) + 2\mathbf{Re}\left\{\beta\right\} \mathbf{Re}\left\{T_{23}\right\} \sin\left(4\theta_\mathrm{odd}\right)$$

$$\frac{\partial^2 F}{\partial f_\mathrm{s} \partial \mathbf{Im}\left\{\beta\right\}} = 2\mathbf{Im}\left\{\beta\right\} f_\mathrm{c} + 2\mathbf{Im}\left\{\beta\right\} f_\mathrm{d} + 4\mathbf{Im}\left\{\beta\right\} f_\mathrm{s} + 7\left(\mathbf{Im}\left\{\beta\right\}\right)^3 f_\mathrm{s}\ldots$$

$$+ 7\mathbf{Im}\left\{\beta\right\} \left(\mathbf{Re}\left\{\beta\right\}\right)^2 f_\mathrm{s} + 2b\mathbf{Im}\left\{\beta\right\} f_\mathrm{v} + 2c\mathbf{Im}\left\{\beta\right\} f_\mathrm{v}\ldots$$

$$- 2\mathbf{Im}\left\{\beta\right\} T_{22} - 2\mathbf{Im}\left\{\beta\right\} T_{33} + \frac{3}{2}\mathbf{Im}\left\{\beta\right\} f_\mathrm{d} \cos\left(4\left(\theta_\mathrm{dbl} - \theta_\mathrm{odd}\right)\right)\ldots$$

$$- 2\mathbf{Im}\left\{\alpha\right\} f_\mathrm{d} \cos\left(2\left(\theta_\mathrm{dbl} - \theta_\mathrm{odd}\right)\right) + 2b\mathbf{Im}\left\{\beta\right\} f_\mathrm{v} \cos\left(4\theta_\mathrm{odd}\right)\ldots$$

$$- 2c\mathbf{Im}\left\{\beta\right\} f_\mathrm{v} \cos\left(4\theta_\mathrm{odd}\right) - 2\mathbf{Im}\left\{\beta\right\} T_{22} \cos\left(4\theta_\mathrm{odd}\right)\ldots$$

$$+ 2\mathbf{Im}\left\{\beta\right\} T_{33} \cos\left(4\theta_\mathrm{odd}\right) + \left(\mathbf{Im}\left\{\beta\right\}\right)^3 f_\mathrm{s} \cos\left(8\theta_\mathrm{odd}\right)\ldots$$

$$+ \mathbf{Im}\left\{\beta\right\} \left(\mathbf{Re}\left\{\beta\right\}\right)^2 f_\mathrm{s} \cos\left(8\theta_\mathrm{odd}\right) + \frac{1}{2}\mathbf{Im}\left\{\beta\right\} f_\mathrm{d} \cos\left(4\left(\theta_\mathrm{dbl} - \theta_\mathrm{odd}\right)\right)\ldots$$

$$- 2 f_\mathrm{v} \cos\left(2\theta_\mathrm{odd}\right) \mathbf{Im}\left\{d\right\} + 2\cos\left(\theta_\mathrm{odd}\right) \mathbf{Im}\left\{T_{12}\right\} + 2 f_\mathrm{v} \mathbf{Im}\left\{e\right\} \sin\left(2\theta_\mathrm{odd}\right)\ldots$$

$$- 2\mathbf{Im}\left\{T_{13}\right\} \sin\left(2\theta_\mathrm{odd}\right) - 2\mathbf{Im}\left\{\beta\right\} f_\mathrm{v} \mathbf{Re}\left\{f\right\} \sin\left(\theta_\mathrm{odd}\right)\ldots$$

(304)
$$+ 2\mathbf{Im}\left\{\beta\right\} \mathbf{Re}\left\{T_{23}\right\} \sin\left(4\theta_\mathrm{odd}\right)$$

The first partial derivative of the objective function with respect to f_d is

$$
\begin{aligned}
\frac{\partial F}{\partial f\mathrm{d}} = {}& -2|\alpha|^2 \left(T_{11} - f_\mathrm{s} - f_\mathrm{d}|\alpha|^2 - a\,f_\mathrm{v} \right) \ldots \\
& - 2\cos^2\left(2\theta_\mathrm{dbl}\right) \left(T_{22} - f_\mathrm{s}|\beta|^2 \cos^2\left(2\theta_\mathrm{odd}\right) - f_\mathrm{d}\cos^2\left(2\theta_{dbl}\right) - b\,f_\mathrm{v} - \frac{f_\mathrm{c}}{2} \right) \ldots \\
& - 2\sin^2\left(2\theta_\mathrm{dbl}\right) \left(T_{33} - f_\mathrm{s}|\beta|^2 \sin^2\left(2\theta_\mathrm{odd}\right) - f_\mathrm{d}\sin^2\left(2\theta_{dbl}\right) - c\,f_\mathrm{v} - \frac{f_\mathrm{c}}{2} \right) \ldots \\
& - 2\mathbf{Re}\left\{\alpha\right\}\cos\left(2\theta_\mathrm{dbl}\right) \left(\mathbf{Re}\left\{T_{12}\right\} - f_\mathrm{s}\mathbf{Re}\left\{\beta\right\}\cos\left(2\theta_\mathrm{odd}\right) \ldots \right. \\
& \qquad \left. - f_\mathrm{d}\mathbf{Re}\left\{\alpha\right\}\cos\left(2\theta_\mathrm{dbl}\right) - f_\mathrm{v}\mathbf{Re}\left\{d\right\} \right) \ldots \\
& + 2\mathbf{Re}\left\{\alpha\right\}\sin\left(2\theta_\mathrm{dbl}\right) \left(\mathbf{Re}\left\{T_{13}\right\} + f_\mathrm{s}\mathbf{Re}\left\{\beta\right\}\sin\left(2\theta_\mathrm{odd}\right) \ldots \right. \\
& \qquad \left. + f_\mathrm{d}\mathbf{Re}\left\{\alpha\right\}\sin\left(2\theta_\mathrm{dbl}\right) - f_\mathrm{v}\mathbf{Re}\left\{e\right\} \right) \ldots \\
& + \sin\left(4\theta_\mathrm{dbl}\right) \left(\mathbf{Re}\left\{T_{23}\right\} + \frac{f_\mathrm{s}}{2}|\beta|^2 \sin\left(\theta_\mathrm{odd}\right) + \frac{f_\mathrm{d}}{2}\sin\left(4\theta_\mathrm{dbl}\right) - f_\mathrm{v}\mathbf{Re}\left\{f\right\} \right) \ldots \\
& - 2\mathbf{Im}\left\{\alpha\right\}\cos\left(2\theta_\mathrm{dbl}\right) \left(\mathbf{Im}\left\{T_{12}\right\} + f_\mathrm{s}\mathbf{Im}\left\{\beta\right\}\cos\left(2\theta_\mathrm{odd}\right) \ldots \right. \\
& \qquad \left. - f_\mathrm{d}\mathbf{Im}\left\{\alpha\right\}\cos\left(\theta_\mathrm{dbl}\right) - f_\mathrm{v}\mathbf{Im}\left\{d\right\} \right) \ldots \\
& + 2\mathbf{Im}\left\{\alpha\right\}\sin\left(2\theta_\mathrm{dbl}\right) \left(\mathbf{Im}\left\{T_{13}\right\} - f_\mathrm{s}\mathbf{Im}\left\{\beta\right\}\sin\left(2\theta_\mathrm{odd}\right) \ldots \right. \\
& \qquad \left. + f_\mathrm{d}\mathbf{Im}\left\{\alpha\right\}\sin\left(\theta_\mathrm{dbl}\right) - f_\mathrm{v}\mathbf{Im}\left\{e\right\} \right).
\end{aligned}
$$

(305)

The second partial derivatives of the form $\frac{\partial^2 F}{\partial f_\mathrm{d}\partial[]}$ that form the second row of the Hessian are as follows:

(306)
$$
\frac{\partial^2 F}{\partial f_\mathrm{d}^2} = \frac{1}{4}\left(7 + 8|\alpha|^4 + \cos\left(8\theta_\mathrm{dbl}\right) + 8|\alpha|^2 \right)
$$

$$\frac{\partial^2 F}{\partial f_{\mathrm{d}} \partial f_{\mathrm{v}}} = b + c + 2a|\alpha|^2 + b\cos(4\theta_{\mathrm{dbl}}) - c\cos(4\theta_{\mathrm{dbl}}) + 2\cos(2\theta_{\mathrm{dbl}})\,\mathbf{Re}\,\{\alpha\}\,\mathbf{Re}\,\{d\}\ldots$$

$$- 2\mathbf{Re}\,\{\alpha\}\,\mathbf{Re}\,\{e\}\sin(2\theta_{\mathrm{dbl}}) + 2\mathbf{Im}\,\{\alpha\}\left(\cos(2\theta_{\mathrm{dbl}})\,\mathbf{Im}\,\{d\} - \mathbf{Im}\,\{e\}\sin(2\theta_{\mathrm{dbl}})\right)\ldots$$

$$(307) \qquad - \mathbf{Re}\,\{f\}\sin(\theta_{\mathrm{dbl}})$$

$$(308) \qquad\qquad \frac{\partial^2 F}{\partial f_{\mathrm{d}} \partial f_{\mathrm{c}}} = 1$$

$$\frac{\partial^2 F}{\partial f_{\mathrm{d}} \partial \theta_{\mathrm{odd}}} = f_{\mathrm{s}}\left(4\left(\mathbf{Re}\,\{\alpha\}\,\mathbf{Re}\,\{\beta\} - \mathbf{Im}\,\{\alpha\}\,\mathbf{Im}\,\{\beta\}\right)\sin\left(2\left(\theta_{\mathrm{dbl}} - \theta_{\mathrm{odd}}\right)\right)\ldots\right.$$

$$(309) \qquad\qquad \left. + |\beta|^2\left(3\sin(4\theta_{\mathrm{dbl}} - 4\theta_{\mathrm{odd}}) - \sin(4\theta_{\mathrm{dbl}} + 4\theta_{\mathrm{odd}})\right)\right)$$

$$\frac{\partial^2 F}{\partial f_{\mathrm{d}} \partial \theta_{\mathrm{dbl}}} = -4f_{\mathrm{v}}\cos(4\theta_{\mathrm{dbl}})\,\mathbf{Re}\,\{f\} + 4\cos(4\theta_{\mathrm{dbl}})\,\mathbf{Re}\,\{T_{23}\}\ldots$$

$$- 4bf_{\mathrm{v}}\sin(4\theta_{\mathrm{dbl}}) + 4cf_{\mathrm{v}}\sin(4\theta_{\mathrm{dbl}}) + 4T_{22}\sin(4\theta_{\mathrm{dbl}})\ldots$$

$$- 4T_{33}\sin(4\theta_{\mathrm{dbl}}) - 2f_{\mathrm{d}}\sin(8\theta_{\mathrm{dbl}}) - 3f_{\mathrm{s}}|\beta|^2\sin(4\theta_{\mathrm{dbl}} - 4\theta_{\mathrm{odd}})\ldots$$

$$+ 4\mathbf{Im}\,\{\alpha\}\left(\cos(2\theta_{\mathrm{dbl}})\,\mathbf{Im}\,\{T_{13}\} - f_{\mathrm{v}}\cos(2\theta_{\mathrm{dbl}})\,\mathbf{Im}\,\{e\} - f_{\mathrm{v}}\mathbf{Im}\,\{d\}\sin(2\theta_{\mathrm{dbl}})\ldots\right.$$

$$\left. + \mathbf{Im}\,\{T_{12}\}\sin(2\theta_{\mathrm{dbl}}) + f_{\mathrm{s}}\mathbf{Im}\,\{\beta\}\sin(2\theta_{\mathrm{dbl}} - 2\theta_{\mathrm{odd}})\right)\ldots$$

$$- 4\mathbf{Re}\,\{\alpha\}\left(f_{\mathrm{v}}\cos(2\theta_{\mathrm{dbl}})\,\mathbf{Im}\,\{e\} - \cos(2\theta_{\mathrm{dbl}})\,\mathbf{Re}\,\{T_{13}\} + f_{\mathrm{v}}\mathbf{Re}\,\{d\}\sin(2\theta_{\mathrm{dbl}})\ldots\right.$$

$$\left. - \mathbf{Re}\,\{T_{12}\}\sin(2\theta_{\mathrm{dbl}}) + f_{\mathrm{s}}\mathbf{Re}\,\{\beta\}\sin(2\theta_{\mathrm{dbl}} - 2\theta_{\mathrm{dbl}})\right)\ldots$$

$$(310) \qquad - f_{\mathrm{s}}|\beta|^2\sin(4\theta_{\mathrm{dbl}} + 4\theta_{\mathrm{odd}})$$

$$\frac{\partial^2 F}{\partial f_\mathrm{d} \partial \mathbf{Re}\{\alpha\}} = 4\mathbf{Re}\{\alpha\}\,|\alpha|^2 f_\mathrm{d} + 4\mathbf{Re}\{\alpha\}\left(|\alpha|^2 f_\mathrm{d} + f_\mathrm{s} + a\,f_\mathrm{v} - T_{11}\right) + 2\mathbf{Re}\{\alpha\}\,f_\mathrm{d}\ldots$$

$$+\,2\cos\left(2\theta_\mathrm{dbl}\right)\Big(\mathbf{Re}\{\alpha\}\,f_\mathrm{d}\cos\left(2\theta_\mathrm{dbl}\right)\ldots$$

$$+\,\mathbf{Re}\{\beta\}\,f_\mathrm{s}\cos\left(2\theta_\mathrm{odd}\right) + f_\mathrm{v}\mathbf{Re}\{d\} - \mathbf{Re}\{T_{12}\}\Big)\ldots$$

$$+\,2\sin\left(2\theta_\mathrm{dbl}\right)\Big(\mathbf{Re}\{T_{13}\} - f_\mathrm{v}\mathbf{Re}\{e\} + \mathbf{Re}\{\alpha\}\,f_\mathrm{d}\sin\left(2\theta_\mathrm{dbl}\right)\ldots$$

(311) $$\qquad +\,\mathbf{Re}\{\beta\}\,f_\mathrm{s}\sin\left(2\theta_\mathrm{odd}\right)\Big)$$

$$\frac{\partial^2 F}{\partial f_\mathrm{d} \partial \mathbf{Im}\{\alpha\}} = 4\mathbf{Im}\{\alpha\}\,|\alpha|^2 f_\mathrm{d} + 4\mathbf{Im}\{\alpha\}\left(|\alpha|^2 f_\mathrm{d} + f_\mathrm{s} + a\,f_\mathrm{v} - T_{11}\right) + 2\mathbf{Im}\{\alpha\}\,f_\mathrm{d}\ldots$$

$$+\,2\cos\left(2\theta_\mathrm{dbl}\right)\Big(\mathbf{Im}\{\alpha\}\,f_\mathrm{d}\cos\left(2\theta_\mathrm{dbl}\right)\ldots$$

$$-\mathbf{Im}\{\beta\}\,f_\mathrm{s}\cos\left(\theta_\mathrm{odd}\right) + f_\mathrm{v}\mathbf{Im}\{f\} - \mathbf{Im}\{T_{12}\}\Big)\ldots$$

$$+\,2\sin\left(2\theta_\mathrm{dbl}\right)\left(\mathbf{Im}\{T_{13}\} - f_\mathrm{v}\mathbf{Im}\{e\}\ldots\right.$$

(312) $$\qquad +\,\mathbf{Im}\{\alpha\}\,f_\mathrm{d}\sin\left(2\theta_\mathrm{dbl}\right) -\mathbf{Im}\{\beta\}\,f_\mathrm{s}\sin\left(2\theta_\mathrm{odd}\right)\Big)$$

$$\frac{\partial^2 F}{\partial f_\mathrm{d} \partial \mathbf{Re}\{\beta\}} = 2\mathbf{Re}\{\alpha\}\,f_\mathrm{s}\cos\left(2\theta_{dbl}\right)\cos\left(2\theta_\mathrm{odd}\right) + 4\mathbf{Re}\{\beta\}\,f_\mathrm{s}\cos^2\left(2\theta_\mathrm{dbl}\right)\cos^2\left(2\theta_\mathrm{odd}\right)\ldots$$

$$+\,2\mathbf{Re}\{\alpha\}\,f_\mathrm{s}\sin\left(2\theta_{dbl}\right)\sin\left(2\theta_\mathrm{odd}\right) + 4\mathbf{Re}\{\beta\}\,f_\mathrm{s}\sin^2\left(2\theta_\mathrm{dbl}\right)\sin^2\left(2\theta_\mathrm{odd}\right)\ldots$$

(313) $$\qquad +\,\mathbf{Re}\{\beta\}\,f_\mathrm{s}\sin\left(4\theta_\mathrm{dbl}\right)\sin\left(4\theta_\mathrm{odd}\right)$$

$$\frac{\partial^2 F}{\partial f_{\mathrm{d}} \partial \mathbf{Im}\left\{\beta\right\}} = -2\mathbf{Im}\left\{\alpha\right\} f_{\mathrm{s}} \cos\left(2\theta_{\mathrm{dbl}}\right) \cos\left(2\theta_{\mathrm{odd}}\right) + 4\mathbf{Im}\left\{\beta\right\} f_{\mathrm{s}} \cos^2\left(2\theta_{\mathrm{dbl}}\right) \cos^2\left(2\theta_{\mathrm{odd}}\right) \ldots$$

$$- 2\mathbf{Im}\left\{\alpha\right\} f_{\mathrm{s}} \sin\left(2\theta_{\mathrm{dbl}}\right) \sin\left(2\theta_{\mathrm{odd}}\right) + 4\mathbf{Im}\left\{\beta\right\} f_{\mathrm{s}} \sin^2\left(2\theta_{\mathrm{dbl}}\right) \sin^2\left(2\theta_{\mathrm{odd}}\right) \ldots$$

$$(314) \qquad + \mathbf{Im}\left\{\beta\right\} f_{\mathrm{s}} \sin\left(4\theta_{\mathrm{dbl}}\right) \sin\left(4\theta_{\mathrm{odd}}\right)$$

B.3. PARTIAL DERIVATIVES OF $\frac{\partial F}{\partial FV}$

The first partial derivative of the objective function with respect to f_{v} is

$$\frac{\partial F}{\partial f\mathrm{v}} = -2a\left(T_{11} - f_{\mathrm{s}} - f_{\mathrm{d}}|\alpha|^2 - a\,f_{\mathrm{v}}\right) \ldots$$

$$- 2b\left(T_{22} - f_{\mathrm{s}}|\beta|^2 \cos^2\left(2\theta_{\mathrm{odd}}\right) - f_{\mathrm{d}} \cos^2\left(2\theta_{dbl}\right) - b\,f_{\mathrm{v}} - \frac{f_{\mathrm{c}}}{2}\right) \ldots$$

$$- 2c\left(T_{33} - f_{\mathrm{s}}|\beta|^2 \sin^2\left(2\theta_{\mathrm{odd}}\right) - f_{\mathrm{d}} \sin^2\left(2\theta_{dbl}\right) - c\,f_{\mathrm{v}} - \frac{f_{\mathrm{c}}}{2}\right) \ldots$$

$$- 2\mathbf{Re}\left\{d\right\}\left(\mathbf{Re}\left\{T_{12}\right\} - f_{\mathrm{s}}\mathbf{Re}\left\{\beta\right\} \cos\left(2\theta_{\mathrm{odd}}\right) - f_{\mathrm{d}}\mathbf{Re}\left\{\alpha\right\} \cos\left(2\theta_{\mathrm{dbl}}\right) - f_{\mathrm{v}}\mathbf{Re}\left\{d\right\}\right) \ldots$$

$$- 2\mathbf{Re}\left\{e\right\}\left(\mathbf{Re}\left\{T_{13}\right\} + f_{\mathrm{s}}\mathbf{Re}\left\{\beta\right\} \sin\left(2\theta_{\mathrm{odd}}\right) + f_{\mathrm{d}}\mathbf{Re}\left\{\alpha\right\} \sin\left(2\theta_{\mathrm{dbl}}\right) - f_{\mathrm{v}}\mathbf{Re}\left\{e\right\}\right) \ldots$$

$$- 2\mathbf{Re}\left\{f\right\}\left(\mathbf{Re}\left\{T_{23}\right\} + \frac{f_{\mathrm{s}}}{2}|\beta|^2 \sin\left(\theta_{\mathrm{odd}}\right) + \frac{f_{\mathrm{d}}}{2} \sin\left(4\theta_{\mathrm{dbl}}\right) - f_{\mathrm{v}}\mathbf{Re}\left\{f\right\}\right) \ldots$$

$$- 2\mathbf{Im}\left\{d\right\}\left(\mathbf{Im}\left\{T_{12}\right\} + f_{\mathrm{s}}\mathbf{Im}\left\{\beta\right\} \cos\left(2\theta_{\mathrm{odd}}\right) - f_{\mathrm{d}}\mathbf{Im}\left\{\alpha\right\} \cos\left(\theta_{\mathrm{dbl}}\right) - f_{\mathrm{v}}\mathbf{Im}\left\{d\right\}\right) \ldots$$

$$- 2\mathbf{Im}\left\{e\right\}\left(\mathbf{Im}\left\{T_{13}\right\} - f_{\mathrm{s}}\mathbf{Im}\left\{\beta\right\} \sin\left(2\theta_{\mathrm{odd}}\right) + f_{\mathrm{d}}\mathbf{Im}\left\{\alpha\right\} \sin\left(\theta_{\mathrm{dbl}}\right) - f_{\mathrm{v}}\mathbf{Im}\left\{e\right\}\right)$$

$$- 2\mathbf{Im}\left\{f\right\}\left(\mathbf{Im}\left\{T_{23}\right\} - \mathbf{Im}\left\{f\right\} f_{\mathrm{v}} - \frac{f_{\mathrm{c}}}{2}\right).$$

(315)

The second partial derivatives of the form $\frac{\partial^2 F}{\partial f_v \partial []}$ that form the third row of the Hessian are as follows:

$$(316) \qquad \frac{\partial^2 F}{\partial f_v \partial f_v} = 2\left(a^2 + b^2 + c^2 + |d|^2 + |e|^2 + |f|^2\right)$$

$$(317) \qquad \frac{\partial^2 F}{\partial f_v \partial f_c} = b + c + \mathbf{Im}\{f\}$$

$$\frac{\partial^2 F}{\partial f_v \partial \theta_{odd}} = -4f_s \Big(-\mathbf{Im}\{\beta\}\left(\cos\left(2\theta_{odd}\right)\mathbf{Im}\{e\} + \mathbf{Im}\{d\}\sin\left(2\theta_{odd}\right)\right) \ldots$$
$$+ \mathbf{Re}\{\beta\}\left(\cos\left(2\theta_{odd}\right)\mathbf{Re}\{e\} + \mathbf{Re}\{d\}\sin\left(2\theta_{odd}\right)\right) \ldots$$
$$(318) \qquad + |\beta|^2\left(\cos\left(4\theta_{odd}\right)\mathbf{Re}\{f\} + (b-c)\sin\left(4\theta_{odd}\right)\right) \Big)$$

$$\frac{\partial^2 F}{\partial f_v \partial \theta_{dbl}} = -4f_d \Big(\cos\left(4\theta_{dbl}\right)\mathbf{Re}\{f\} + \mathbf{Im}\{\alpha\}\left(\cos\left(2\theta_{dbl}\right)\mathbf{Im}\{e\} + \mathbf{Im}\{d\}\sin\left(2\theta_{dbl}\right)\right) \ldots$$
$$(319) \qquad + \mathbf{Re}\{\alpha\}\left(\cos\left(2\theta_{dbl}\right)\mathbf{Re}\{e\} + \mathbf{Re}\{d\}\sin\left(2\theta_{dbl}\right) + (b-c)\sin\left(4\theta_{dbl}\right)\right) \Big)$$

$$(320) \qquad \frac{\partial^2 F}{\partial f_v \partial \mathbf{Re}\{\alpha\}} = 2f_d\Big(2a\mathbf{Re}\{\alpha\} + \cos\left(2\theta_{dbl}\right)\mathbf{Re}\{d\} - \mathbf{Re}\{e\}\sin\left(2\theta_{dbl}\right)\Big)$$

$$(321) \qquad \frac{\partial^2 F}{\partial f_v \partial \mathbf{Im}\{\alpha\}} = 2f_d\Big(2a\mathbf{Im}\{\alpha\} + \cos\left(2\theta_{dbl}\right)\mathbf{Im}\{d\} - \mathbf{Im}\{e\}\sin\left(2\theta_{dbl}\right)\Big)$$

$$\frac{\partial^2 F}{\partial f_v \partial \mathbf{Re}\{\beta\}} = 2f_s \bigg(\cos\left(2\theta_{\text{odd}}\right) \mathbf{Re}\{d\} - \mathbf{Re}\{e\}\sin\left(2\theta_{\text{odd}}\right) \dots$$

$$(322) \qquad + \mathbf{Re}\{\beta\}\left(b + c + (b-c)\cos\left(4\theta_{\text{odd}}\right) - \mathbf{Re}\{f\}\sin\left(4\theta_{\text{odd}}\right)\right)\bigg)$$

$$\frac{\partial^2 F}{\partial f_v \partial \mathbf{Im}\{\beta\}} = 2f_s \bigg(-\cos\left(2\theta_{\text{odd}}\right) \mathbf{Im}\{d\} + \mathbf{Im}\{e\}\sin\left(2\theta_{\text{odd}}\right) \dots$$

$$(323) \qquad + \mathbf{Im}\{\beta\}\left(b + c + (b-c)\cos\left(4\theta_{\text{odd}}\right) - \mathbf{Re}\{f\}\sin\left(4\theta_{\text{odd}}\right)\right)\bigg)$$

B.4. PARTIAL DERIVATIVES OF $\frac{\partial F}{\partial FC}$

The first partial derivative of the objective function with respect to f_c is

$$(324) \qquad \frac{\partial F}{\partial fc} = \frac{3}{2}f_c + f_d + f_v\left(b + c_{\mathbf{Im}}\{f\}\right) + f_s|\beta|^2 - T_{22} - T_{33} - \mathbf{Im}\{T_{23}\}.$$

The second partial derivatives of the form $\frac{\partial^2 F}{\partial f_c \partial []}$ that form the fourth row of the Hessian are as follows:

$$(325) \qquad \frac{\partial^2 F}{\partial f_c^2} = \frac{3}{2}$$

$$(326) \qquad \frac{\partial^2 F}{\partial f_c \partial \theta_{\text{odd}}} = 0$$

$$(327) \qquad \frac{\partial^2 F}{\partial f_c \partial \theta_{\text{dbl}}} = 0$$

$$(328) \qquad \frac{\partial^2 F}{\partial f_{\mathrm{c}} \partial \mathbf{Re}\left\{\alpha\right\}} = 0$$

$$(329) \qquad \frac{\partial^2 F}{\partial f_{\mathrm{c}} \partial \mathbf{Im}\left\{\alpha\right\}} = 0$$

$$(330) \qquad \frac{\partial^2 F}{\partial f_{\mathrm{c}} \partial \mathbf{Re}\left\{\beta\right\}} = 2 f_{\mathrm{s}} \mathbf{Re}\left\{\beta\right\}$$

$$(331) \qquad \frac{\partial^2 F}{\partial f_{\mathrm{c}} \partial \mathbf{Im}\left\{\beta\right\}} = 2 f_{\mathrm{s}} \mathbf{Im}\left\{\beta\right\}$$

B.5. PARTIAL DERIVATIVES OF $\frac{\partial F}{\partial \theta_{\mathrm{ODD}}}$

The first partial derivative of the objective function with respect to θ_{odd} is

$$
\begin{aligned}
\frac{\partial F}{\partial \theta_{\mathrm{odd}}} &= 4 f_{\mathrm{s}} |\beta|^2 \sin\left(4\theta_{\mathrm{odd}}\right) \left(T_{22} - f_{\mathrm{s}} |\beta|^2 \cos^2\left(2\theta_{\mathrm{odd}}\right) - f_{\mathrm{d}} \cos^2\left(2\theta_{\mathrm{dbl}}\right) - b\, f_{\mathrm{v}} - \frac{f_{\mathrm{c}}}{2} \right) \ldots \\
&\quad - 4 f_{\mathrm{s}} |\beta|^2 \sin\left(4\theta_{\mathrm{odd}}\right) \left(T_{33} - f_{\mathrm{s}} |\beta|^2 \sin^2\left(2\theta_{\mathrm{odd}}\right) - f_{\mathrm{d}} \sin^2\left(2\theta_{\mathrm{dbl}}\right) - c\, f_{\mathrm{v}} - \frac{f_{\mathrm{c}}}{2} \right) \ldots \\
&\quad + 4 f_{\mathrm{s}} \mathbf{Re}\left\{\beta\right\} \sin\left(2\theta_{\mathrm{odd}}\right) \left(\mathbf{Re}\left\{T_{12}\right\} - f_{\mathrm{s}} \left\{\beta\right\} \cos\left(2\theta_{\mathrm{odd}}\right) \ldots \right. \\
&\qquad \left. - f_{\mathrm{d}} \mathbf{Re}\left\{\alpha\right\} \cos\left(2\theta_{\mathrm{dbl}}\right) - \mathbf{Re}\left\{d\right\} f_{\mathrm{v}} \right) \ldots \\
&\quad + 4 f_{\mathrm{s}} \mathbf{Re}\left\{\beta\right\} \cos\left(2\theta_{\mathrm{odd}}\right) \left(\mathbf{Re}\left\{T_{13}\right\} + f_{\mathrm{s}} \left\{\beta\right\} \sin\left(2\theta_{\mathrm{odd}}\right) \ldots \right. \\
&\qquad \left. + f_{\mathrm{d}} \mathbf{Re}\left\{\alpha\right\} \sin\left(2\theta_{\mathrm{dbl}}\right) - \mathbf{Re}\left\{e\right\} f_{\mathrm{v}} \right) \ldots \\
&\quad + f_{\mathrm{s}} |\beta|^2 \cos\left(4\theta_{\mathrm{odd}}\right) \left(\mathbf{Re}\left\{T_{23}\right\} + \frac{f_{\mathrm{s}}}{2} |\beta|^2 \sin\left(4\theta_{\mathrm{odd}}\right) + \frac{f_{\mathrm{d}}}{2} \sin\left(4\theta_{\mathrm{dbl}}\right) - \mathbf{Re}\left\{f\right\} f_{\mathrm{v}} \right) \ldots
\end{aligned}
$$

97

$$-4f_s \mathbf{Im}\left\{\beta\right\} \sin\left(2\theta_{\text{odd}}\right) \Bigg(\mathbf{Im}\left\{T_{12}\right\} + f_s \mathbf{Im}\left\{\beta\right\} \cos\left(2\theta_{\text{odd}}\right) \ldots$$

$$-f_d \mathbf{Im}\left\{\alpha\right\} \cos\left(2\theta_{\text{dbl}}\right) - \mathbf{Im}\left\{d\right\} f_v \Bigg) \ldots$$

$$-4f_s \mathbf{Im}\left\{\beta\right\} \cos\left(2\theta_{\text{odd}}\right) \Bigg(\mathbf{Im}\left\{T_{13}\right\} - f_s \mathbf{Im}\left\{\beta\right\} \sin\left(2\theta_{\text{odd}}\right) \ldots$$

(332)
$$+f_d \mathbf{Im}\left\{\alpha\right\} \sin\left(2\theta_{\text{dbl}}\right) - \mathbf{Im}\left\{e\right\} f_v \Bigg).$$

The second partial derivatives of the form $\frac{\partial^2 F}{\partial\theta_{\text{odd}}\partial[]}$ that form the fifth row of the Hessian are as follows:

$$\frac{\partial^2 F}{\partial\theta_{\text{odd}}^2} = -4f_s \Bigg[2f_s|\beta|^4 \cos\left(8\theta_{\text{odd}}\right) - 2\Bigg(f_d \cos\left(2\theta_{\text{dbl}} - 2\theta_{\text{odd}}\right) \mathbf{Im}\left\{\alpha\right\} \mathbf{Im}\left\{\beta\right\} \ldots$$

$$+\mathbf{Im}\left\{\beta\right\} \Bigg(f_v \cos\left(2\theta_{\text{odd}}\right) \mathbf{Im}\left\{d\right\} - \cos\left(2\theta_{\text{odd}}\right) \mathbf{Im}\left\{T_{12}\right\} \ldots$$

$$+ \left(\mathbf{Im}\left\{T_{13}\right\} - f_v \mathbf{Im}\left\{e\right\}\right) \sin\left(2\theta_{\text{odd}}\right) \Bigg) \ldots$$

$$- \mathbf{Re}\left\{\beta\right\} \Bigg(f_d \cos\left(2\theta_{\text{dbl}} - 2\theta_{\text{odd}}\right) \mathbf{Re}\left\{\alpha\right\} + f_v \cos\left(2\theta_{\text{odd}}\right) \mathbf{Re}\left\{d\right\} \ldots$$

$$- \cos\left(2\theta_{\text{odd}}\right) \mathbf{Re}\left\{T_{12}\right\} - f_v \mathbf{Re}\left\{e\right\} \sin\left(2\theta_{\text{odd}}\right) + \mathbf{Re}\left\{T_{13}\right\} \sin\left(2\theta_{\text{odd}}\right) \Bigg) \Bigg) \ldots$$

$$+ |\beta|^2 \Bigg(3f_d \cos\left(4\theta_{\text{dbl}} - 4\theta_{\text{odd}}\right) + 4\left(b - c\right) f_v \cos\left(4\theta_{\text{odd}}\right) + 4\left(T_{33} - T_{22}\right) \cos\left(4\theta_{\text{odd}}\right) \ldots$$

$$+ f + d \cos\left(4\theta_{\text{dbl}} + 4\theta_{\text{odd}}\right) - 4f_v \mathbf{Re}\left\{f\right\} \sin\left(4\theta_{\text{odd}}\right) + 4\mathbf{Re}\left\{T_{23}\right\} \sin\left(4\theta_{\text{odd}}\right) \Bigg) \Bigg]$$

(333)

$$\frac{\partial^2 F}{\partial\theta_{\text{odd}}\partial\theta_{\text{dbl}}} = -4f_d f_s \Bigg(|\beta|^2 \Big(- 3 \cos\left(4\theta_{\text{dbl}} - 4\theta_{\text{odd}}\right) + \cos\left(4\theta_{\text{dbl}} + 4\theta_{\text{odd}}\right) \Big) \ldots$$

(334)
$$+ 2\cos\left(2\theta_{\text{dbl}} - 2\theta_{\text{odd}}\right) \Big(\mathbf{Im}\left\{\alpha\right\} \mathbf{Im}\left\{\beta\right\} - \mathbf{Re}\left\{\alpha\right\} \mathbf{Re}\left\{\beta\right\} \Big) \Bigg)$$

$$(335) \qquad \frac{\partial^2 F}{\partial \theta_{\text{odd}} \partial \mathbf{Re}\{\alpha\}} = 4\mathbf{Re}\{\beta\}\, f_{\text{d}} f_{\text{s}} \sin\left(2\theta_{\text{dbl}} - 2\theta\text{odd}\right)$$

$$(336) \qquad \frac{\partial^2 F}{\partial \theta_{\text{odd}} \partial \mathbf{Im}\{\alpha\}} = -4\mathbf{Im}\{\beta\}\, f_{\text{d}} f_{\text{s}} \sin\left(2\theta_{\text{dbl}} - 2\theta\text{odd}\right)$$

$$\frac{\partial^2 F}{\partial \theta_{\text{odd}} \partial \mathbf{Re}\{\beta\}} = -2 f_{\text{s}} \Bigg[2 f_{\text{v}} \cos\left(2\theta_{\text{odd}}\right) \mathbf{Re}\{e\} + 4\mathbf{Re}\{\beta\}\, f_{\text{v}} \cos\left(4\theta_{\text{odd}}\right) \mathbf{Re}\{f\} \ldots$$

$$- 2\cos\left(2\theta_{\text{odd}}\right) \mathbf{Re}\{T_{13}\} - 4\mathbf{Re}\{\beta\} \cos\left(4\theta_{\text{odd}}\right) \mathbf{Re}\{T_{23}\} \ldots$$

$$- 3\mathbf{Re}\{\beta\}\, f_{\text{d}} \sin\left(4\theta_{\text{dbl}} - 4\theta_{\text{odd}}\right) - 2\mathbf{Re}\{\alpha\}\, f_{\text{d}} \sin\left(2\theta_{\text{dbl}} - 2\theta_{\text{odd}}\right) \ldots$$

$$+ 2 f_{\text{v}}\mathbf{Re}\{d\} \sin\left(2\theta_{\text{odd}}\right) - 2\mathbf{Re}\{T_{12}\} \sin\left(2\theta_{\text{odd}}\right) + 4\left(b - c\right) \mathbf{Re}\{\beta\}\, f_{\text{v}} \sin\left(4\theta_{\text{odd}}\right) \ldots$$

$$+ 4\left(T_{33} - T_{22}\right) \mathbf{Re}\{\beta\} \sin\left(4\theta_{\text{odd}}\right) + 2\left(\mathbf{Im}\{\beta\}\right)^2 \mathbf{Re}\{\beta\}\, f_{\text{s}} \sin\left(8\theta_{\text{odd}}\right) \ldots$$

$$(337) \qquad + 2\left(\mathbf{Re}\{\beta\}\right)^3 f_{\text{s}} \sin\left(8\theta_{\text{odd}}\right) + \mathbf{Re}\{\beta\}\, f_{\text{d}} \sin\left(4\theta_{\text{dbl}} + 4\theta_{\text{odd}}\right) \Bigg]$$

$$\frac{\partial^2 F}{\partial \theta_{\text{odd}} \partial \mathbf{Im}\{\beta\}} = -2 f_{\text{s}} \Bigg[- 2 f_{\text{v}} \cos\left(2\theta_{\text{odd}}\right) \mathbf{Im}\{e\} + 4\mathbf{Im}\{\beta\}\, f_{\text{v}} \cos\left(4\theta_{\text{odd}}\right) \mathbf{Re}\{f\} \ldots$$

$$+ 2\cos\left(2\theta_{\text{odd}}\right) \mathbf{Im}\{T_{13}\} - 4\mathbf{Im}\{\beta\} \cos\left(4\theta_{\text{odd}}\right) \mathbf{Re}\{T_{23}\} \ldots$$

$$- 3\mathbf{Im}\{\beta\}\, f_{\text{d}} \sin\left(4\theta_{\text{dbl}} - 4\theta_{\text{odd}}\right) + 2\mathbf{Im}\{\alpha\}\, f_{\text{d}} \sin\left(2\theta_{\text{dbl}} - 2\theta_{\text{odd}}\right) \ldots$$

$$- 2 f_{\text{v}}\mathbf{Im}\{d\} \sin\left(2\theta_{\text{odd}}\right) + 2\mathbf{Im}\{T_{12}\} \sin\left(2\theta_{\text{odd}}\right) + 4\left(b - c\right) \mathbf{Im}\{\beta\}\, f_{\text{v}} \sin\left(4\theta_{\text{odd}}\right) \ldots$$

$$+ 4\left(T_{33} - T_{22}\right) \mathbf{Im}\{\beta\} \sin\left(4\theta_{\text{odd}}\right) + 2\left(\mathbf{Im}\{\beta\}\right)^3 f_{\text{s}} \sin\left(8\theta_{\text{odd}}\right) \ldots$$

$$(338) \qquad + 2\mathbf{Im}\{\beta\}\left(\mathbf{Re}\{\beta\}\right)^2 f_{\text{s}} \sin\left(8\theta_{\text{odd}}\right) + \mathbf{Im}\{\beta\}\, f_{\text{d}} \sin\left(4\theta_{\text{dbl}} + 4\theta_{\text{odd}}\right) \Bigg]$$

The first partial derivative of the objective function with respect to θ_{dbl} is

$$
\begin{aligned}
\frac{\partial F}{\partial \theta_{\text{dbl}}} = {} & 4f_{\text{d}} \sin\left(4\theta_{\text{dbl}}\right) \left(T_{22} - f_{\text{s}}|\beta|^2 \cos^2\left(2\theta_{\text{odd}}\right) - f_{\text{d}}\cos^2\left(2\theta_{\text{dbl}}\right) - b\, f_{\text{v}} - \frac{f_{\text{c}}}{2} \right) \dots \\
& - 4f_{\text{d}} \sin\left(4\theta_{\text{dbl}}\right) \left(T_{33} - f_{\text{s}}|\beta|^2 \sin^2\left(2\theta_{\text{odd}}\right) - f_{\text{d}}\sin^2\left(2\theta_{\text{dbl}}\right) - c\, f_{\text{v}} - \frac{f_{\text{c}}}{2} \right) \dots \\
& + 4f_{\text{d}}\mathbf{Re}\left\{\alpha\right\} \sin\left(2\theta_{\text{dbl}}\right) \left(\mathbf{Re}\left\{T_{12}\right\} - f_{\text{s}}\left\{\beta\right\}\cos\left(2\theta_{\text{odd}}\right) \dots \right. \\
& \left. qquad - f_{\text{d}}\mathbf{Re}\left\{\alpha\right\}\cos\left(2\theta_{\text{dbl}}\right) - \mathbf{Re}\left\{d\right\} f_{\text{v}} \right) \dots \\
& + 4f_{\text{d}}\mathbf{Re}\left\{\alpha\right\} \cos\left(2\theta_{\text{dbl}}\right) \left(\mathbf{Re}\left\{T_{13}\right\} + f_{\text{s}}\left\{\beta\right\}\sin\left(2\theta_{\text{odd}}\right) \dots \right. \\
& \left. + f_{\text{d}}\mathbf{Re}\left\{\alpha\right\}\sin\left(2\theta_{\text{dbl}}\right) - \mathbf{Re}\left\{e\right\} f_{\text{v}} \right) \dots \\
& + f_{\text{d}}\cos\left(4\theta_{\text{dbl}}\right) \left(\mathbf{Re}\left\{T_{23}\right\} + \frac{f_{\text{s}}}{2}|\beta|^2 \sin\left(4\theta_{\text{odd}}\right) + \frac{f_{\text{d}}}{2}\sin\left(4\theta_{\text{dbl}}\right) - \mathbf{Re}\left\{f\right\} f_{\text{v}} \right) \dots \\
& + 4f_{\text{d}}\mathbf{Im}\left\{\alpha\right\} \sin\left(2\theta_{\text{dbl}}\right) \left(\mathbf{Im}\left\{T_{12}\right\} + f_{\text{s}}\mathbf{Im}\left\{\beta\right\}\cos\left(2\theta_{\text{odd}}\right) \dots \right. \\
& \left. - f_{\text{d}}\mathbf{Im}\left\{\alpha\right\}\cos\left(2\theta_{\text{dbl}}\right) - \mathbf{Im}\left\{d\right\} f_{\text{v}} \right) \dots \\
& + 4f_{\text{d}}\mathbf{Im}\left\{\alpha\right\} \cos\left(2\theta_{\text{dbl}}\right) \left(\mathbf{Im}\left\{T_{13}\right\} - f_{\text{s}}\mathbf{Im}\left\{\beta\right\}\sin\left(2\theta_{\text{odd}}\right) \dots \right. \\
& \left. + f_{\text{d}}\mathbf{Im}\left\{\alpha\right\}\sin\left(2\theta_{\text{dbl}}\right) - \mathbf{Im}\left\{e\right\} f_{\text{v}} \right).
\end{aligned}
$$

(339)

The second partial derivatives of the form $\frac{\partial^2 F}{\partial \theta_{\text{dbl}}\partial[]}$ that form the sixth row of the Hessian are as follows:

$$
\frac{\partial^2 F}{\partial \theta_{\text{dbl}}^2} = -4f_{\text{d}} \left[f_{\text{s}}|\beta|^2 \left(3\cos\left(4\theta_{\text{dbl}} - 4\theta_{\text{odd}}\right) + \cos\left(4\theta_{\text{dbl}} + 4\theta_{\text{odd}}\right) \right) \dots \right.
$$

$$+ 2 \left(2 \left(b - c \right) f_{\text{v}} \cos \left(4\theta_{\text{dbl}} \right) + 2 \left(T_{33} - T_{22} \right) \cos \left(4\theta_{\text{dbl}} \right) + f_{\text{d}} \cos \left(8\theta_{\text{dbl}} \right) \ldots \right.$$

$$- \, \mathbf{Im} \left\{ \alpha \right\} \left(f_{\text{s}} \cos \left(2\theta_{\text{dbl}} - 2\theta_{\text{odd}} \right) \mathbf{Im} \left\{ \beta \right\} - f_{\text{v}} \cos \left(2\theta_{\text{dbl}} \right) \mathbf{Im} \left\{ d \right\} \ldots \right.$$

$$\left. + \, \cos \left(2\theta_{\text{dbl}} \right) \mathbf{Im} \left\{ T_{12} \right\} + f_{\text{v}} \mathbf{Im} \left\{ e \right\} \sin \left(2\theta_{\text{dbl}} \right) - \mathbf{Im} \left\{ T_{13} \right\} \sin \left(2\theta_{\text{dbl}} \right) \right) \ldots$$

$$+ \, \mathbf{Re} \left\{ \alpha \right\} \left(f_{\text{s}} \cos \left(2\theta_{\text{dbl}} - 2\theta_{\text{odd}} \right) \mathbf{Re} \left\{ \beta \right\} + f_{\text{v}} \cos \left(2\theta_{\text{dbl}} \right) \mathbf{Re} \left\{ d \right\} \ldots \right.$$

$$\left. - \, \cos \left(2\theta_{\text{dbl}} \right) \mathbf{Re} \left\{ T_{12} \right\} - f_{\text{v}} \mathbf{Re} \left\{ e \right\} \sin \left(2\theta_{\text{dbl}} \right) + \mathbf{Re} \left\{ T_{13} \right\} \sin \left(2\theta_{\text{dbl}} \right) \right) \ldots$$

$$\left. \left. - \, f_{\text{v}} \mathbf{Re} \left\{ f \right\} \sin \left(4\theta_{\text{dbl}} \right) + 2 \mathbf{Re} \left\{ T_{23} \right\} \sin \left(4\theta_{\text{dbl}} \right) \right) \right]$$

(340)

$$\frac{\partial^2 F}{\partial \theta_{\text{dbl}} \partial \mathbf{Re} \left\{ \alpha \right\}} = -4 f_{\text{d}} \left(f_{\text{v}} \cos \left(2\theta_{\text{dbl}} \right) \mathbf{Re} \left\{ e \right\} - \cos \left(2\theta_{\text{dbl}} \right) \mathbf{Re} \left\{ T_{13} \right\} + f_{\text{v}} \mathbf{Re} \left\{ d \right\} \sin \left(2\theta_{\text{dbl}} \right) \ldots \right.$$

$$\left. - \, \mathbf{Re} \left\{ T_{12} \right\} \sin \left(2\theta_{\text{dbl}} \right) + \mathbf{Re} \left\{ \beta \right\} f_{\text{s}} \sin \left(2\theta_{\text{dbl}} - 2\theta_{\text{odd}} \right) \right)$$

(341)

$$\frac{\partial^2 F}{\partial \theta_{\text{dbl}} \partial \mathbf{Im} \left\{ \alpha \right\}} = -4 f_{\text{d}} \left(f_{\text{v}} \cos \left(2\theta_{\text{dbl}} \right) \mathbf{Im} \left\{ e \right\} - \cos \left(2\theta_{\text{dbl}} \right) \mathbf{Im} \left\{ T_{13} \right\} + f_{\text{v}} \mathbf{Im} \left\{ d \right\} \sin \left(2\theta_{\text{dbl}} \right) \ldots \right.$$

$$\left. - \, \mathbf{Im} \left\{ T_{12} \right\} \sin \left(2\theta_{\text{dbl}} \right) - \mathbf{Im} \left\{ \beta \right\} f_{\text{s}} \sin \left(2\theta_{\text{dbl}} - 2\theta_{\text{odd}} \right) \right)$$

(342)

$$\frac{\partial^2 F}{\partial \theta_{\text{dbl}} \partial \mathbf{Re} \left\{ \beta \right\}} = -2 f_{\text{s}} f_{\text{d}} \left(3 \mathbf{Re} \left\{ \beta \right\} \sin \left(4\theta_{\text{dbl}} - 4\theta_{\text{odd}} \right) + 2 \mathbf{Re} \left\{ \alpha \right\} \sin \left(2\theta_{\text{dbl}} - 2\theta_{\text{odd}} \right) \ldots \right.$$

$$\left. + \, \mathbf{Re} \left\{ \beta \right\} \sin \left(4\theta_{\text{dbl}} + 4\theta_{\text{odd}} \right) \right)$$

(343)

$$\frac{\partial^2 F}{\partial \theta_{\text{dbl}} \partial \mathbf{Im}\{\beta\}} = -2f_s f_d \left(3\mathbf{Im}\{\beta\} \sin\left(4\theta_{\text{dbl}} - 4\theta_{\text{odd}}\right) - 2\mathbf{Im}\{\alpha\} \sin\left(2\theta_{\text{dbl}} - 2\theta_{\text{odd}}\right) \ldots \right.$$

(344)
$$\left. + \mathbf{Im}\{\beta\} \sin\left(4\theta_{\text{dbl}} + 4\theta_{\text{odd}}\right) \right)$$

B.7. PARTIAL DERIVATIVES OF $\frac{\partial F}{\partial \mathbf{RE}\{\alpha\}}$

The first partial derivative of the objective function with respect to $\mathbf{Re}\{\alpha\}$ is

$$\frac{\partial F}{\mathbf{Re}\{\alpha\}} = -4f_d \mathbf{Re}\{\alpha\} \left(T_{11} - f_s - f_d|\alpha|^2 - a\, f_v \right) \ldots$$

$$+ 2f_d \cos\left(2\theta_{\text{dbl}}\right) \left(\mathbf{Re}\{T_{12}\} - f_s\{\beta\} \cos\left(2\theta_{\text{odd}}\right) - f_d \mathbf{Re}\{\alpha\} \cos\left(2\theta_{\text{dbl}}\right) - \mathbf{Re}\{d\}\, f_v \right) \ldots$$

$$+ 2f_d \sin\left(2\theta_{\text{dbl}}\right) \left(\mathbf{Re}\{T_{13}\} + f_s\{\beta\} \sin\left(2\theta_{\text{odd}}\right) + f_d \mathbf{Re}\{\alpha\} \sin\left(2\theta_{\text{dbl}}\right) - \mathbf{Re}\{e\}\, f_v \right).$$

(345)

The second partial derivatives of the form $\frac{\partial^2 F}{\partial \mathbf{Re}\{\alpha\}\partial[]}$ that form the seventh row of the Hessian are as follows:

(346)
$$\frac{\partial^2 F}{\partial \mathbf{Re}\{\alpha\}^2} = 8\left(\mathbf{Re}\{\alpha\}\right)^2 f_d^2 - f_d\left(-|\alpha|^2 f_d - f_s - a\, f_v + T_{11}\right) + 2f_d^2$$

(347)
$$\frac{\partial^2 F}{\partial \mathbf{Re}\{\alpha\}\,\partial \mathbf{Im}\{\alpha\}} = 8\mathbf{Im}\{\alpha\}\,\mathbf{Re}\{\alpha\}\, f_d^2$$

(348)
$$\frac{\partial^2 F}{\partial \mathbf{Re}\{\alpha\}\,\partial \mathbf{Re}\{\beta\}} = 2f_s f_d \cos\left(2\theta_{\text{dbl}} - 2\theta_{\text{odd}}\right)$$

$$(349) \qquad \frac{\partial^2 F}{\partial \mathbf{Re}\left\{\alpha\right\} \partial \mathbf{Im}\left\{\beta\right\}} = 0$$

B.8. PARTIAL DERIVATIVES OF $\frac{\partial F}{\partial \mathbf{IM}\{\alpha\}}$

The first partial derivative of the objective function with respect to $\mathbf{Im}\left\{\alpha\right\}$ is

$$\frac{\partial F}{\mathbf{Im}\left\{\alpha\right\}} = -4 f_{\mathrm{d}} \mathbf{Im}\left\{\alpha\right\} \left(T_{11} - f_{\mathrm{s}} - f_{\mathrm{d}} |\alpha|^2 - a\, f_{\mathrm{v}}\right) \ldots$$

$$- 2 f_{\mathrm{d}} \cos\left(2\theta_{\mathrm{dbl}}\right) \left(\mathbf{Re}\left\{T_{12}\right\} - f_{\mathrm{s}}\left\{\beta\right\} \cos\left(2\theta_{\mathrm{odd}}\right) - f_{\mathrm{d}} \mathbf{Re}\left\{\alpha\right\} \cos\left(2\theta_{\mathrm{dbl}}\right) - \mathbf{Re}\left\{d\right\} f_{\mathrm{v}}\right) \ldots$$

$$+ 2 f_{\mathrm{d}} \sin\left(2\theta_{\mathrm{dbl}}\right) \left(\mathbf{Re}\left\{T_{13}\right\} + f_{\mathrm{s}}\left\{\beta\right\} \sin\left(2\theta_{\mathrm{odd}}\right) + f_{\mathrm{d}} \mathbf{Re}\left\{\alpha\right\} \sin\left(2\theta_{\mathrm{dbl}}\right) - \mathbf{Re}\left\{e\right\} f_{\mathrm{v}}\right).$$

(350)

The second partial derivatives of the form $\frac{\partial^2 F}{\partial \mathbf{Im}\{\alpha\}\partial []}$ that form the eighth row of the Hessian are as follows:

$$(351) \qquad \frac{\partial^2 F}{\partial \mathbf{Im}\left\{\alpha\right\}^2} = 2 f_{\mathrm{d}} \left(f_{\mathrm{d}} + 6\left(\mathbf{Im}\left\{\alpha\right\}\right)^2 f_{\mathrm{d}} + 2\left(\mathbf{Re}\left\{\alpha\right\}\right)^2 f_{\mathrm{d}} + 2 f_{\mathrm{s}} + 2a\, f_{\mathrm{v}} - 2T_{11}\right)$$

$$(352) \qquad \frac{\partial^2 F}{\partial \mathbf{Im}\left\{\alpha\right\} \partial \mathbf{Re}\left\{\beta\right\}} = 0$$

$$(353) \qquad \frac{\partial^2 F}{\partial \mathbf{Im}\left\{\alpha\right\} \partial \mathbf{Im}\left\{\beta\right\}} = -2 f_{\mathrm{d}} f_{\mathrm{s}} \cos\left(2\theta_{\mathrm{dbl}} - 2\theta_{\mathrm{odd}}\right)$$

103

B.9. PARTIAL DERIVATIVES OF $\frac{\partial F}{\partial \mathbf{RE}\{\beta\}}$

The first partial derivative of the objective function with respect to $\mathbf{Re}\{\beta\}$ is

$$
\begin{aligned}
\frac{\partial F}{\mathbf{Re}\{\beta\}} &= -4f_{\mathrm{s}} \cos^2\left(2\theta_{\mathrm{odd}}\right) \mathbf{Re}\{\beta\} \left(T_{22} - f_{\mathrm{s}}|\beta|^2 \cos^2\left(2\theta_{\mathrm{odd}}\right) - f_{\mathrm{d}} \cos^2\left(2\theta_{\mathrm{dbl}}\right) - b\,f_{\mathrm{v}} - \frac{f_{\mathrm{c}}}{2}\right) \ldots \\
&\quad - 4f_{\mathrm{s}} \sin^2\left(2\theta_{\mathrm{odd}}\right) \mathbf{Re}\{\beta\} \left(T_{33} - f_{\mathrm{s}}|\beta|^2 \sin^2\left(2\theta_{\mathrm{odd}}\right) - f_{\mathrm{d}} \sin^2\left(2\theta_{\mathrm{dbl}}\right) - c\,f_{\mathrm{v}} - \frac{f_{\mathrm{c}}}{2}\right) \ldots \\
&\quad - 2f_{\mathrm{s}} \cos\left(2\theta_{\mathrm{odd}}\right) \left(\mathbf{Re}\{T_{12}\} - f_{\mathrm{s}}\{\beta\} \cos\left(2\theta_{\mathrm{odd}}\right) - f_{\mathrm{d}}\mathbf{Re}\{\alpha\} \cos\left(2\theta_{\mathrm{dbl}}\right) - \mathbf{Re}\{d\}\,f_{\mathrm{v}}\right) \ldots \\
&\quad + 2f_{\mathrm{s}} \sin\left(2\theta_{\mathrm{odd}}\right) \left(\mathbf{Re}\{T_{13}\} + f_{\mathrm{s}}\{\beta\} \sin\left(2\theta_{\mathrm{odd}}\right) + f_{\mathrm{d}}\mathbf{Re}\{\alpha\} \sin\left(2\theta_{\mathrm{dbl}}\right) - \mathbf{Re}\{e\}\,f_{\mathrm{v}}\right) \ldots \\
&\quad + 2f_{\mathrm{s}} \sin\left(4\theta_{\mathrm{odd}}\right) \mathbf{Re}\{\beta\} \left(\mathbf{Re}\{T_{23}\} + \frac{f_{\mathrm{s}}}{2}|\beta|^2 \sin\left(4\theta_{\mathrm{odd}}\right) + \frac{f_{\mathrm{d}}}{2} \sin\left(4\theta_{\mathrm{dbl}}\right) - \mathbf{Re}\{f\}\,f_{\mathrm{v}}\right).
\end{aligned}
$$

(354)

The second partial derivatives of the form $\frac{\partial^2 F}{\partial \mathbf{Re}\{\beta\}\partial[]}$ that form the ninth row of the Hessian are as follows:

$$
\begin{aligned}
\frac{\partial^2 F}{\partial \mathbf{Re}\{\beta\}^2} &= \frac{f_{\mathrm{s}}}{2} \left(4f_{\mathrm{c}} + 4f_{\mathrm{d}} + 4f_{\mathrm{s}} + 7\left(\mathbf{Re}\{\beta\}\right)^2 + 21\left(\mathbf{Im}\{\beta\}\right)^2 f_{\mathrm{s}} + (b+c)\,f_{\mathrm{v}} \ldots \right. \\
&\quad - (T_{22} + T_{33}) \cos\left(4\theta_{\mathrm{odd}}\right) + \left(\mathbf{Im}\{\beta\}\right)^2 f_{\mathrm{s}} \cos\left(8\theta_{\mathrm{odd}}\right) + 3\left(\mathbf{Re}\{\beta\}\right)^2 f_{\mathrm{s}} \cos\left(8\theta_{\mathrm{odd}}\right) \ldots \\
&\quad \left. + f_{\mathrm{d}} \cos\left(4\theta_{\mathrm{dbl}} + 4\theta_{\mathrm{odd}}\right) - 4f_{\mathrm{v}}\mathbf{Re}\{f\} \sin\left(4\theta_{\mathrm{odd}}\right) + 4\mathbf{Re}\{T_{23}\} \sin\left(4\theta_{\mathrm{odd}}\right) \right)
\end{aligned}
$$

(355)

$$
\frac{\partial^2 F}{\partial \mathbf{Re}\{\beta\}\,\partial \mathbf{Im}\{\beta\}} = \mathbf{Im}\{\beta\}\,\mathbf{Re}\{\beta\}\,f_{\mathrm{s}}^2 \left(7 + \cos\left(8\theta_{\mathrm{odd}}\right)\right)
$$

(356)

B.10. PARTIAL DERIVATIVES OF $\frac{\partial F}{\partial \mathbf{IM}\{\beta\}}$

The first partial derivative of the objective function with respect to $\mathbf{Im}\{\beta\}$ is

$$
\frac{\partial F}{\mathbf{Im}\{\beta\}} = -4f_{\mathrm{s}} \cos^2\left(2\theta_{\mathrm{odd}}\right) \mathbf{Im}\{\beta\} \left(T_{22} - f_{\mathrm{s}}|\beta|^2 \cos^2\left(2\theta_{\mathrm{odd}}\right) - f_{\mathrm{d}} \cos^2\left(2\theta_{\mathrm{dbl}}\right) - b\,f_{\mathrm{v}} - \frac{f_{\mathrm{c}}}{2}\right) \ldots
$$

$$- 4f_s \sin^2 (2\theta_{\mathrm{odd}}) \, \mathbf{Im} \{\beta\} \left(T_{33} - f_s |\beta|^2 \sin^2 (2\theta_{\mathrm{odd}}) - f_d \sin^2 (2\theta_{\mathrm{dbl}}) - c\, f_v - \frac{f_c}{2} \right) \ldots$$

$$+ 2f_s \sin (4\theta_{\mathrm{odd}}) \, \mathbf{Im} \{\beta\} \left(\mathbf{Re} \{T_{23}\} + \frac{f_s}{2} |\beta|^2 \sin (4\theta_{\mathrm{odd}}) + \frac{f_d}{2} \sin (4\theta_{\mathrm{dbl}}) - f_v \mathbf{Re} \{f\} \right) \ldots$$

$$+ 2f_s \cos (2\theta_{\mathrm{odd}}) \left(\mathbf{Im} \{T_{12}\} + f_s \mathbf{Im} \{\beta\} \cos (2\theta_{\mathrm{odd}}) - f_d \mathbf{Im} \{\alpha\} \cos (2\theta_{\mathrm{dbl}}) - f_v \mathbf{Im} \{d\} \right) \ldots$$

$$+ 2f_s \cos (2\theta_{\mathrm{odd}}) \left(\mathbf{Im} \{T_{12}\} + f_s \mathbf{Im} \{\beta\} \cos (2\theta_{\mathrm{odd}}) - f_d \mathbf{Im} \{\alpha\} \cos (2\theta_{\mathrm{dbl}}) - f_v \mathbf{Im} \{d\} \right).$$

(357)

The second partial of the form $\frac{\partial^2 F}{\partial (\mathbf{Re}\{\beta\})^2}$ and completes the tenth (and last, phew!) row of the Hessian is as follows:

$$\frac{\partial^2 F}{\partial \mathbf{Im} \{\beta\}^2} = \frac{f_s}{2} \left(4f_c + 4f_d + 4f_s + 7 \left(\mathbf{Re} \{\beta\} \right)^2 + 21 \left(\mathbf{Im} \{\beta\} \right)^2 f_s + (b + c)\, f_v \ldots \right.$$

$$- (T_{22} + T_{33}) \cos (4\theta_{\mathrm{odd}}) + 3 \left(\mathbf{Im} \{\beta\} \right)^2 f_s \cos (8\theta_{\mathrm{odd}}) + \left(\mathbf{Re} \{\beta\} \right)^2 f_s \cos (8\theta_{\mathrm{odd}}) \ldots$$

$$(358) \qquad \left. + f_d \cos (4\theta_{\mathrm{dbl}} + 4\theta_{\mathrm{odd}}) - 4f_v \mathbf{Re} \{f\} \sin (4\theta_{\mathrm{odd}}) + 4 \mathbf{Re} \{T_{23}\} \sin (4\theta_{\mathrm{odd}}) \right)$$